NASA-CR-166,046

NASA Contractor Report 166046

PERFORMANCE OF A QUANTITATIVE STUDY OF INSTABILITY-RELATED DELAMINATION GROWTH

R.L RAMKUMAR

NORTHROP CORPORATION
AIRCRAFT DIVISION
HAWTHORNE, CA 90250

CONTRACT NAS1-16727
MARCH 1983

National Aeronautics and
Space Administration

Langley Research Center
Hampton, Virginia 23665

NASA Contractor Report 166046

PERFORMANCE OF A QUANTITATIVE STUDY OF INSTABILITY-RELATED DELAMINATION GROWTH

R.L. RAMKUMAR

NORTHROP CORPORATION
AIRCRAFT DIVISION
HAWTHORNE, CA 90250

CONTRACT NAS1-16727
MARCH 1983

NASA
National Aeronautics and
Space Administration

Langley Research Center
Hampton, Virginia 23665

N83-29314#

ACKNOWLEDGEMENT

The author is thankful to Mr. J. D. Whitcomb, the project engineer at NASA, Langley Research Center, for his technical comments that aided and ensured the proper conduct of the reported program. Nonlinear finite element analysis of the CLS specimen was performed at NASA, Langley Research Center.

Thanks are also due to the following personnel for the cited contributions:

Specimen Fabrication - Ms. B. A. Fourcher, Mr. J. Welbourn, Mr. A. Cecka, Mr. A. Hall

Machining Operations - Mr. N. P. Barrett, Mr. B. J. Mays

DCB and CLS Testing - Mr. P. J. Dager, Mr. L. J. Heller

ITTW Delamination Testing - Mr. T. R. Miller

Graphics - Ms. R. Cordero

Typing - Ms. B. Parish

TABLE OF CONTENTS

TABLE OF CONTENTS (CONCLUDED)

NOMENCLATURE

a	delamination length in DCB specimens, or half-length of delamination in specimens with ITTW delamination
A	cross-sectional area of specimens
C	compliance
CLS	abbreviation for "cracked lap shear"
da/dN	delamination growth rate
dC/da	rate of change of compliance with delamination growth
DCB	abbreviation for "double cantilever beam"
E	Young's modulus in the loading direction
E_{11}	Young's modulus in the fiber direction
E_{22}	Young's modulus perpendicular to the fiber direction
G	total strain energy release rate = $P^2(dC/da)/2w$
G_I	mode I strain energy release rate (opening mode)
G_{II}	mode II strain energy release rate (shear mode)
G_{III}	mode III strain energy release rate (out-of-plane shear mode).
G_{12}	Shear modulus of an orthotropic lamina
G_c	critical value of the total strain energy release rate
G_{IC}, G_{IIC}, G_{IIIC}	critical strain energy release rates under modes I, II, and III, respectively
ITTW	abbreviation for "imbedded through the width"
L	half gage length of specimens with ITTW delaminations
L_1	length of thinner load-carrying portion of CLS specimens
L_2	length of thicker load-carrying portion of CLS specimens
N	number of cycles of constant amplitude fatigue loading at specified ω, R, S values
P	load applied on DCB specimens
P_T	total tensile load applied on CLS specimens
P_{cr}	load at which delamination starts to propagate

R	algebraic minimum-to-maximum cyclic load ratio
S	ratio of the absolute maximum cyclic stress to the absolute static strength
u_1	axial elongation of the thinner load-carrying portion of CLS specimens
u_2	axial elongation of the thicker load-carrying portion of CLS specimens
w	specimen width
X_{max}	distance from the tab edge to the location of maximum out-of-plane displacement of delaminated plies in specimens with ITTW delaminations
δ	total opening displacement in DCB specimens
δ_L	out-of-plane displacement of delaminated plies at mid-length of specimens with ITTW delaminations
ε_L	axial strain in delaminated plies at mid-length of specimens with ITTW delaminations
ν_{12}	Poisson's ratio for an orthoropic lamina
ω	frequency of constant amplitude fatigue loading.

SECTION 1

INTRODUCTION AND SUMMARY

1.1 INTRODUCTION

Delaminations are precipitated in laminated composites under many process and service conditions. Their presence and growth have been shown to induce significant strength losses under static compressive loading, and have proven to be life-limiting under constant amplitude fatigue loading conditions (References 1, 2). The severity of the problem is a result of local instability induced in the delaminated region by a compressive load. The onset of instability is manifested by the local buckling of the delaminated region. Static compression and constant-amplitude compression fatigue tests on specimens containing realistic or idealized (imbedded) delaminations have identified delamination propagation as the primary failure mechanism. and have demonstrated the deleterious effect of these flaws on the strength and lifetime of the laminate (References 1,2, 3).

In a realistic situation, delaminations of various planforms exist alongside many intraply cracks. Failure under compressive loading is induced by a simultaneous progression of these local defects. Analysis of this complex behavior requires an understanding of the interaction of various failure modes, and the availability of failure criteria that appropriately quantify this interaction. A quantitative assessment of the effect of delaminations on the strength and lifetime of a laminate is difficult. Consequently, analytical efforts to date have only attempted to quantify the effect of idealized (imbedded) delaminations (References 4-12). In every case, the delamination is also assumed to propagate along the same interfacial surface.

Delamination growth may be predicted based on point stresses, average stresses or strain energy release rates at the delamination boundary. In this report, predictions are based on strain energy release rates, G_I and G_{II}, corresponding to the opening or peeling mode (mode I) and the inplane shear mode (mode II), respectively. G_{III}, the strain energy release rate corresponding to out-of-plane shear (mode III), is assumed to be negligible in the test specimens.

1.2 SUMMARY

The objectives of the reported program were: (a) to characterize a pure mode I delamination growth in T300/5208 graphite/epoxy laminates, under static and fatigue loading conditions; (b) to monitor delamination growth in T300/5208 laminates in a mixed mode (modes I and II) situation, under static and fatigue loading conditions; (c) to perform a finite element analysis of the mixed mode test specimen to compute the G_I and G_{II} values corresponding to various delamination sizes and load levels; (d) to incorporate the computed G_I and G_{II} values, mode I test results, and mixed mode test results into assumed static failure criteria and delamination growth rate equations, to separate the effects of G_I and G_{II} on delamination growth in T300/5208 laminates under static and fatigue loading conditions; and (e) to generate delamination growth data on T300/5208 specimens with imbedded through-the-width (ITTW) delaminations, under static compression and compression fatigue loading conditions.

Double cantilever beam (DCB) specimens were used for pure mode I tests. Cracked lap shear (CLS) specimens were used for mixed mode tests. DCB and CLS tests were conducted in a displacement-controlled mode to obtain stable delamination growth. Delaminations were introduced during fabrication by inserting folded Kapton films of specified sizes between selected plies. Delaminations were placed between two 0^{0} plies in all the specimens, to minimize G_{III} (out-of-plane shear) effects, and to obtain "clean" delamination growths by inhibiting failure propagation across plies into adjacent interfaces.

The critical mode I strain energy release rate, G_{IC}, was obtained directly from static DCB tests, conducted in accordance with ASTM standards (Reference 13). G_{IC} for the T300/5208 material system was compared with results from similar tests on other materials (References 14-17). Static tests on the mixed mode CLS specimens measured the critical value of the total strain energy release rate (G_C) at which delamination growth occurred. A geometrically nonlinear finite element analysis of the CLS specimen was carried out at NASA, Langley Research Center to determine the G_I and G_{II} components of the total strain energy release rate at various load levels for different delamination lengths. Incorporating the finite element results and DCB measurements into assumed failure criteria, the critical mode II strain energy release rate (G_{IIC}) was computed.

A similar procedure was used to characterize fatigue-induced delamination growth. Constant amplitude fatigue tests on DCB specimens were conducted to derive a power law relationship between delamination growth rate (da/dN) and G_I, for a pure mode I delamination growth. Similar tests on CLS specimens provided mixed mode delamination growth data. Because the fatigue tests were conducted in a displacement-controlled mode, the total strain energy release rate decreased with delamination growth. During the tests, the total strain energy release rate and the delamination size were monitored. The effects of G_I and G_{II} components on mixed mode delamination growth were assumed to be additive. Hence, the power law for a pure mode II delamination growth was derived from CLS test results by subtracting out the contribution due to G_I, as determined using the power law derived from the DCB tests.

Finally, specimens with imbedded through-the-width (ITTW) delaminations were subjected to static compression and constant amplitude compression fatigue loading conditions. Delaminations were imbedded between adjacent 0^o plies and different delamination locations in the thickness direction were considered. The out-of-plane deflection of the delaminated set of plies was monitored during static compression tests. The load corresponding to delamination growth to the tab region, and the load at total failure, were recorded. Delamination growth rates under constant amplitude compression fatigue loading conditions were also measured.

A description of the experimental procedure is presented in Section 2. Results are discussed in Section 3. Conclusions and recommendations are presented in Section 4.

SECTION 2

DETAILS OF THE EXPERIMENTAL PROGRAM

Details of the experimental program and a description of the various tests are presented below:

2.1 TEST MATERIAL

T300/5208 graphite/epoxy was selected to be the test material from which all the specimens were fabricated. The material was purchased in prepreg form to conform to Lockheed specification LAC-C-22-1379/114, with a nominal ply thickness of 0.132 mm (0.0052 in.) in the cured laminate.

Quality control (QC) tests were conducted on the procured material to qualify it for use in the program. Prepreg QC data, shown in Table 1, and $[0]_{16T}$ laminate QC data, shown in Table 2, indicate that the material met purchase specifications. Vendor-supplied data on T300/5208 graphite/epoxy are also presented in Table 3 for comparison.

2.2 FABRICATION OF TEST PANELS

Test panels were fabricated to yield the required number of test specimens for the program. Panels were laid up as specified in fabrication drawings. Imbedded folded Kapton films (0.0254 mm thick unfolded) introduced the desired initial delaminations in the test specimens. Thick laminates were debulked under vacuum in sets of 8 to 12 plies. No bleeder ply was used because of the low resin content (35% by weight uncured) in the T300/5208 prepreg. Test panels were cured in accordance with the following cure cycle:

(1) Apply full vacuum
(2) Heat to 408°K at 1-2°K per minute.
(3) Dwell at 408°K for 45 minutes (starting at 403°K).
(4) Apply 689.5 kPa, venting vacuum at 137.9 kPa.
(5) Heat to 453°K at 1-2°K per minute.

TABLE 1. AVERAGE T300/5208 PREPREG QUALITY CONTROL (QC) DATA

Property	Measurement*	Requirement**
Resin Content (% by weight)	34.7	(34 ± 3)
% Volatiles	0.30	(3.0 maximum)
Areal fiber weight (gm/m^2)	142.5^+	(144 ± 5)
Gel Time	17'30"	
% Flow	8.64	
Tack	Acceptable	

*Tests conducted per Northrop specification number NAI-1371
**Requirements per Lockheed specification number C-22-1379/114, to which the prepreg was purchased.
+Vendor (NARMCO) - supplied data.

TABLE 2. AVERAGE LAMINATE QC DATA ON T300/5208*

Test Type	Property	Measurement
Transverse Tension Tests	Failure stress (MPa)	62.40 (44.8 minimum)**
	Failure strain (μmm/mm)	6680 (4000 minimum)
	Modulus (GPa)	9.65 (9.65 minimum)
Longitudinal Flexure Tests	Failure Stress (MPa)	1630.1 (1448 minimum)
	Modulus (GPa)	132.4 (124.1 minimum)
Short Beam Shear Tests	Shear Strength (MPa)	130.0 (89.6 minimum)

*Tests were conducted on $[0]_{16T}$ laminates.
**Numbers within parentheses are requirements per Lockheed specification number C-22-1379/114 to which the prepreg was purchased.

TABLE 3. AVERAGE VENDOR (NARMCO) DATA ON T300/5208

Resin Content (by weight)	35% (uncured)
Areal Fiber Weight	144 gm/m^2
Volatile Content	0.3%
Flow	14/12%
Gel Time	22'47"
Tack	Acceptable
Specific Gravity	1.59
Fiber Volume	67%
Cured Ply Thickness	0.012954cm (.0051 in.) -8 ply 0.013208cm (.0052 in.) -16 ply
Longitudinal (0^o) Flexural Strength (RT)	2004 MPa (291 ksi)
Longitudinal (0^o) Flexural Modulus (RT)	136.7 GPa (19.83 Msi)
0^o Tensile Strength (RT)	1458 MPa (211.5 ksi)
0^o Tensile Modulus (RT)	146 GPa (21.2 Msi)
0^o Flex. Strength (355°K)	1924 MPa (279 ksi)
0^o Flex. Modulus (355°K)	131.1 GPa (19.02 Msi)
Short Beam Shear Strength (RT)	147.1 MPa (21.34 ksi)
Short Beam Shear Strength (355°K)	130.0 MPa (18.85 ksi)

(6) Cure at 453°K for 120 +10, -0 minutes.

(7) Cool to 350°K under pressure.

Fabricated panels were inspected visually and via ultrasonic through-transmission to ensure acceptable quality. Accepted panels were block-machined and pre-cured tabs were bonded to them secondarily, if required. The tabs contained ten 0° plies of 1581/3203 glass/epoxy, and were bonded to selected blocks using FM73 adhesive. The blocks were subsequently machined to extract the various test specimens.

Layup errors in the initial cracked lap shear test panel were not detected until most of the specimens from this panel were tested. Instead of the specified $[(0_2/\pm45)_s]_s$ layup, which forms symmetric layups on either side of the imbedded delamination (at the midplane), a $[0_2/\pm45_2/0_2]_s$ layup was fabricated. The $[0_2/\pm45_2/0_2]_s$ laminate resulted in unsymmetric layups on either side of the imbedded delamination. Nevertheless, tests on the $[0_2/\pm45_2/0_2]_s$ specimens were completed, and were then repeated on specimens from a $[(0_2/\pm45)_s]_s$ panel that was subsequently fabricated.

2.3 DESCRIPTION OF TEST SPECIMENS

Three types of specimens were tested in the program--double cantilever beam (DCB) specimens, cracked lap shear (CLS) specimens, and specimens with imbedded through-the-width (ITTW) delaminations. Schematic drawings of the three specimens are presented in Figures 1 to 3.

Two 0.51 mm thick aluminum foils were bonded to the DCB specimens using a structural adhesive, along with two 1.27 mm thick aluminum pieces (see Figure 1). Loads were introduced through the flexible aluminum foils, ensuring a pure mode I delamination growth over a length of 76 to 102 mm.

0.51 mm thick stainless steel strips, with large axial stiffness and low bending rigidity, were pin-connected to secondarily bonded aluminum pieces on selected CLS specimens and specimens with ITTW delaminations (see Figures 2, 3). These strips, called flexures, provided constraints against specimen lateral deflection at the locations where they were present. In selected CLS specimens flexures were located in the vicinity of the

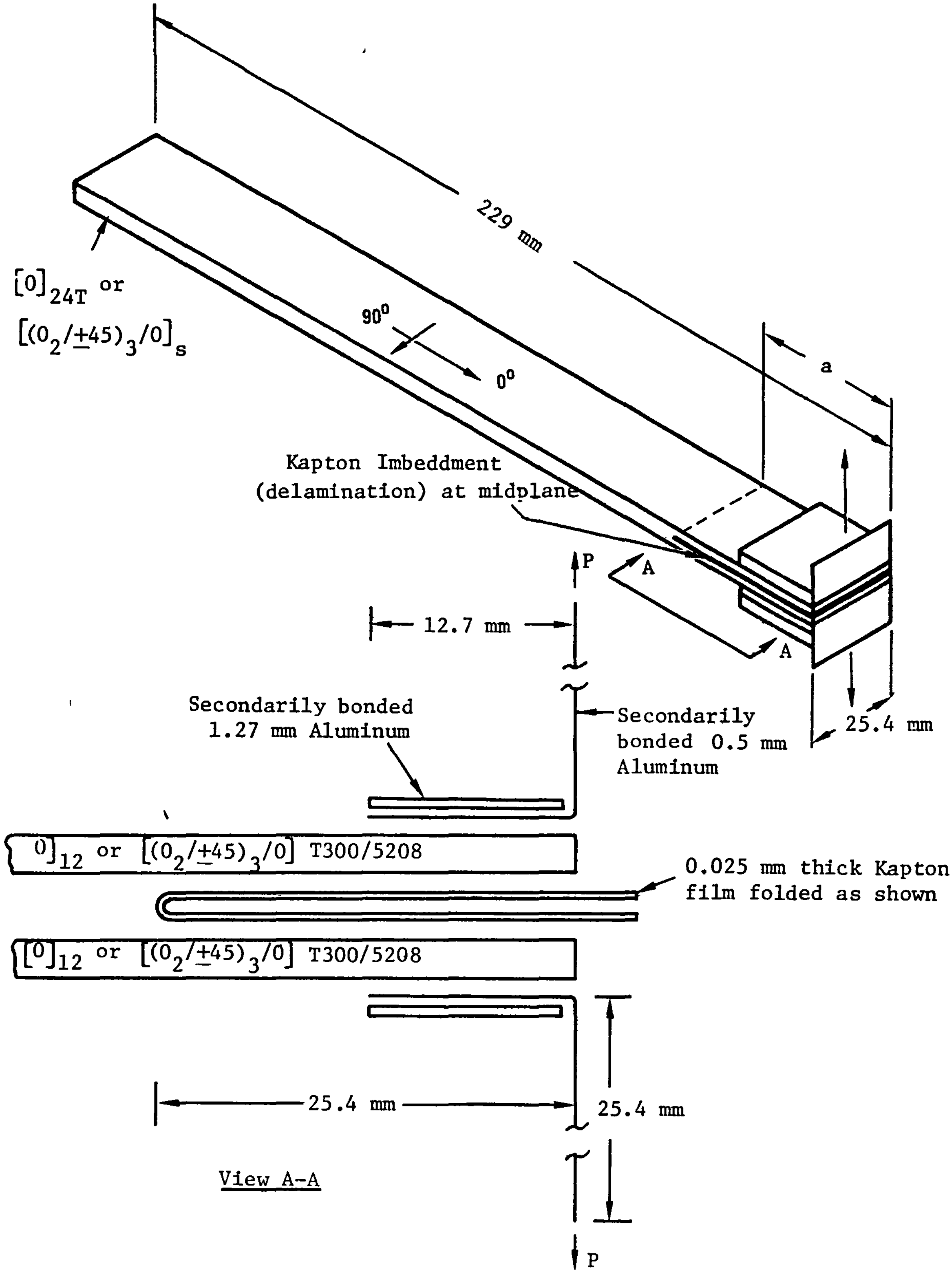

Figure 1. Double Cantilever Beam (DCB) Test Specimen.

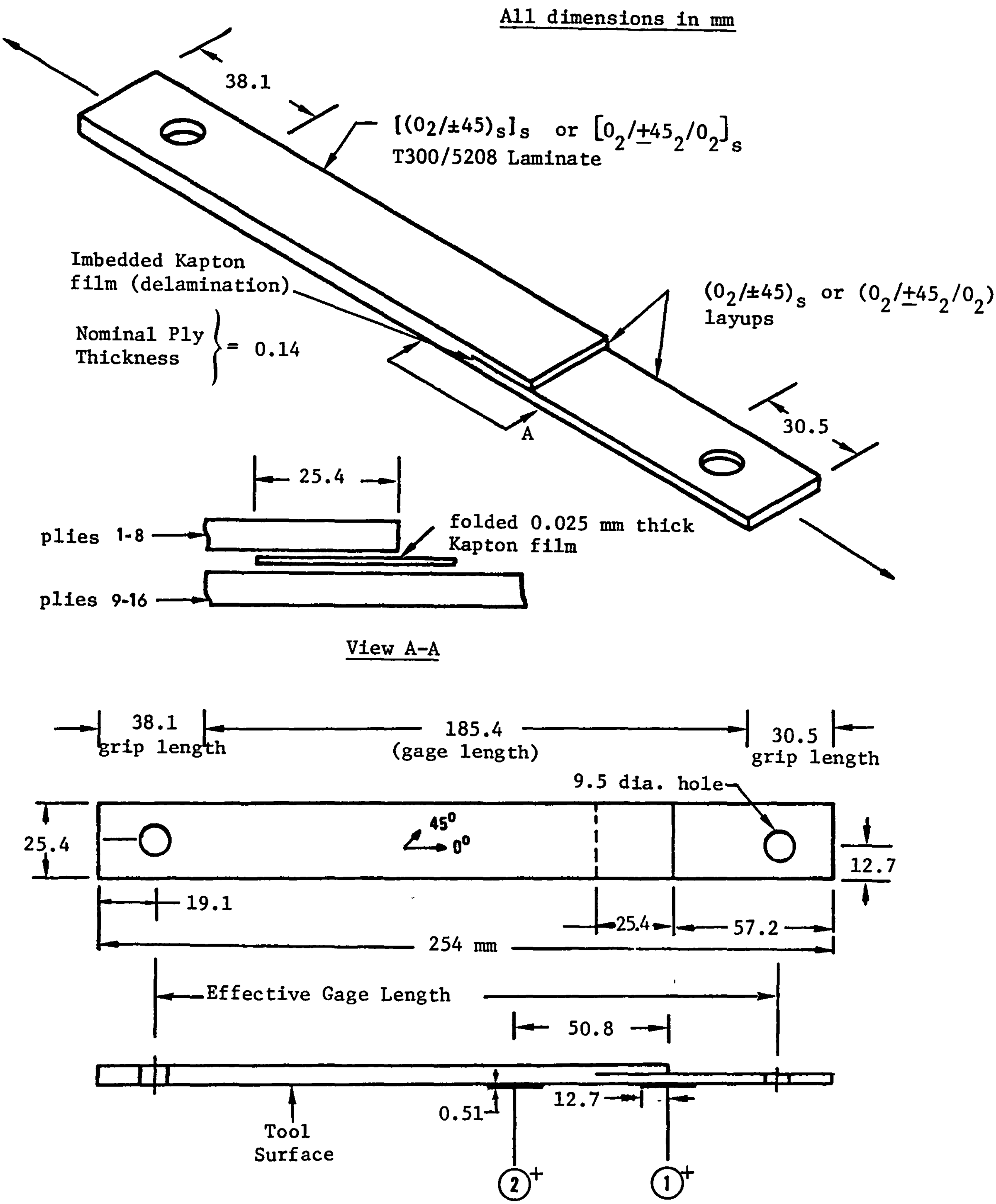

+ (1) and (2) are flexures bonded to the tool surface, 50.8 mm apart, for selected tests.

Figure 2. Details of the Cracked Lap Shear Test Specimen.

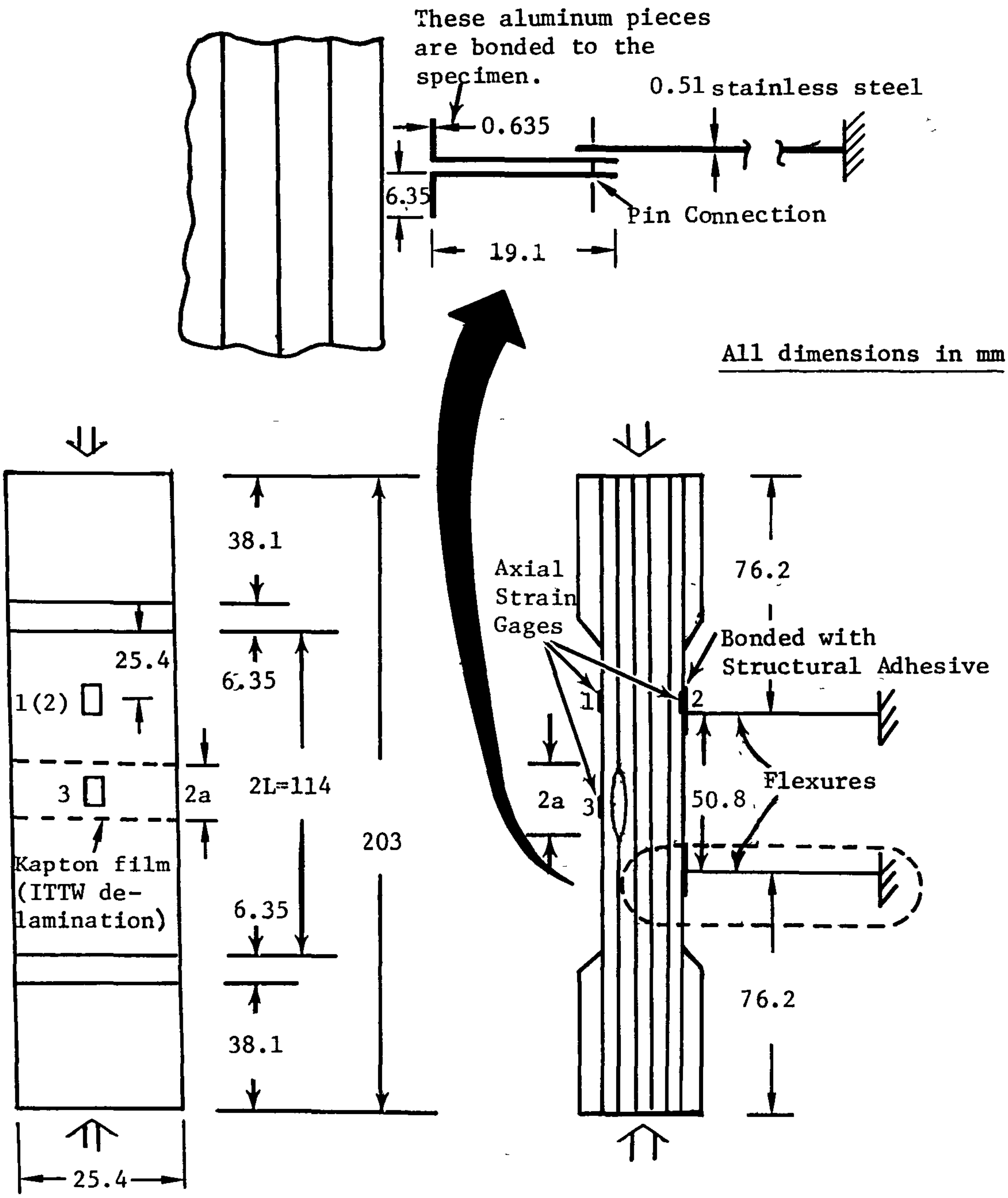

NOTE: Tabs contain ten 0° plies of 1581/3203 glass/epoxy material, and were bonded to the specimen using FM73 adhesive.

Figure 3. Geometry of Test Specimens with ITTW Delaminations.

delaminated step region to constrain possible large rotations. In specimens with ITTW delaminations, the flexures precluded gross (Euler) buckling of the 11.4 cm long test section under compression loading.

Two DCB laminate configurations were tested -- $[0]_{24T}$ and $[(0_2/\pm45)_3/0]_s$. Both layups had a 2.54 cm (1.0 in.) long initial delamination at the midplane (see Figure 1).

Cracked lap shear (CLS) tests were conducted on $[0_2/\pm45_2/0_2]_s$ and $[(0_2/\pm45)_s]_s$ T300/5208 specimens with a 2.54 cm (1 in.) long initial delamination at the step location (see Figure 2). Half of the $[0_2/\pm45_2/0_2]_s$ CLS specimens were provided lateral constraints through flexures on the longer surface, near the step region (see Figure 2).

Three laminate configurations were chosen for tests on specimens with ITTW delaminations: (1) a $[0_4/(0/45/90/-45)_7]_s$ layup with a 1.91 cm (0.75 in.) long delamination between plies 3 and 4 (0/0 interface); (2) a $[0/45_2/0/(0/45/90/-45)_7]_s$ layup with a 2.54 cm (1 in.) long delamination between plies 4 and 5 (0/0 interface); and (3) a $[0/45/90_2/45/0_3/(0/45/90/-45)_6]_s$ layup with a 3.18 cm (1.25 in.) long delamination between plies 6 and 7 (0/0 interface).

2.4 TEST MATRICES

The various tests conducted on DCB specimens are listed in Table 4. Five static and ten constant amplitude fatigue tests were conducted on each laminate configuration. DCB tests were conducted in a displacement-controlled mode to obtain stable delamination growth under static loading. Fatigue tests were conducted at a frequency (ω) of 10 Hertz, with a minimum to maximum cyclic displacement ratio (R) of 0.05.

CLS specimens were subjected to static tension and constant amplitude fatigue loading at ω = 10 Hertz and R = 0.05 as shown in Table 5. CLS tests were also displacement-controlled to obtain stable delamination growth under static loading.

TABLE 4. TESTS ON DOUBLE CANTILEVER BEAM (DCB) SPECIMENS

Test Case	Laminate*	Delamination Between Plies	Loading	No. of Specimens
1	D	12 and 13	Static	5
2	D	12 and 13	Fatigue**	10
3	E	13 and 14	Static	5
4	E	13 and 14	Fatigue**	10

*Laminates D and E had $[0]_{24T}$ and $[(0_2/\pm45)_3/0]_s$ layups, respectively.

**These displacement-controlled tests were conducted at R = 0.05 and ω = 10 Hertz.

TABLE 5. TESTS ON CRACKED LAP SHEAR (CLS) SPECIMENS

Test Case	Laminate	Lateral Supports	Loading	No. of Specimens
5	F	None	Static Tension	4
6	F	None	Tension Fatigue**	11
7	F	Flexures	Static Tension	4
8	F	Flexures	Tension Fatigue**	11
9	H	None	Static Tension	4
10	H	None	Tension Fatigue**	6

*All the laminates had a delamination at the midplane (between plies 8 and 9). A thickness change from 16 plies to 8 plies occurred 2.54 cm (1 in.) from the delamination boundary.

Laminates F and H had $[0_2/\pm45_2/0_2]_s$ and $[(0_2/\pm45)_s]_s$ layups, respectively.

**These were conducted at R = 0.05 and ω = 10 Hertz.

The various tests on specimens with ITTW delaminations are listed in Table 6. Static compression and constant amplitude compression fatigue tests were conducted in a load-controlled mode. Fatigue tests were conducted at ω = 10 Hertz and R = 10. The ratio (S) of the minimum cyclic stress to the static stress at which the ITTW delamination propagated to the tab region was varied to obtain different delamination growth rates.

2.5 DESCRIPTION OF DCB TESTS

DCB tests were conducted in a displacement-controlled mode in the setup shown in Figure 4. Stable delamination growth was achieved by controlling the tip displacement (see Section 3.1). If these tests had been conducted in a load-controlled mode, delamination growth would have been unstable and limited data would have been gathered from each test (see Section 3.1). Prior to mounting the specimen as shown in Figure 4, its free edges were coated with a typewriter correction fluid. After the fluid dried out, fine visible marks were made on these edges, at 2.54 mm (0.10 in.) intervals on either side, to aid in the measurement of the extent of delamination. Prior to recording test data, the DCB specimen was loaded to cause the folded Kapton imbeddment to debond and introduce a sharply defined, visible delamination. The initial delamination length was recorded with the help of a microscope mounted adjacent to the specimen (see Figure 4).

Static tests were initiated at slow crosshead speeds (approximately 0.51 mm/minute) to induce slow delamination growth. The crosshead speed was increased to approximately 5.1 mm/minute when the delamination extended beyond 76.2 mm. The load (P) corresponding to the applied displacement (δ) was also monitored. P increased linearly with δ when the delamination length (a) remained constant. This continued until a critical value (P_{cr}, δ_{cr}) was reached. When the tip displacement exceeded δ_{cr}, a delamination growth (Δa) was observed, accompanied by a reduction in the load from the P_{cr} value (Section 3.1). The applied displacement was increased until the delamination growth was observed to be 1.27 cm (0.5 in). The applied displacement was then decreased until a zero load reading was observed. It should be noted that a zero load reading did not correspond

TABLE 6. TESTS ON COUPONS WITH IMBEDDED THROUGH-THE-WIDTH (ITTW) DELAMINATIONS

Test Series	Laminate	N_D^*	$2a^*$ mm (in.)	Load Type++	S^*	No. of Specimens
11	A	3	19.1 (0.75)	SC	---	4
12	A	3	19.1 (0.75)	CF	0.41, 0.46	10
13	B	4	25.4 (1.00)	SC	---	4
14	B	4	25.4 (1.00)	CF	0.67	6
15	C	6	31.8 (1.25)	SC	---	4
16	C	6	31.8 (1.25)	CF	0.75	6

+ A, B and C are 64-ply, T300/5208 laminates with $[0_4/(0/45/90/-45)_7]_s$, $[0/45_2/0/(0/45/90/-45)_7]_s$, and $[0/45/90_2/45/0_3/(0/45/90/-45)_6]_s$ layups, respectively.

++SC denotes static compression
CF denotes constant amplitude, compression fatigue loading at ω = 10 Hertz and R = 10.

*N_D is the number of plies that are delaminated (smaller number)

2a is the initial length of the through-the-width delamination.

S is the ratio of the minimum cyclic stress to the static strength.

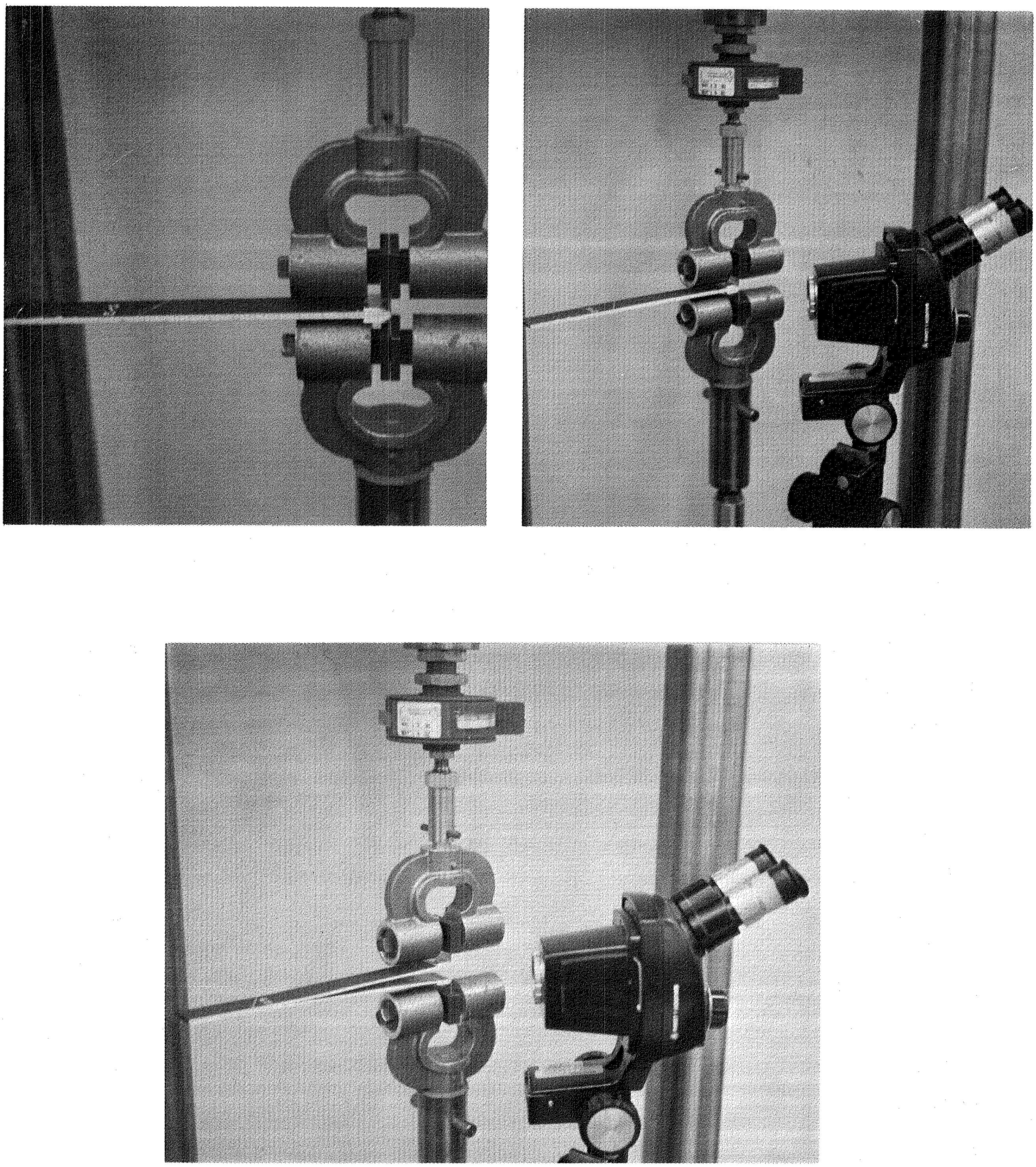

Figure 4. Double Cantilever Beam Test Setup.

to a zero displacement reading (Section 3.1). This has been observed by other investigators (Reference 15). The loading/unloading procedure was repeated for every 1.27 cm (0.5 in.) growth of delamination. The slopes of the load-deflection plots indicated an increase in compliance with an increase in delamination size. The critical load and deflection values, and the compliance measurements corresponding to delamination sizes that were 1.27 cm (0.5 in.) apart, were recorded during each static test. Plots of critical loads and compliances as a function of the delamination size were obtained, and the slopes of the curves were used to compute G_{IC}, the mode I critical strain energy release rate. The computational procedure is explained in Section 3.

Constant amplitude fatigue tests on DCB specimens were conducted at ω = 10 Hertz and R = 0.05. Based on the static test data, the maximum cyclic displacement value was selected to cause a desired initial rate of delamination growth. Fatigue test specimens had their free edges marked at 2.54 mm (0.1 in.) intervals. A microscope was used to monitor delamination growth (see Figure 4). Since the tests were displacement-controlled, delamination growth rates reduced significantly as the delamination propagated in a stable manner. The slowest rate monitored corresponded to 250,000 cycles for a delamination growth of 1.27 cm (0.5 in.). Consequently, the maximum cyclic displacement was increased after each 12.7 mm delamination growth was measured. In a limited number of specimens, the initial displacement amplitude was unaltered and delamination growth was monitored for approximately 1.5 million cycles. Denoting delamination growth rate by da/dN, its variation with delamination size (a) was obtained for each applied maximum displacement level. Using available static test data, these were converted to da/dN versus G_I plots that are conventional delamination growth rate records.

2.6 DESCRIPTION OF CLS TESTS

Static tension and constant amplitude tension fatigue tests were conducted on $[0_2/\pm45_2/0_2]_s$ and $[(0_2/\pm45)_s]_s$ CLS specimens. Half of the $[0_2/\pm45_2/0_2]_s$ specimens were constrained laterally by flexures at two locations (see Figure 5). The remaining specimens were laterally

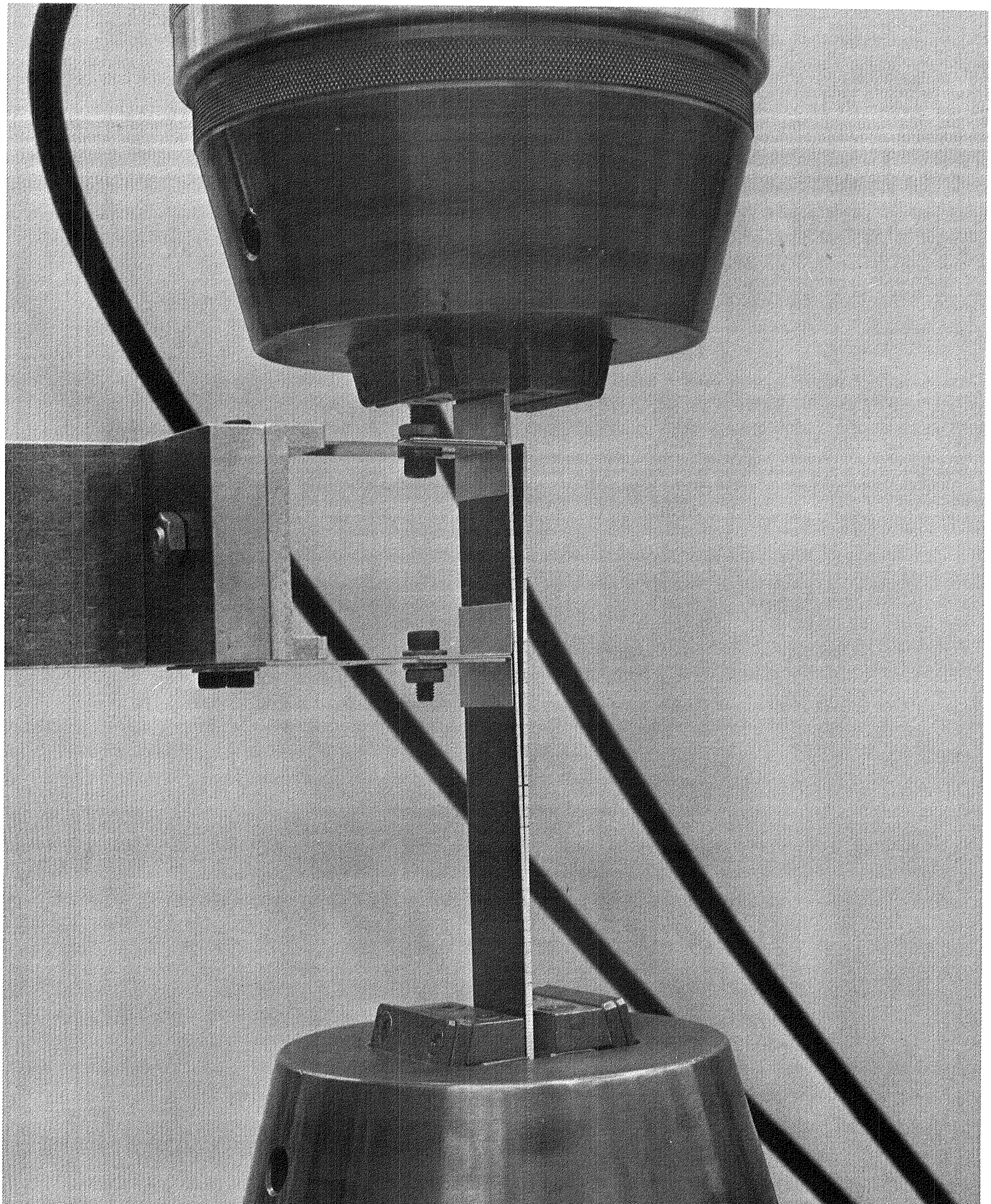

Figure 5. Cracked Lap Shear Test Setup Showing a Laterally Constrained $[0_2/\pm45_2/0_2]_s$ Specimen.

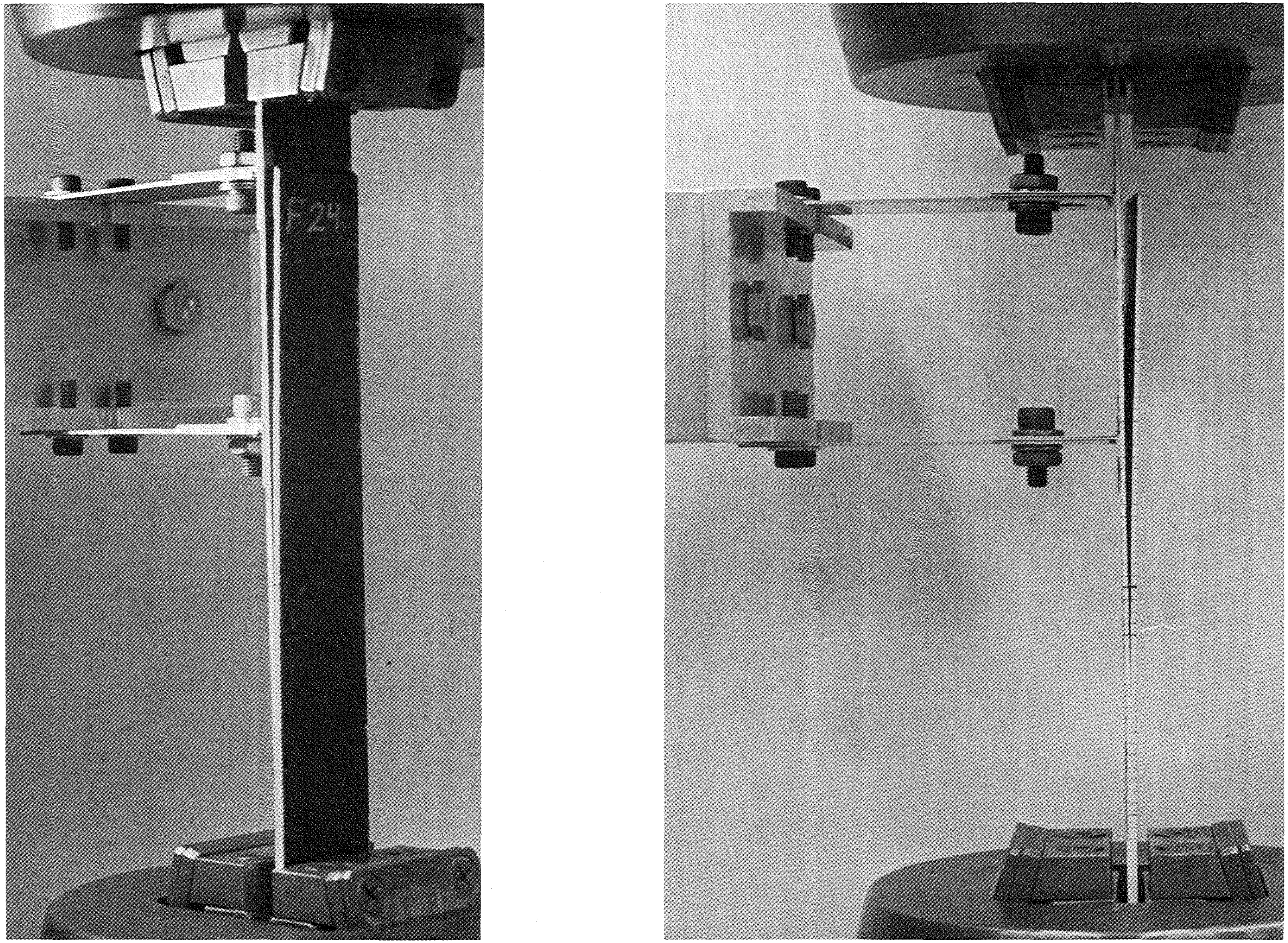

Figure 5. Cracked Lap Shear Test Setup Showing a Laterally Constrained $[0_2/\pm45_2/0_2]_s$ Specimen (Concluded).

unconstrained during testing. Photographs of an unconstrained $[(0_2/\pm45)_s]_s$ CLS specimen in the test fixture are presented in Figure 6.

The applied displacements on $[0_2/\pm45_2/0_2]_s$ specimens corresponded to the relative displacement of one grip fixture (attached to the loading cylinder) with respect to the other. As explained later (Section 3.3), the recorded stroke (displacement) was effectively between the centers of the holes at either end of the specimen (See Figure 2). Therefore, the effective gage length for the $[0_2/\pm45_2/0_2]_s$ CLS specimen was 21.6 cm (8.5 in.). The $[(0_2/\pm45)_s]_s$ specimens, on the other hand, had extensometers mounted on them (see Figure 6). The extensometer gage length was chosen to be large enough (14 cm or 5.5 in.) to record useful compliance measurements until the imbedded delamination propagated over approximately 10 cm (see Figure 7).

Static tension tests on CLS specimens were conducted in a displacement-controlled mode to ensure stable delamination growth (see Section 3.3). Prior to testing, specimen edges were marked to monitor delamination growth (see Section 2.5). The applied displacement was increased slowly, and the corresponding load varied linearly with displacement until the delamination started to propagate. Delamination growth occurred only along the imbeddment 0/0 interface (see Figure 8), and was accompanied by an unloading (see Section 3.3). The applied displacement was slowly increased during this propagation phase until a 1.27 cm (0.5 in.) delamination growth was recorded. At this point, the applied displacement was reduced until a zero load reading was obtained. This procedure was repeated for every 1.27 cm (0.5 in.) growth of the delamination, and the corresponding critical load, critical deflection and compliance measurements were recorded. These data were used, as explained in Section 3, to compute the critical total strain energy release rate (G_C) for the CLS specimen.

Constant amplitude tension fatigue tests on CLS specimens were conducted in a displacement-controlled mode at ω = 10 Hertz and R = 0.05 (see Table 5). The maximum cyclic displacement was selected, based on static test data, to induce delamination growth rates that were large (10 to 60 mm growth in 1000 cycles) at the beginning. As the delami-

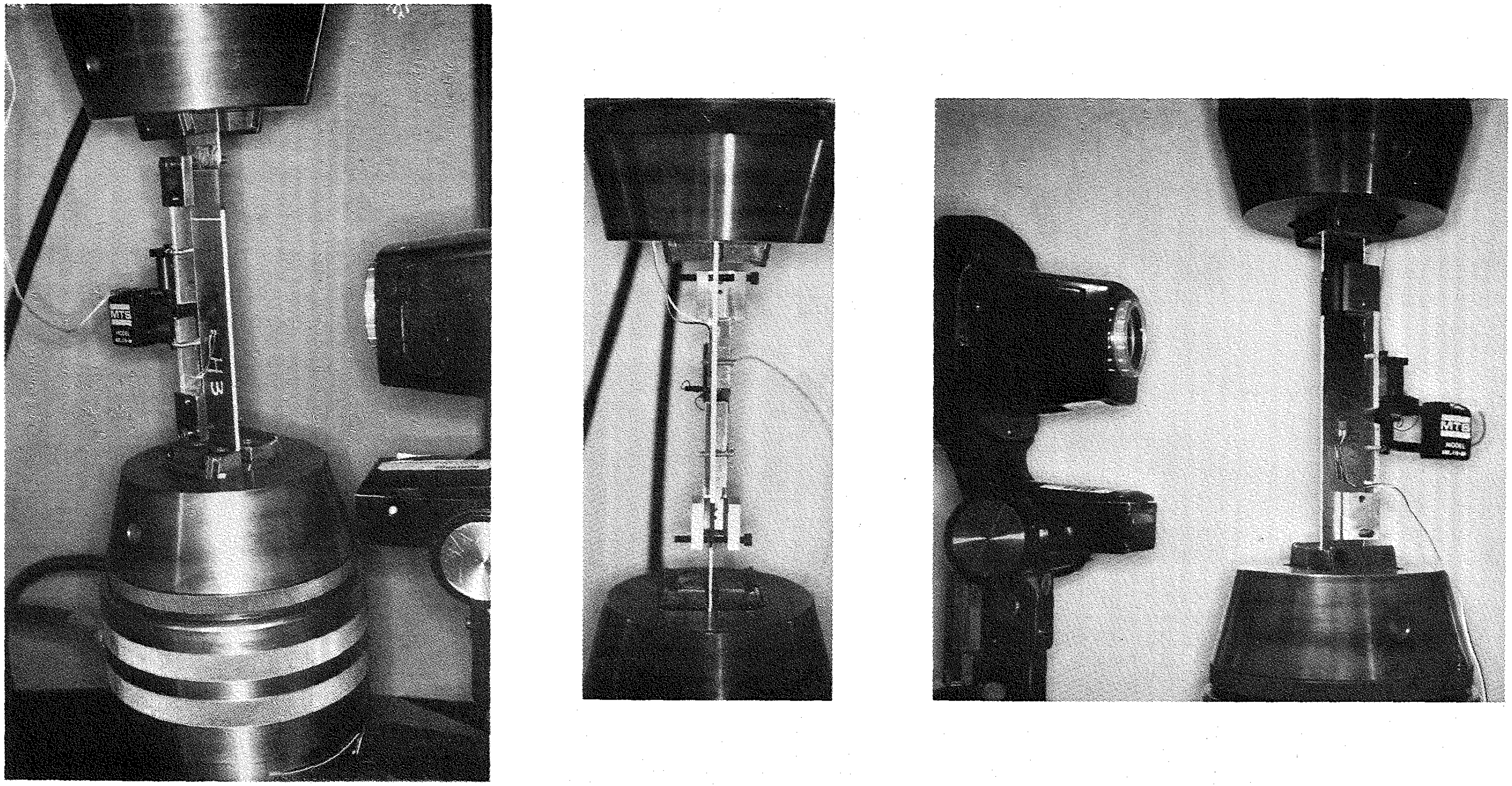

Figure 6. Cracked Lap Shear Test Setup, Showing a Laterally Unconstrained $[(0_2/\pm 45)_s]_s$ Specimen.

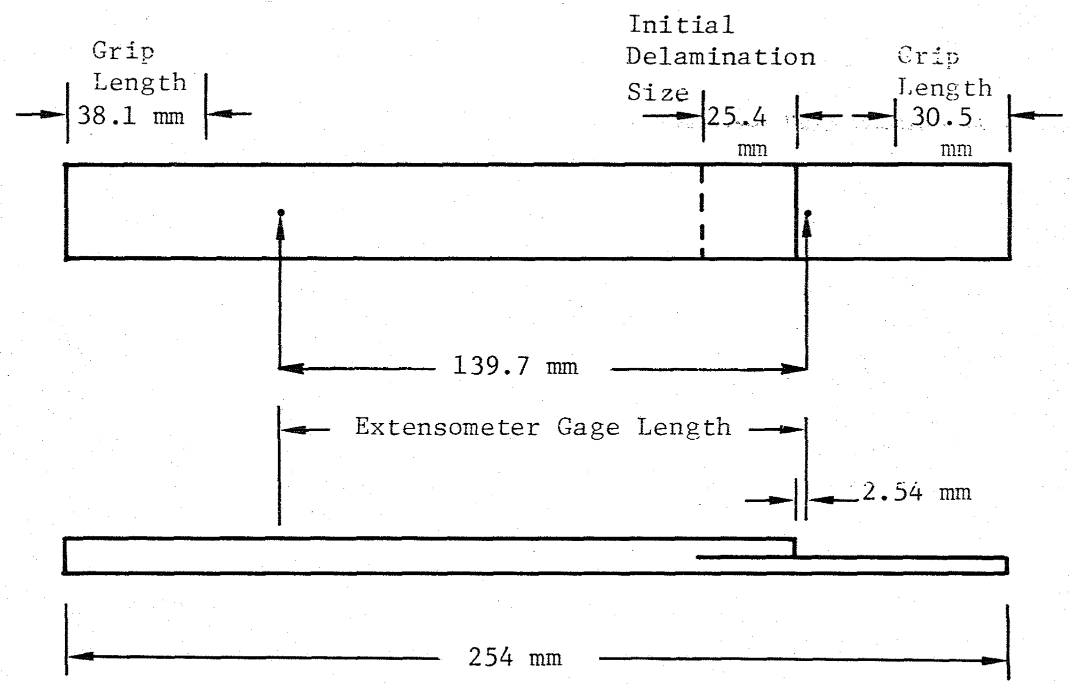

Figure 7. Extensometer Locations on the $[(0_2/\pm45)_s]_s$ CLS Test Specimens.

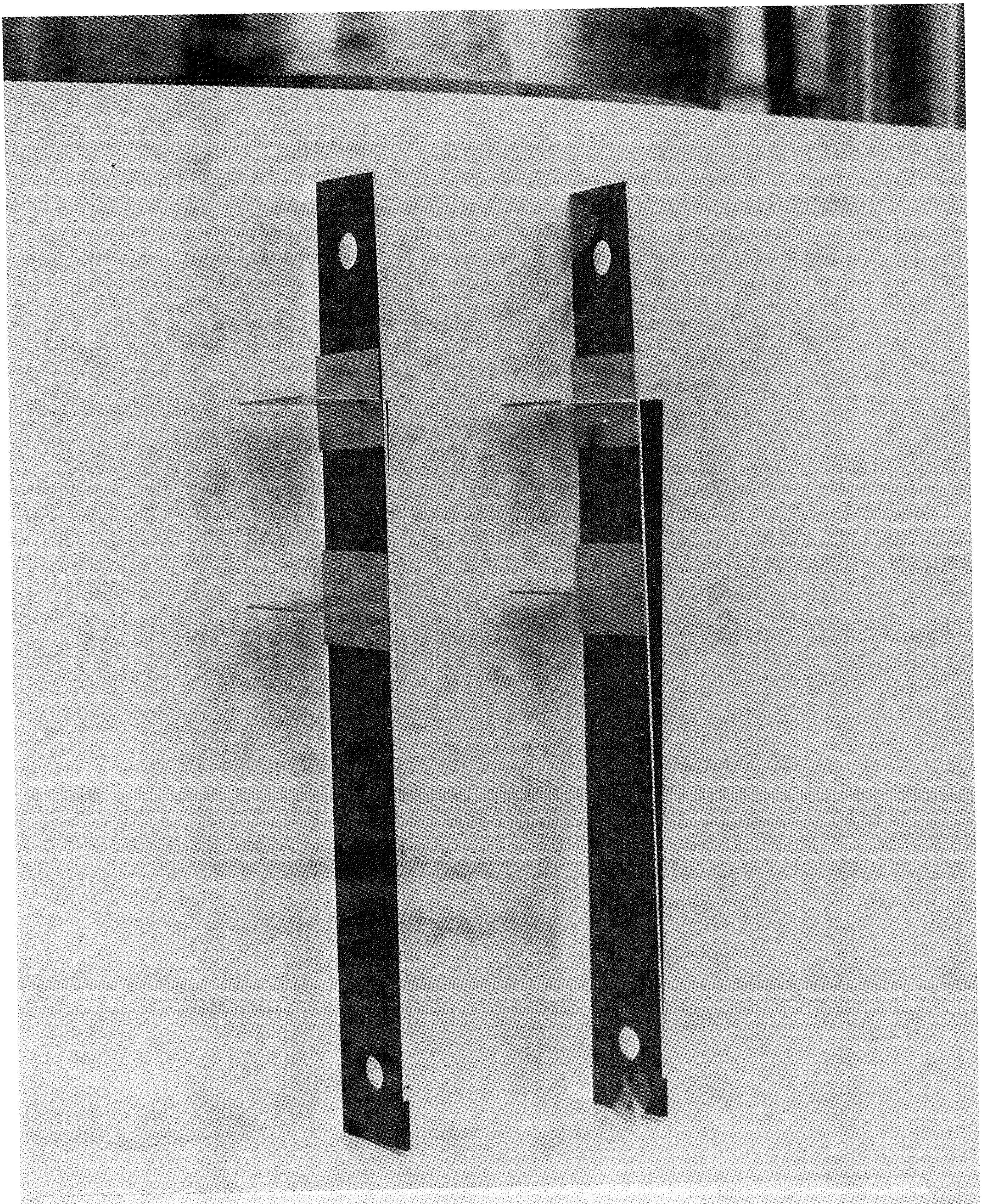

Figure 8. Photographs Showing Delamination Growth Along the Imbeddment 0/0 Interface In $[0_2/\pm45_2/0_2]_s$ CLS Specimens.

nation propagated in a stable manner, its growth rate reduced sharply. In most of the tests, the maximum cyclic displacement was increased after every 12.7 mm delamination growth to reset the growth rate to be large. A few specimens were tested for approximately 1.5 million cycles without altering the maximum cyclic displacement to obtain slow growth rate data.

2.7 DESCRIPTION OF TESTS ON SPECIMENS WITH ITTW DELAMINATIONS

Table 6 lists the various tests--static compression and constant amplitude compression fatigue tests--that were conducted on specimens with ITTW delaminations (see Figure 3). Figure 9 presents the static compression test setup for these specimens, showing how the flexures provide antibuckling constraints. The compression fatigue test setup is shown in Figure 10. During fatigue testing, a microscope was mounted adjacent to the test specimen to monitor delamination growth.

Four static compression tests were conducted on each laminate (Table 6). Three strain gages were bonded to selected specimens (one out of four) to monitor the strain level at which local instability occurred. These gages included back-to-back axial gages located 2.54 cm (1 in.) from the tab edge, and an axial gage centrally located over the delaminated set of plies (Figure 3). During the static tests, the central lateral deflection on the specimen surface closest to the delaminated interface was monitored using a dial indicator. The applied load levels corresponding to delamination failure and total failure were recorded. Delamination failure was defined as the propagation of the imbedded delamination to the tab edge (boundary of the bevelled region). Total failure occurred when other delaminations followed the imbedded delamination, in quick succession, from the outer surface toward the midplane, drastically reducing the load-carrying capacity of the specimen. Static compression loads were introduced slowly and were periodically held constant while the corresponding central lateral deflection and delamination growth, if any, were measured.

Constant amplitude compression fatigue tests on specimens with ITTW delaminations were conducted at ω = 10 Hertz and R = 10. The two free edges of the specimens were coated with a typewriter correction fluid

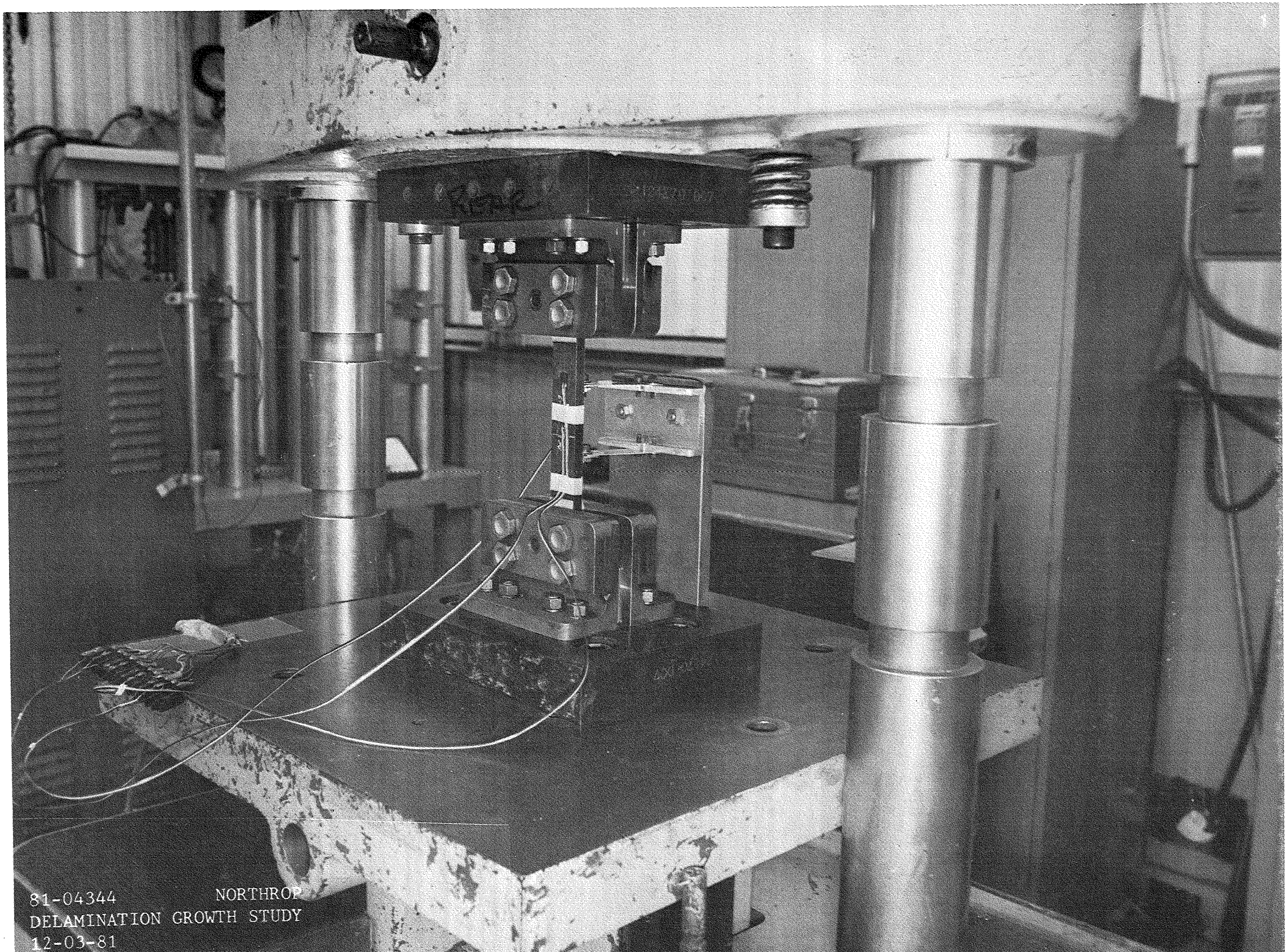

Figure 9. Static Compression Test Setup for Specimens With ITTW Delaminations.

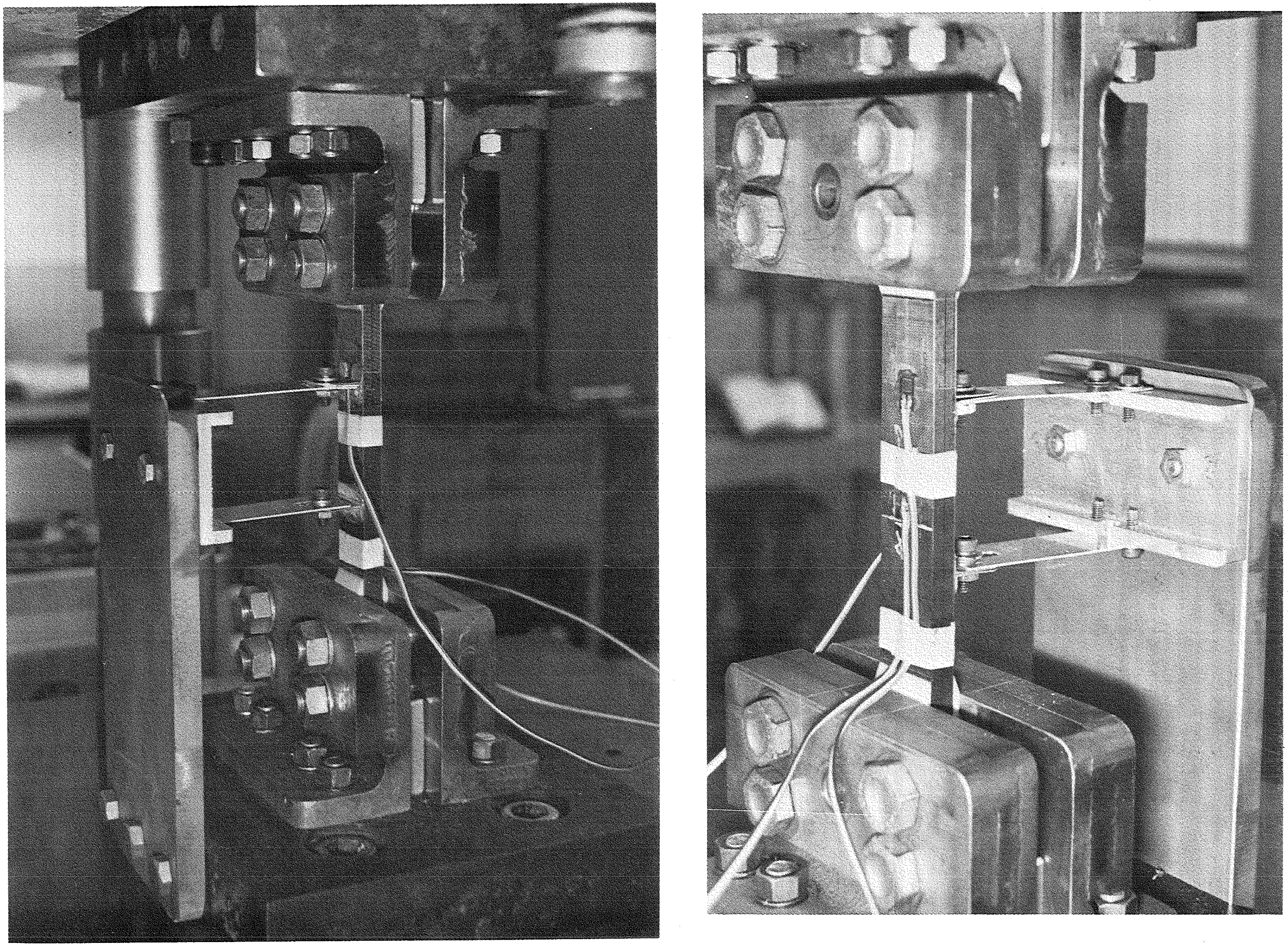

Figure 9. Static Compression Test Setup for Specimens with ITTW Delaminations. (Concluded)

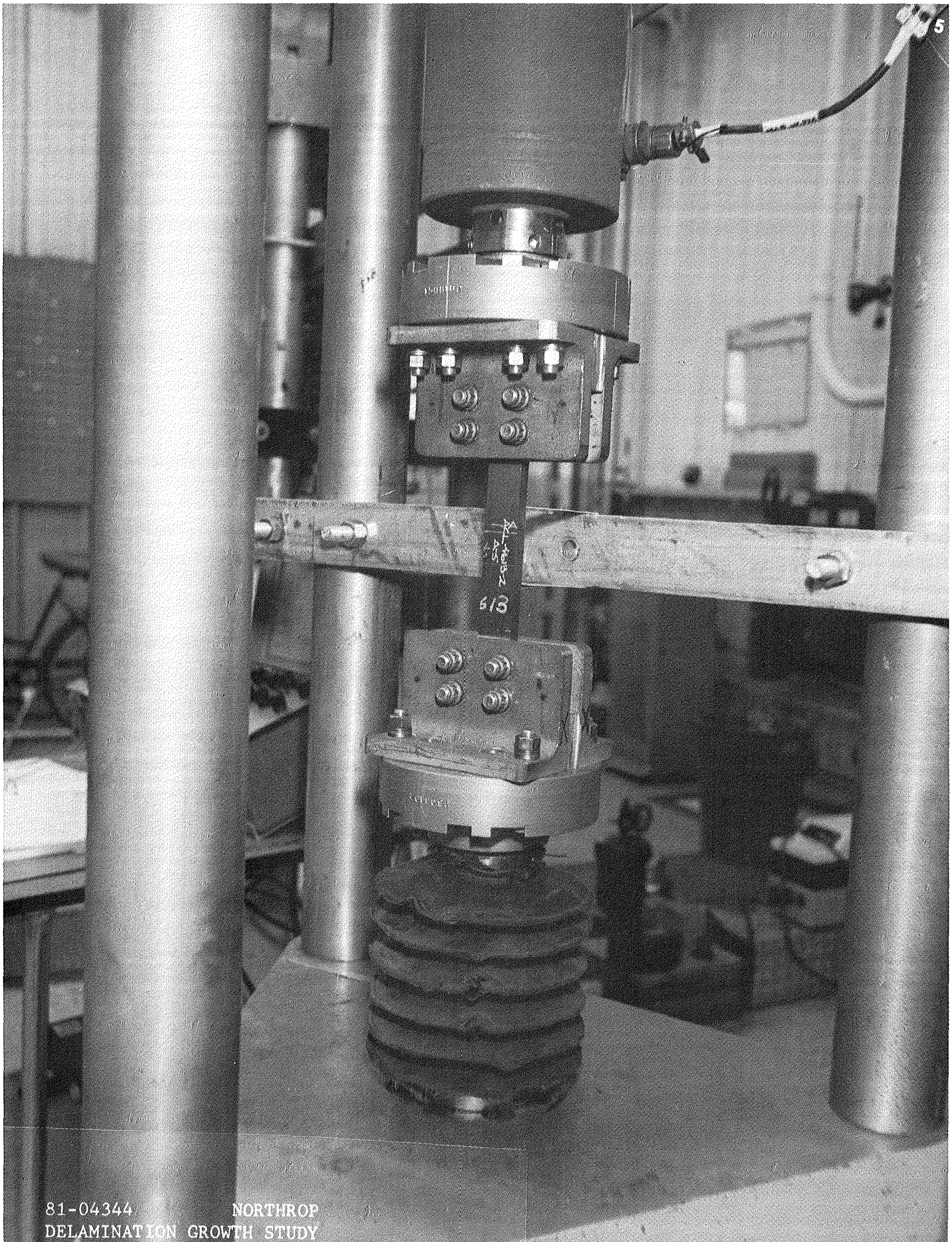

Figure 10. Compression Fatigue Test Setup For Specimens With ITTW Delaminations.

and marked at 6.35 mm (0.25 in.) intervals. A microscope was mounted adjacent to the specimen to monitor upward and downward delamination growth, as seen from either free edge. That is, the movement of two points on each edge was monitored. Cyclic loading was interrupted periodically to measure delamination growth.

Prior to recording fatigue test data, the specimens were cycled, at a load amplitude below the static delamination failure load, to "release" the Kapton inclusion and create a well-defined delaminated region. In laminates B and C, with delamination imbeddments below 4 and 6 plies, respectively, this posed a problem. The ITTW delamination propagated to the tab region when it was "released", resulting in a delamination failure. To preclude this, the remaining specimens were clamped tightly over a 31.8 mm (1.25 in.) length from the tab boundary, on either side, during the "releasing" phase of the test (see Figure 11). The clamps were removed at zero load after the "release" sound was heard. This procedure was only partially successful in preventing delamination failure prior to initiating the fatigue tests on laminates B and C.

The minimum cyclic load was selected to be a fraction (S) of the static strength corresponding to delamination failure (not total failure). Cycling was interrupted periodically to monitor delamination growth. Fatigue failure was assumed to occur when the ITTW delamination propagated to the tab region (delamination failure).

All dimensions in mm.

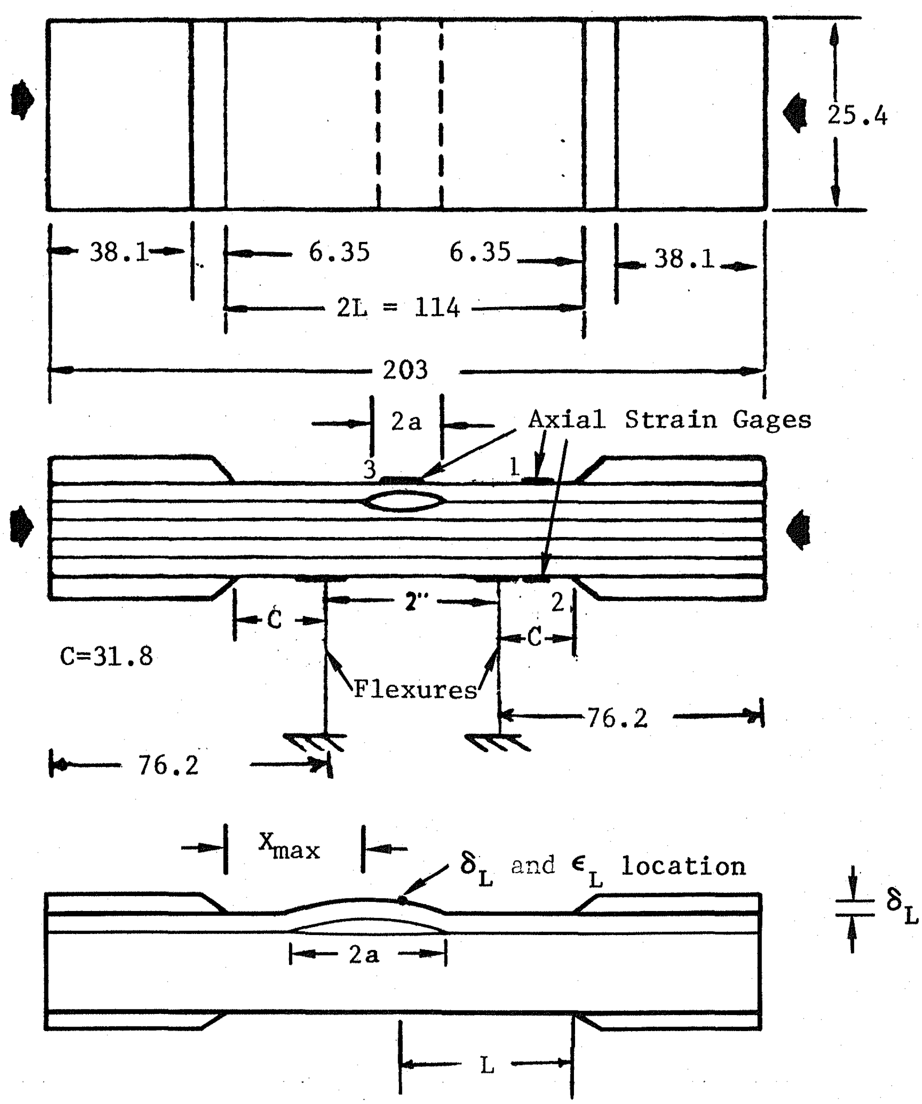

Laminates B and C were clamped over the region marked "C" in the figure prior to initiating fatigue tests. In this state, a low frequency high amplitude load was introduced to "free" the Kapton inclusion within the 51 mm length.

Figure 11. Measurement Locations on Specimens With ITTW Delaminations.

SECTION 3

DISCUSSION OF RESULTS

3.1 STATIC DCB TEST RESULTS

Static double cantilever beam (DCB) tests were conducted to compute the critical strain energy release rate (G_{IC}) for a pure mode I delamination growth in T300/5208 laminates. These displacement - controlled tests produced load-displacement (P versus δ) curves similar to those in Figures 12 and 13. At the onset of delamination growth, the load and the total opening displacement are referred to as P_{cr} and δ_{cr}. The total compliance of the DCB specimen ($C = \delta/P$), P_{cr} and δ_{cr} were obtained from figures similar to those in Figures 12 and 13, and recorded as a function of the delamination length (a). Using the measured C and P_{cr} variations with a, G_{IC} for T300/5208 laminates can be computed using:

$$G_{IC} = P_{cr}^2 \; (dC/da)/(2w) \tag{1}$$

where w is the width of the DCB specimen (25.4 mm). If P_{cr} is replaced by P, G_{IC} becomes G_I, the mode I strain energy release rate corresponding to the load P.

The advantage gained by conducting the tests in a displacement-controlled mode may be understood by invoking a strength of materials expression for the total compliance (C) of the DCB specimen:

$$C = \delta/P = 2a^3/(3D_x) \tag{2}$$

where D_x is the longitudinal flexural stiffness of the delaminated set of plies, assuming bending about its transverse centroidal axis. The expression in equation (2) assumes a clamped condition at the delamination boundary. The validity of this assumption is subsequently discussed. Taking the derivative of C with respect to the delamination length (a),

$$dC/da = 2a^2/D_x \tag{3}$$

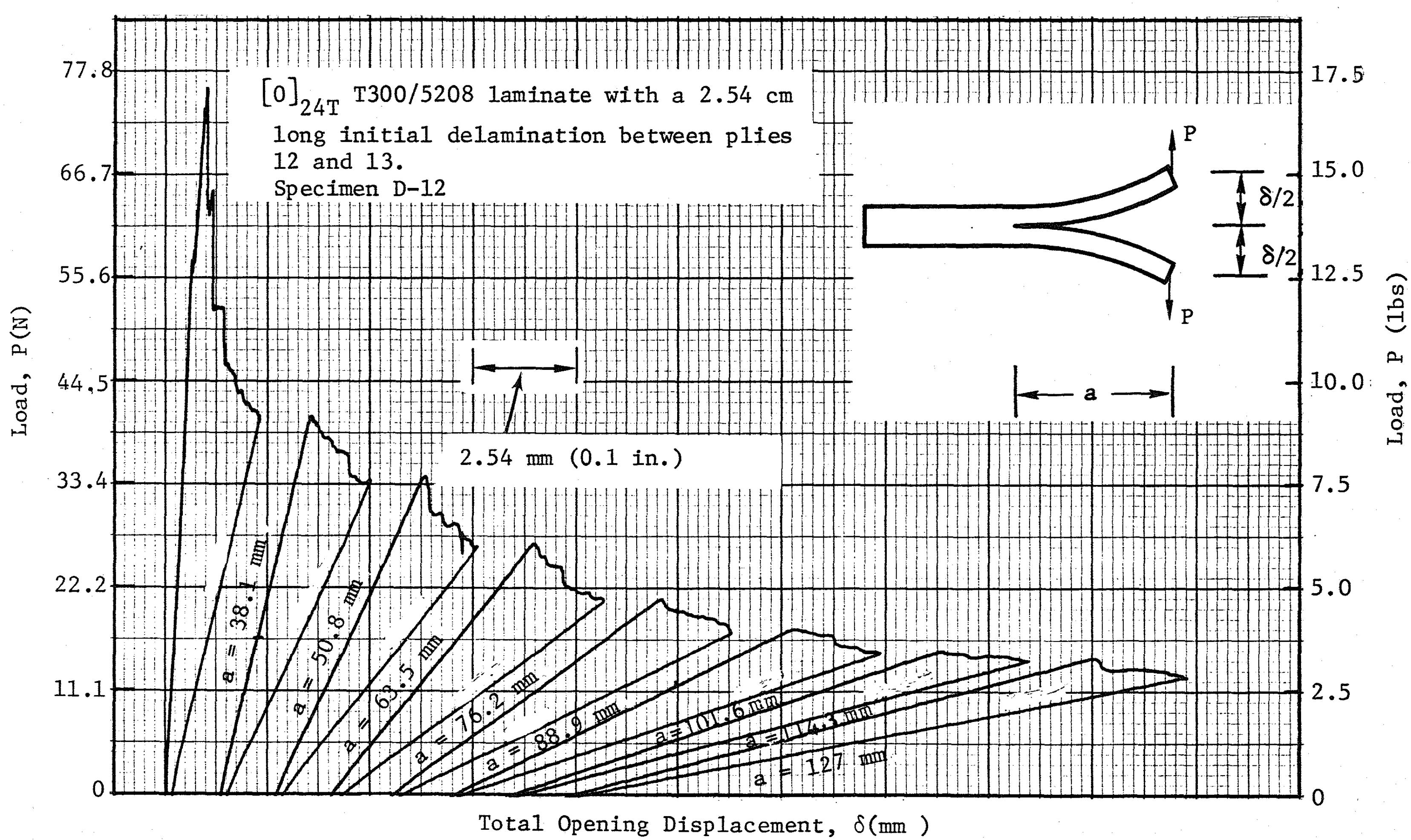

Figure 12. A Typical Load-Deflection Plot From a Static DCB Test on a $[0]_{24T}$ Specimen.

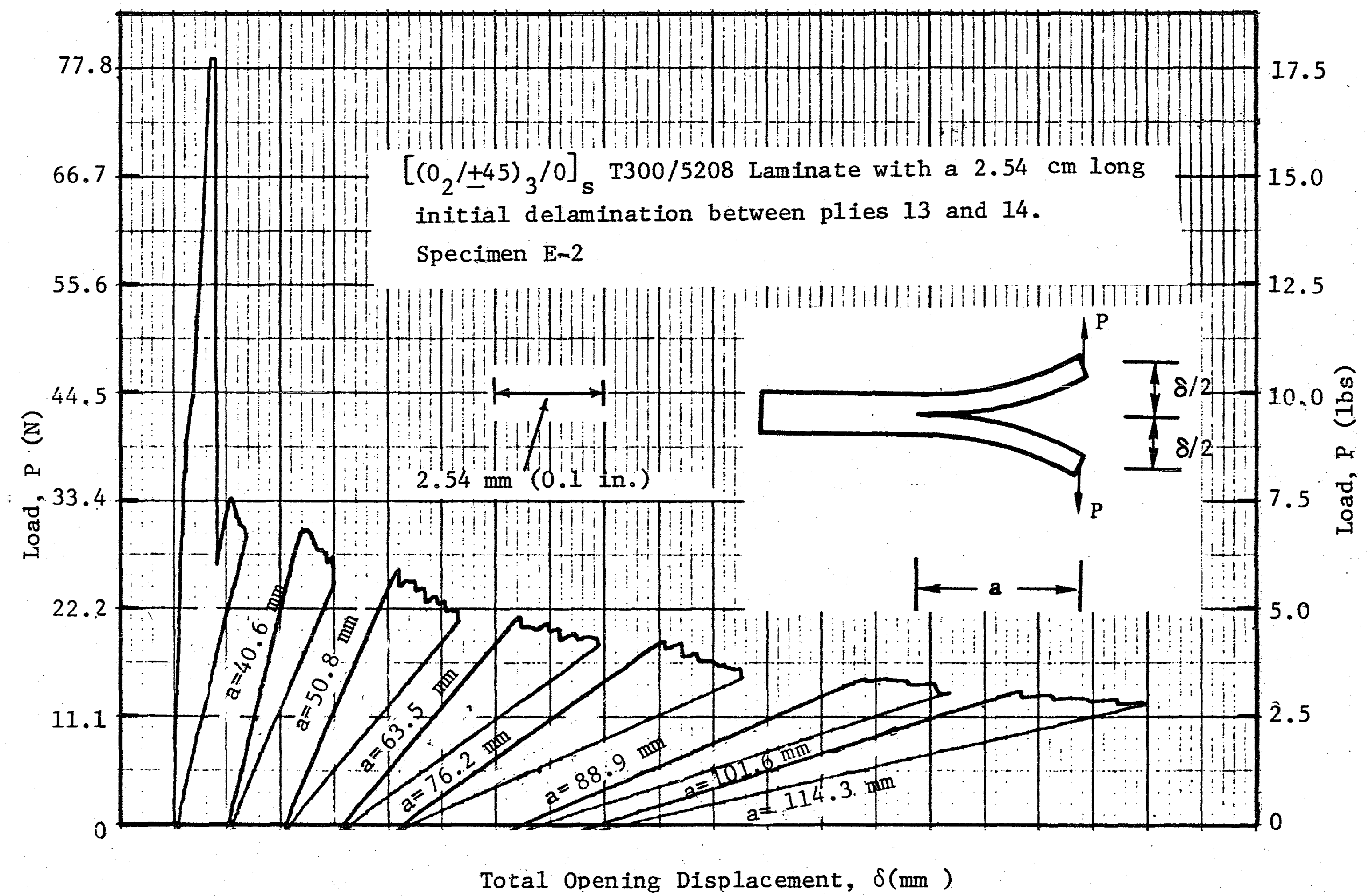

Figure 13. A Typical Load-Deflection Plot Obtained From a Static DCB Test on a $[(0_2/\pm45)_3/0]_s$ Specimen.

It is seen that dC/da increases with a. Since G_{IC} is a material constant (by hypothesis), it is inferred from equation (1) that P_{cr} will decrease when a increases (see Figures 12 and 13). Therefore, if the tests were load-controlled, an unstable growth of the delamination will result at the P_{cr} value corresponding to the initial delamination length. If the tests were displacement-controlled, substituting $C = \delta_{cr}/P_{cr}$ and equations (2) and (3) into equation (1), it is seen that

$$\left.\begin{aligned} G_{IC} &= \delta_{cr}^2 \, (dC/da)/(2wC^2) \\ \text{or } G_{IC} &\;\alpha\; \delta_{cr}^2/a^4 \end{aligned}\right\} \quad (4)$$

Since G_{IC} is a material constant, δ_{cr} will increase with delamination growth (a). Therefore, a stable delamination growth can be achieved by conducting the tests in a displacement-controlled mode.

Static DCB test results from figures similar to those in Figures 12 and 13 yielded critical loads and compliances that varied with delamination size as shown in Figures 14 and 15. The presented plots are on a logarithmic scale, and linear approximations to the plotted data were obtained. The data in Figures 14 and 15 are averages of all the respective static test data. The measured compliances were subsequently compared with strength of materials predictions (equation 2) to assess the validity of the assumed clamped constraint conditions at the delamination boundary in equation (2). Assuming a to be expressed in mm, and E_{11} = 137.9 GPa (20 Msi), E_{22} = 14.5 GPa (2.1 Msi), ν_{12} = 0.21, G_{12} = 5.9 GPa (0.85 Msi), and the nominal cured ply thickness = 0.014 cm (0.0055 in) for T300/5208 graphite/epoxy, equation (2) yielded:

$$\left.\begin{aligned} C &= 0.4850 \text{ X } 10^{-6}\ a^3 \text{ mm/N for the } [0]_{24T} \text{ specimen, and} \\ C &= 0.6133 \text{ X } 10^{-6}\ a^3 \text{ mm/N for the } [(0_2/\pm45)_3/0]_s \text{ specimen} \end{aligned}\right\} \quad (5)$$

Referring to Figures 14 and 15, the measured compliances are seen to be:

$$\left.\begin{aligned} C &= 0.6705 \text{ X } 10^{-6}\ a^3 \text{ mm/N for the } [0]_{24T} \text{ specimen, and} \\ C &= 0.8494 \text{ X } 10^{-6}\ a^3 \text{ mm/N for the } [(0_2/\pm45)_3/0]_s \text{ specimens} \end{aligned}\right\} \quad (6)$$

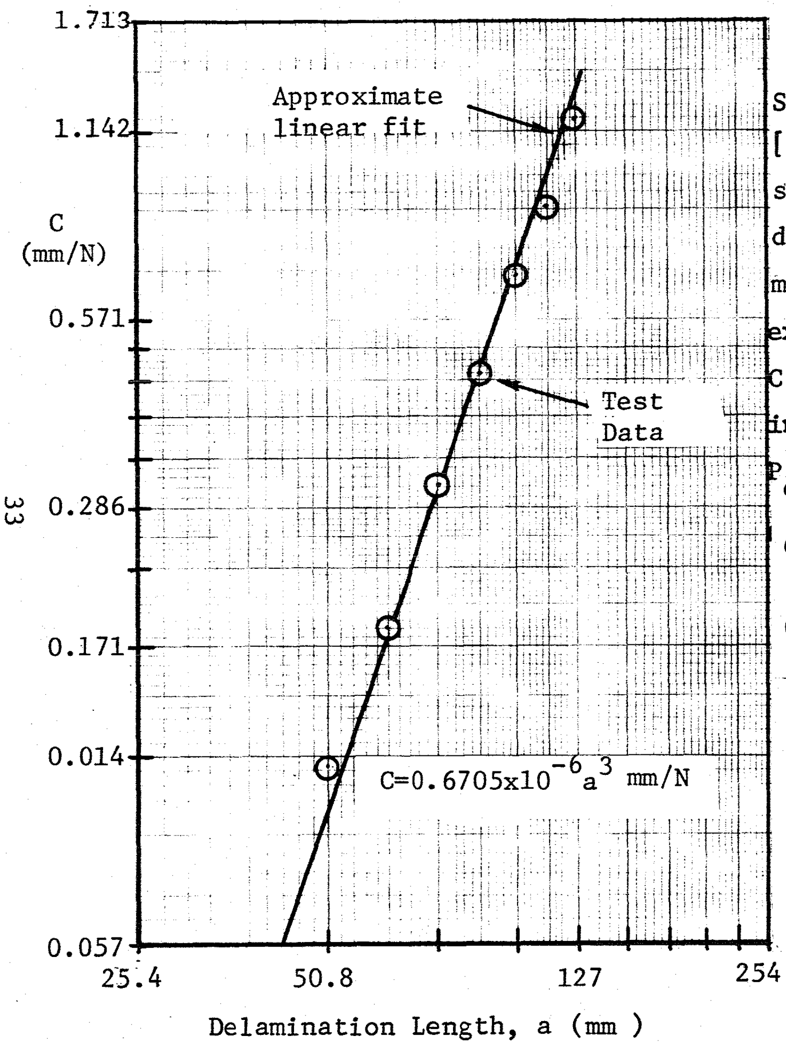

Static DCB tests on $[0]_{24T}$ T300/5208 specimens with a delamination at the midplane. If a is expressed in mm , C in mm/N and P_{cr} in N, $C=0.6705\times10^{-6}a^3$

$P_{cr}=1610.0\ a^{-1}$

$$G_{IC} = \frac{P_{cr}^2\ (dC/da)}{2w}$$

$$G_{IC} = 102.6\ J/m^2$$

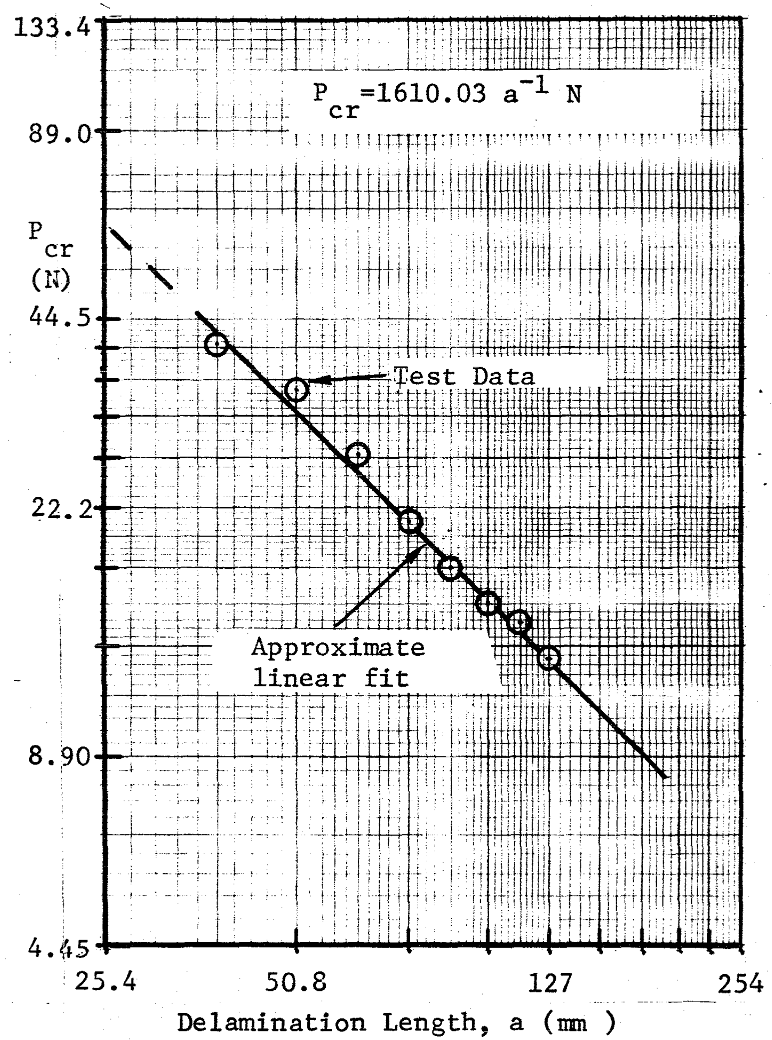

Figure 14. Static DCB Test Data From $[0]_{24T}$ T300/5208 Specimens.

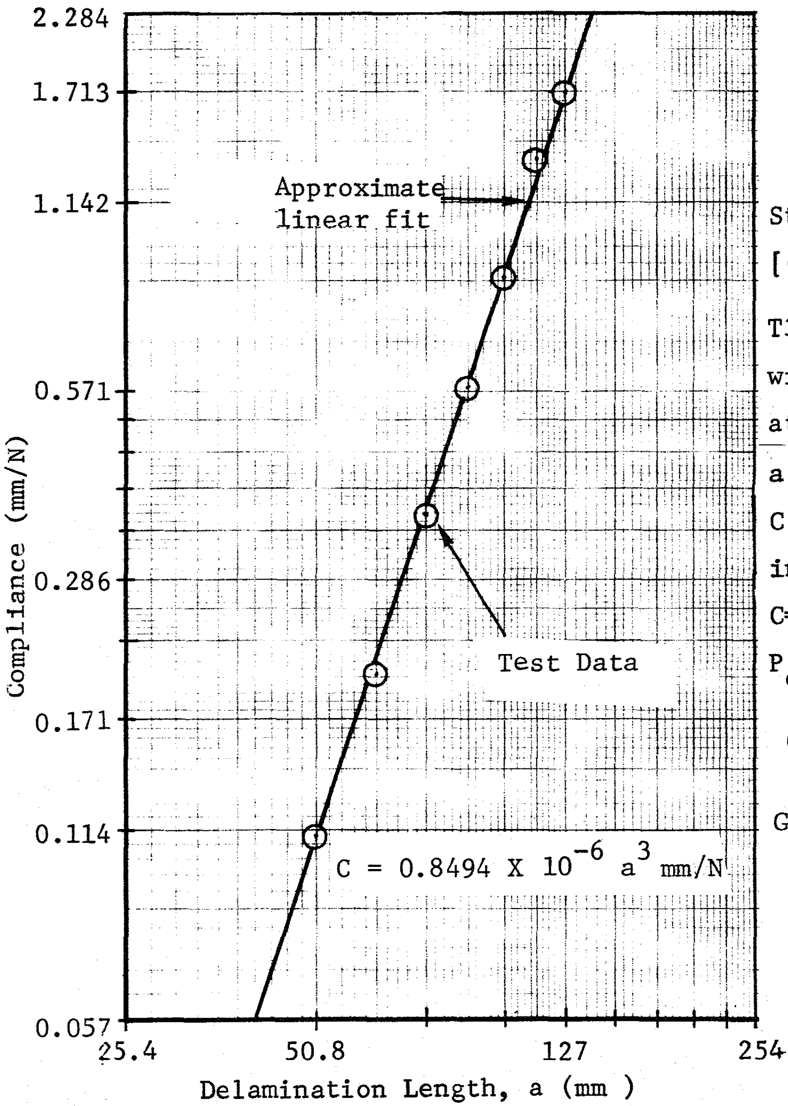

Static DCB tests on $[(0_2/\pm45)_3/0]_s$ T300/5208 specimens with a delamination at the midplane. If a is expressed in mm, C in mm/N, and P_{cr} in N,

$C = 0.8494 \times 10^{-6} a^3$

$P_{cr} = 1412.0\ a^{-1}$

$$G_{IC} = \frac{P_{cr}^2 (dC/da)}{2w}$$

$G_{IC} = 100.0\ J/m^2$

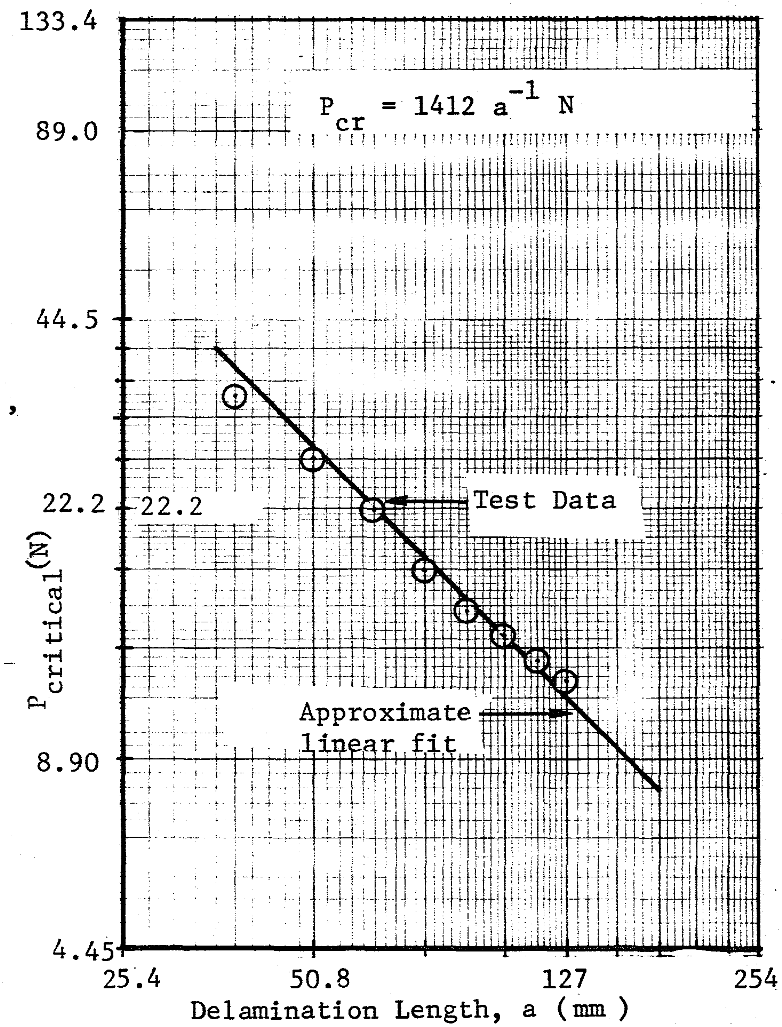

Figure 15. Static DCB Test Data From $[(0_2/\pm45)_3/0]_s$ T300/5208 Specimens.

Compliance predictions based on equation (2) are 28% lower than the measured values. The difference is due to the actual constraint condition at the delamination boundary being less stringent than the clamped condition assumed in equation (2).

It is noted that the log C versus log a results in Figures 14 and 15 were deliberately approximated by straight lines with a slope of three, to conform to the strength of materials expression in equation (2). Likewise, test data corresponding to the log P_{cr} versus log a plots in Figures 14 and 15 were approximated by straight lines with a slope of negative unity:

$$\left.\begin{array}{l} P_{cr} = 1610\ a^{-1}\ \text{N for the } [0]_{24T} \text{ specimen, and} \\ P_{cr} = 1412\ a^{-1}\ \text{N for the } [(0_2/\pm45)_3/0]_s \text{ specimen} \end{array}\right\} \quad (7)$$

where a is expressed in mm. This is a result of the premise that G_{IC} is a material constant that is independent of a, the compliance expressions in equation (6), and the definition of G_{IC} in equation (1). Figures 14 and 15 indicate that the experimental data are adequately represented by the approximations in equations (6) and (7).

Substituting the expressions in equations (6) and (7) into equation (1), the following G_{IC} values were computed:

$$\left.\begin{array}{l} G_{IC} = 102.6\ \text{J/m}^2 \text{ using results from tests on } [0]_{24T} \text{ specimens, and} \\ G_{IC} = 100.0\ \text{J/m}^2 \text{ using results from tests on } [(0_2/\pm45)_3/0]_s \text{ specimens} \end{array}\right\} \quad (8)$$

It is noted that the lack of midplane symmetry in the delaminated portion of the $[(0_2/\pm45)_3/0]_s$ DCB specimens caused them to twist slightly when the load was applied. Nevertheless, a pure mode I propagation of the delamination resulted. The twist probably caused the interlaminar normal stress distribution in the widthwise direction at the delamination boundary, to be non-uniform in these specimens. Referring to equation (8), it is seen that G_{IC} was not adversely affected by this behavior.

G_{IC} based on results from $[0]_{24T}$ specimens (102.6 J/m^2) will henceforth be referred to as the G_{IC} for the T300/5208 material system. In

Reference 14, a G_{IC} value of 87.6 J/m^2 (15% lower than 102.6 J/m^2) was obtained for the T300/5208 material using a similar test procedure.

3.2 DELAMINATION GROWTH RATES IN DCB SPECIMENS

Constant amplitude fatigue tests on $[0]_{24T}$ and $[(0_2/\pm45)_3/0]_s$ DCB specimens were conducted at R = 0.05 and ω = 10 Hertz. Delamination growth was monitored as explained in Section 2.5 The imposed maximum cyclic displacements (δ_{max}) and dC/da expressions from static test results were used to compute the maximum cyclic strain energy release rates ($G_{I_{max}}$) associated with in situ delamination sizes (a) as follows:

$$G_{I_{max}} = P^2_{max}(dC/da)/(2w) \tag{9}$$

where $P_{max} = \delta_{max}/C$ (10)

Therefore, $$G_{I_{max}} = \delta^2_{max} \quad (dC/da)/(2wC^2) \tag{11}$$

Recalling that δ_{max} was held constant during fatigue, substitution of equation (6) into (11) implies that $G_{I_{max}}$ was inversely proportional to a^4:

$$G_{I_{max}} \quad \alpha \ a^{-4} \tag{12}$$

Also, the constant amplitude fatigue tests were run at an R ratio ($\delta_{min}/\delta_{max}$) of 0.05. Therefore, referring to equation (11), the minimum cyclic strain energy release rate ($G_{I_{min}}$) was always:

$$G_{I_{min}} = (0.05)^2 \ G_{I_{max}} = 0.0025 \ G_{I_{max}} \tag{13}$$

During fatigue, the incremental number of cycles (ΔN) corresponding to a 2.54 mm change in the delamination size (Δa) was recorded. The rate of delamination growth (da/dN) was thus monitored as a function of in situ delamination size (a). Substituting the a values and the expressions in (6) into equation (11), relationships between da/dN and $G_{I_{max}}$ were obtained for the two test laminates.

Plots of delamination growth rate (da/dN) as a function of $G_{I_{max}}$ for the two DCB laminates are presented in Figures 16 and 17. Power law fits to the data on these logarithmic plots were obtained using a least squares analysis, and yielded the following relationships:

For $[0]_{24T}$ DCB specimens,

$$da/dN = 0.0283\ (G_{I_{max}}/G_{IC})^{8.02}\ \text{mm/cycle} \tag{14}$$

For $[(0_2/\underline{+}45)_3/0]_s$ DCB specimens,

$$da/dN = 0.0791\ (G_{I_{max}}/G_{IC})^{10.08}\ \text{mm/cycle} \tag{15}$$

Considerable scatter is noticed in the da/dN versus $G_{I_{max}}$ data presented in Figures 16 and 17. Consequently, the exponents in equations (14) and (15) bear a poor correlation to the value of 26 obtained in Reference 14.

Equations (14) and (15) quantify the effect of $G_{I_{max}}/G_{IC}$ on delamination growth rate, for an R ratio of 0.05 and for ω = 10 Hertz. The differences in the growth rate equations for the two specimens are due to the reasons explained in Section 3.1. The delaminated set of plies in the $[(0_2/\underline{+}45)_3/0]_s$ specimens lacked midplane symmetry, and twisted slightly when a tip load was applied. Consequently, a non-uniform distribution of the interlaminar normal stress, in the widthwise direction, existed at the delamination boundary. Hence the difference between equations (14) and (15).

Henceforth, the following approximation of equations (14) will be assumed to quantify the effect of $G_{I_{max}}$ on mode I delamination growth rate in T300/5208 laminates, at R = 0.05 and ω = 10 Hertz:

$$da/dN = 0.0283\ (G_{I_{max}}/G_{IC})^{8}\ \text{mm/cycle} \tag{16}$$

Substituting equation (12) into the above equation, it is seen that:

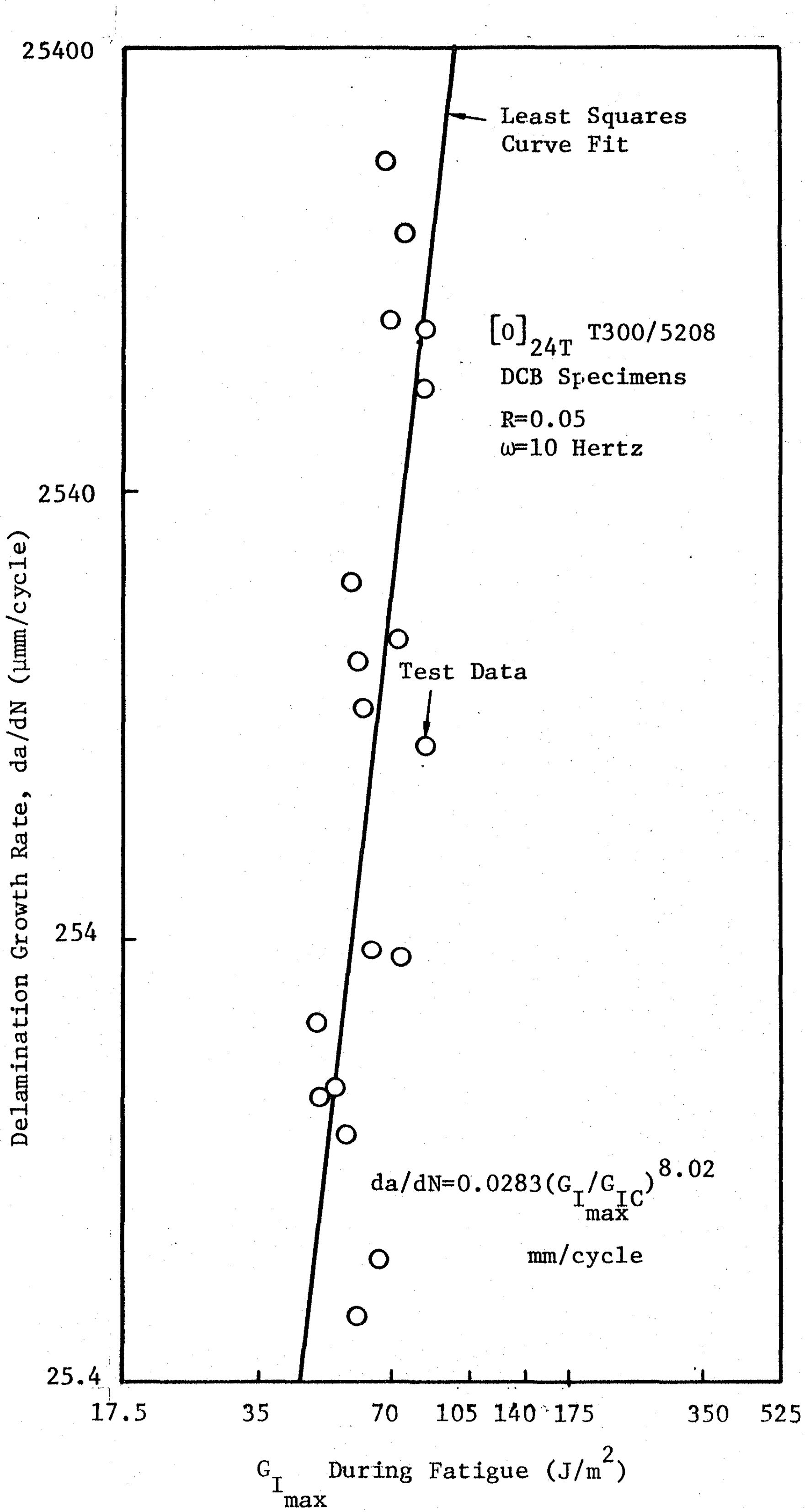

Figure 16. Variation of Delamination growth Rate with Strain Energy Release Rate in $[0]_{24T}$ DCB Specimens.

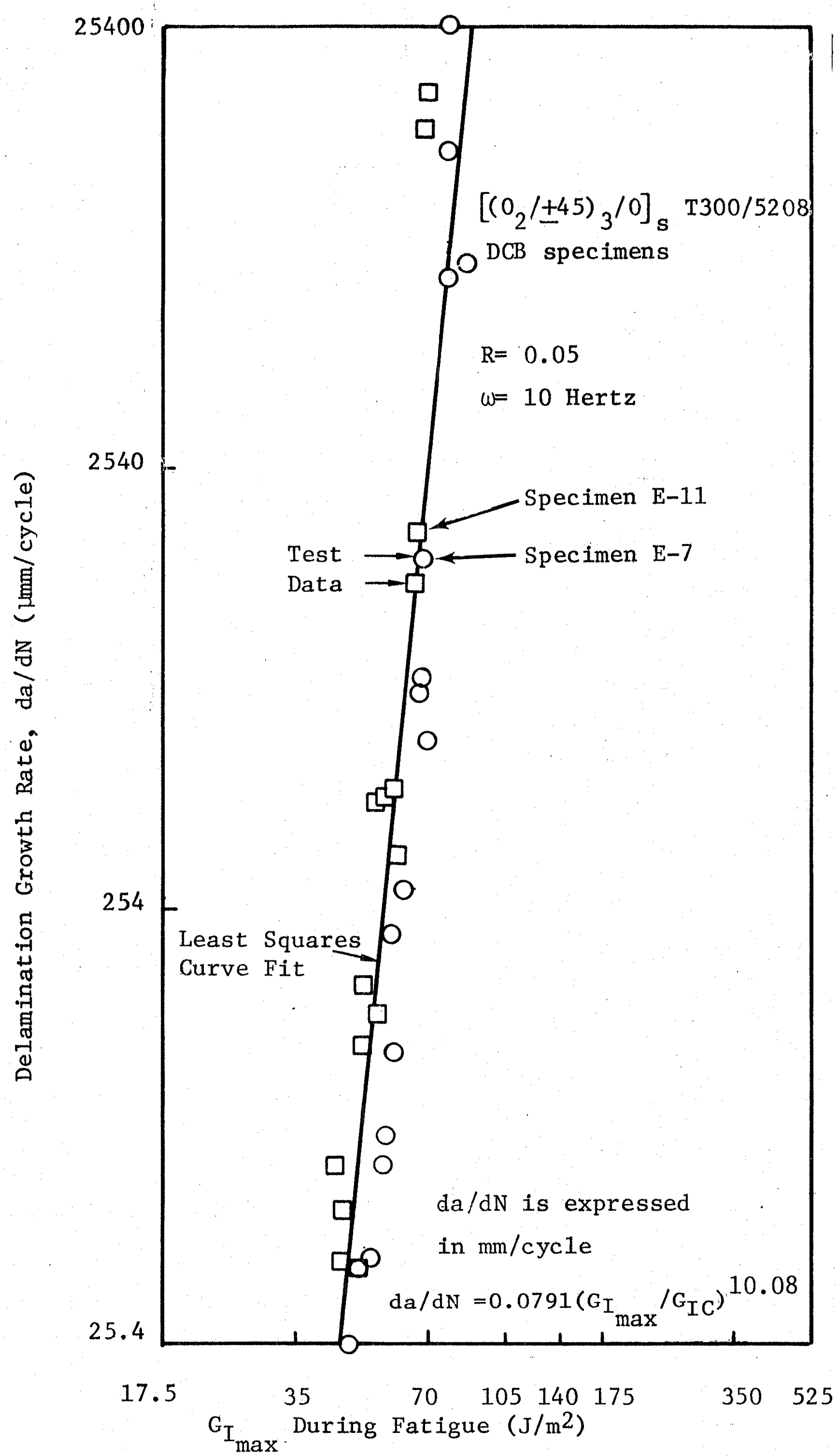

Figure 17. Variation of Delamination Growth Rate with Strain Energy Release Rate in $[(0_2/\pm45)_3/0]_s$ DCB Specimens.

$$da/dN \propto a^{-32} \tag{17}$$

when δ_{max} is held constant during fatigue. Pure mode I delamination growth rate, therefore, decreases drastically as the delamination size increases, in a displacement-controlled fatigue test.

3.3 STATIC CLS TEST RESULTS

Static tensile tests on $[(0_2/\pm45)_s]_s$ and $[0_2/\pm45_2/0_2]_s$ cracked lap shear (CLS) specimens were conducted in a displacement-controlled mode to obtain compliance measurements at various crack (delamination) lengths. The geometry of the CLS specimens is defined in Figure 2. Extensometers were used on $[(0_2/\pm45)_s]_s$ specimens, and the displacement between test grips was monitored on $[0_2/\pm45_2/0_2]_s$ specimens (see Figures 2 and 7). Half the $[0_2/\pm45_2/0_2]_s$ specimens were laterally constrained by flexures, placed 50.8 mm apart on the tool surface, as shown in Figures 2 and 5. The flexures were placed directly below the step location (see Figures 2 and 5), and were originally assumed to be adequate to prevent out-of-plane displacement of the tool surface of these CLS specimens. But, a nonlinear finite element analysis of the CLS specimen, accounting for these lateral constraint (flexure) locations indicated that this assumption was incorrect. The lateral constraints were not sufficient to prevent all lateral displacements. Hence the constrained CLS specimen was not representative of the behavior of one half of a symmetrical double cracked lap shear specimen.

Typical load-displacement records from static tests on $[(0_2/\pm45)_s]_s$ and $[0_2/\pm45_2/0_2]_s$ CLS specimens are presented in Figures 18 and 19. In many specimens--especially the $[0_2/\pm45_2/0_2]_s$ specimens with flexure constraints--delamination growth at P_{cr} could not be controlled to within the 12.7 mm increment shown in Figure 19. A growth (Δa) of 25 mm at P_{cr} was not uncommon during these displacement-controlled tests. The critical loads (P_{cr}) and displacements (u_{cr}), and the compliances (C) corresponding to various delamination sizes (a), were recorded during each static test. dC/da was computed based on a least squares linear fit through the compliance data (see Figures 20 to 22). Table 7 presents the measurements

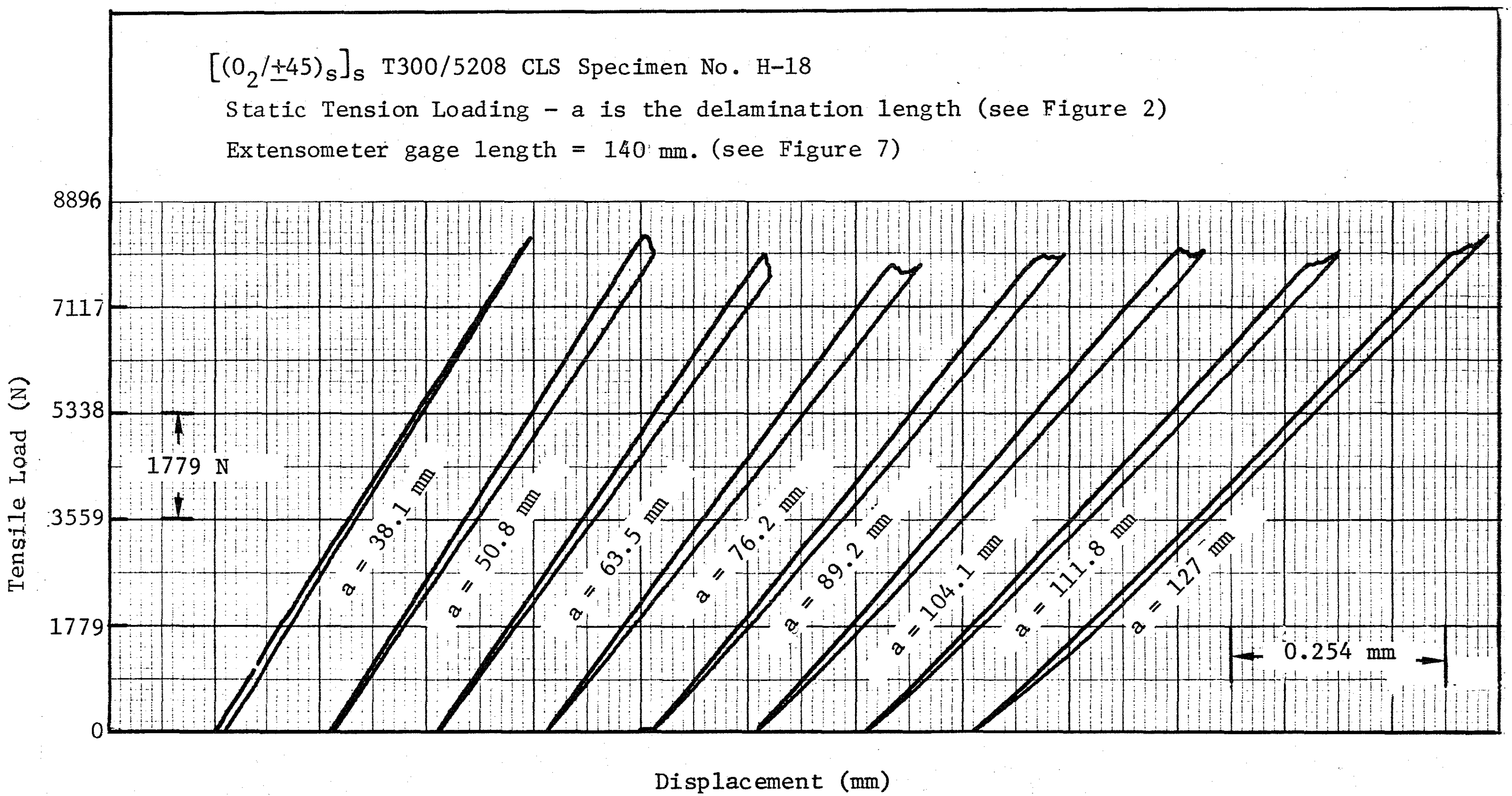

Figure 18. Typical Load-Deflection Curves for a $[(0_2/\pm 45)_s]_s$ CLS Specimen Subjected to Static Tension.

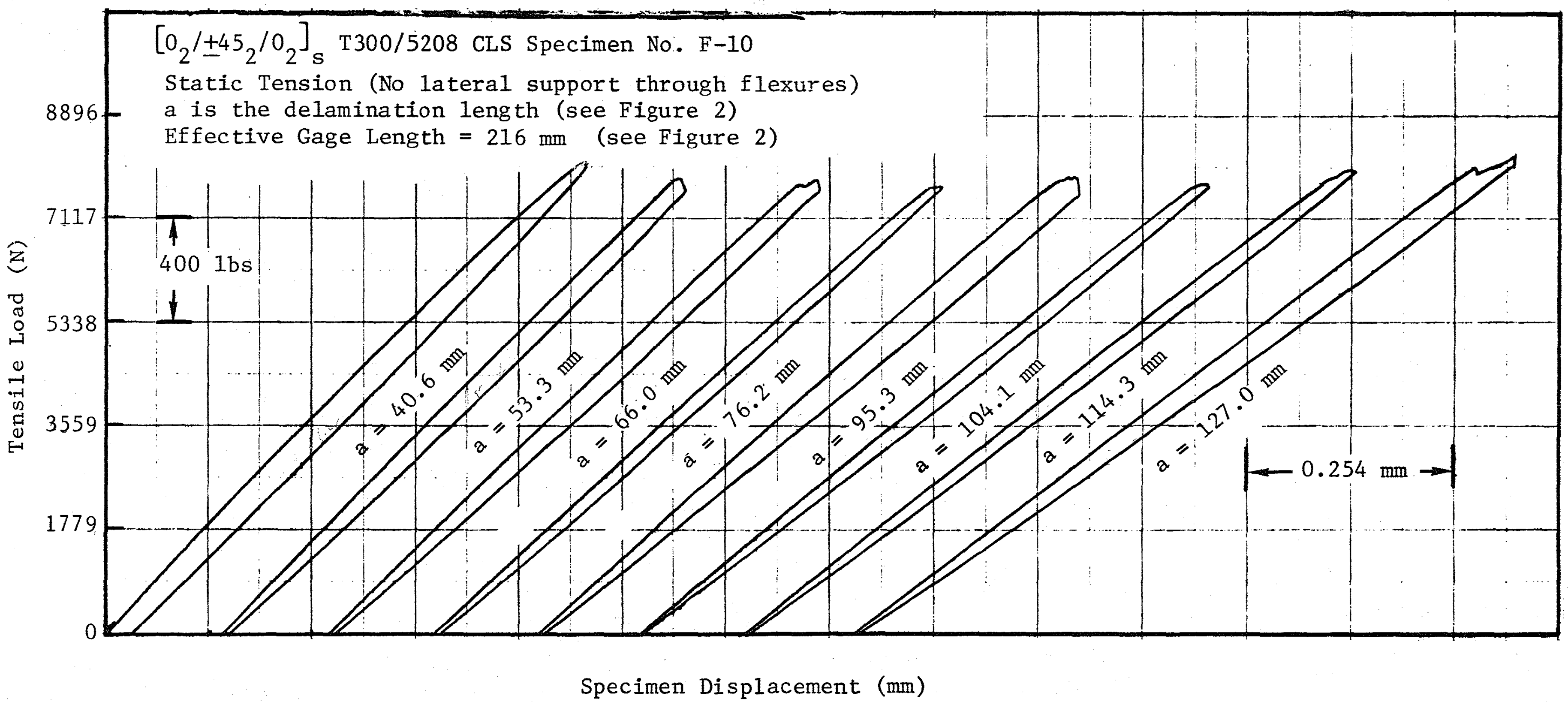

Figure 19. Typical Load-Deflection Curves for a $[0_2/\pm45_2/0_2]_s$ CLS Specimen Subjected to Static Tension.

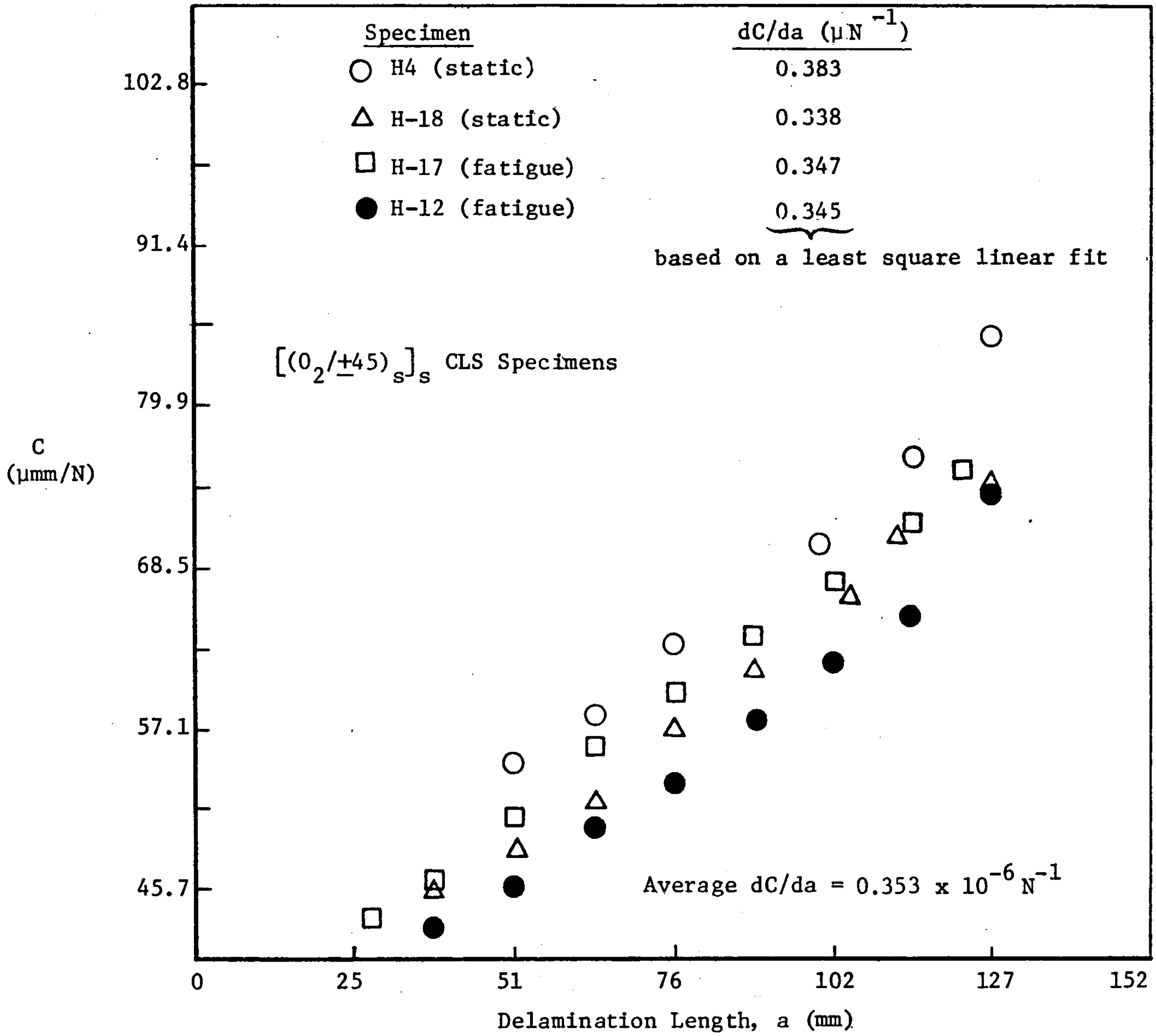

Figure 20. Compliance Variation with Delamination Size in $[0_2/\pm45)_s]_s$ CLS Specimens.

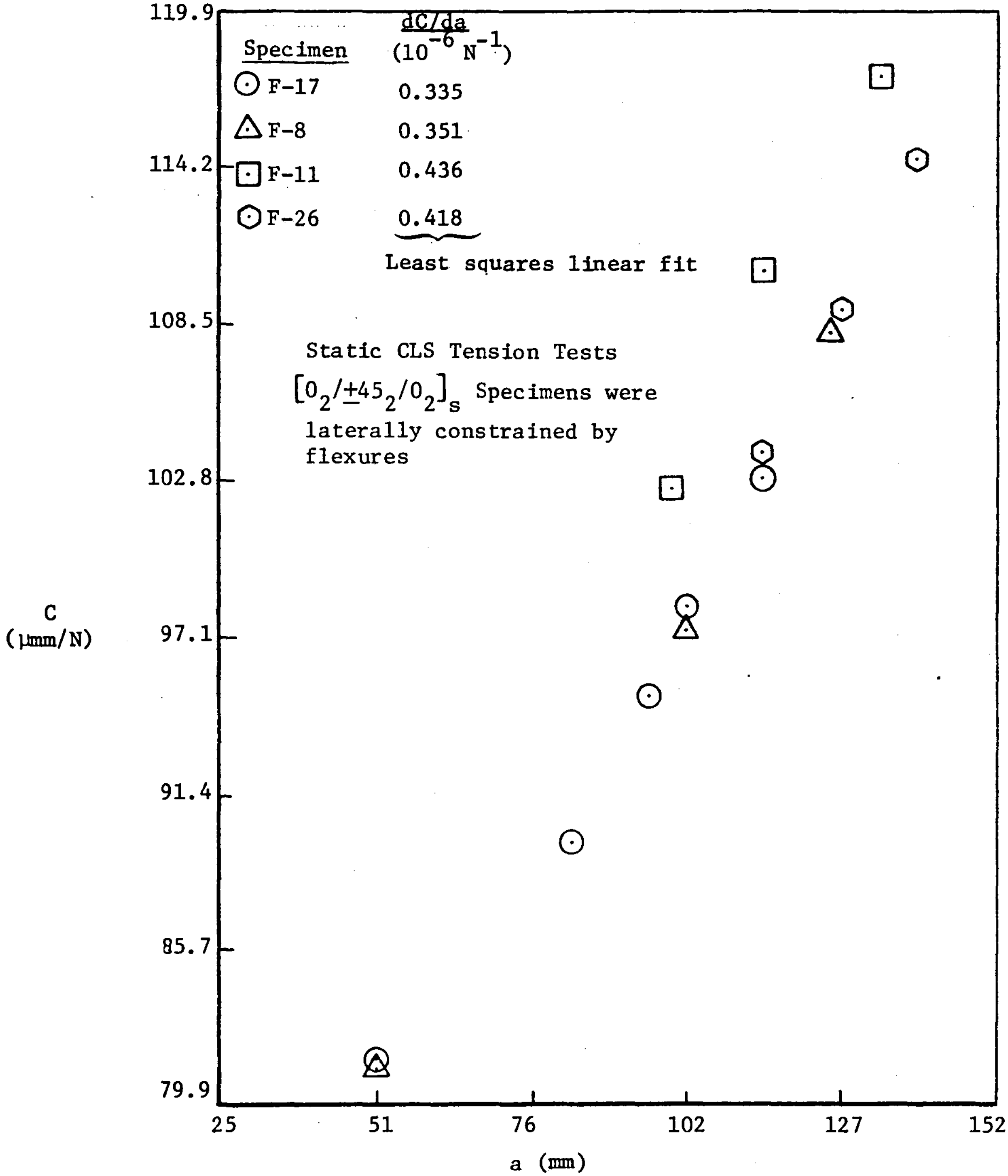

Figure 21. Compliance Variation with Delamination Size in $[0_2/\pm45_2/0_2]_s$ CLS Specimens With Flexure Constraints.

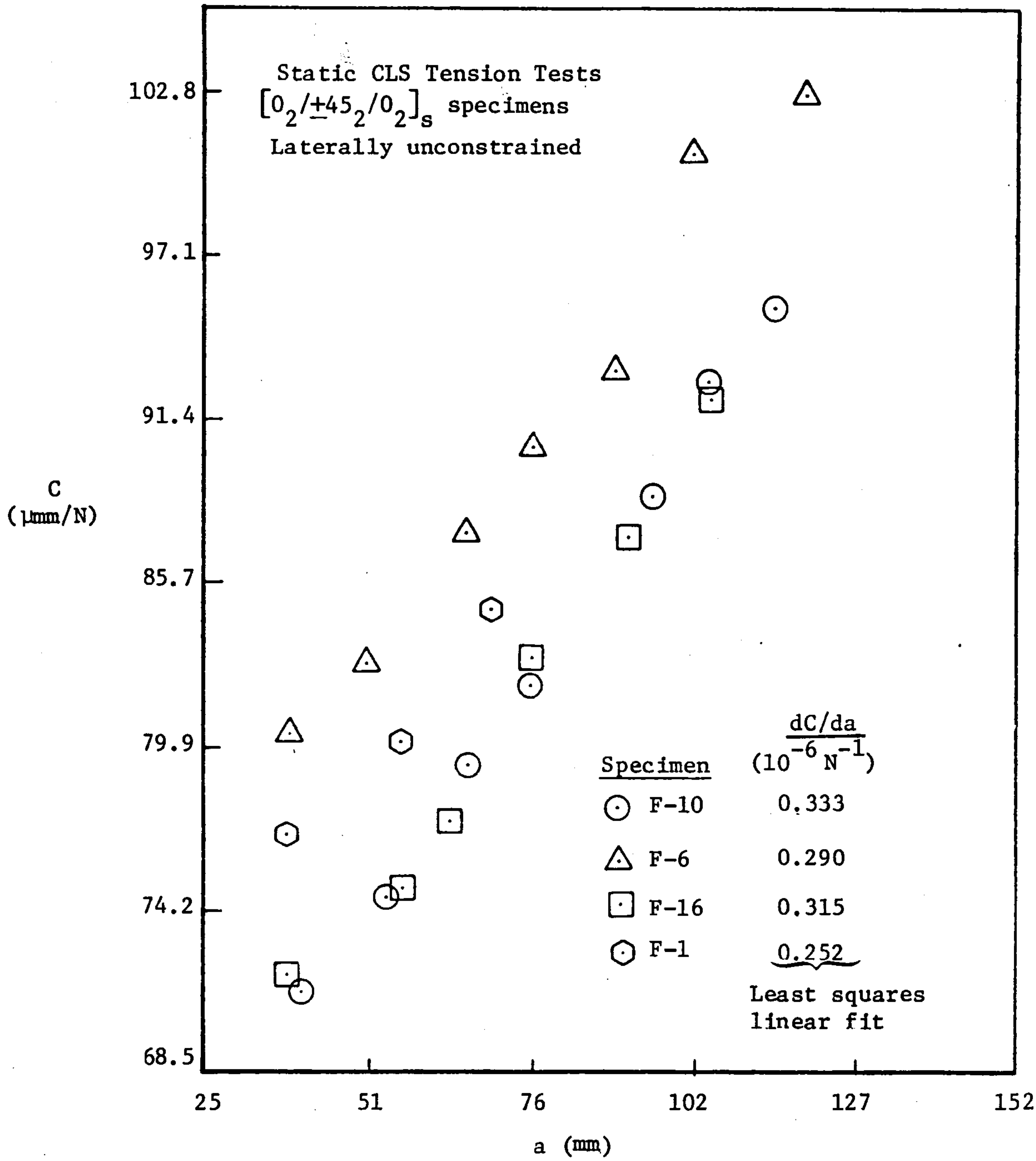

Figure 22. Compliance Variation with Delamination Size in Laterally Unconstrained $[0_2/\pm45_2/0_2]_s$ CLS Specimens.

TABLE 7. STATIC TENSION TEST DATA FROM $[(0_2/\pm 45)_s]_s$ CLS SPECIMENS

Delamination Length, a (mm)	Critical Load, P_{cr} (N)	Critical Displacement u_{cr} (mm)	Compliance C * (μ mm/N)	Critical Total Strain Energy Release Rate, G_c** (J/m^2)
		Specimen H-4		
50.8	7918	0.4318	54.53	472.8
63.5	8185	0.4750	58.19	505.2
76.2	8185	0.5156	62.98	505.2
99.1	8060	0.5664	70.12	489.9
114.3	7793	0.5944	76.34	458.0
127.0	7669	0.6528	84.97	443.5
		Specimen H-18		
38.1	8274	0.3759	45.57	455.9
50.8	8007	0.3886	48.59	427.0
63.5	7651	0.3962	51.91	389.9
76.2	7829	0.4470	57.10	408.2
89.2	7980	0.4877	61.27	424.1
104.1	8042	0.5334	66.35	430.8
111.8	8060	0.5715	70.75	432.7
127.0	8309	0.6172	74.40	459.8

* Based on an extensometer gage length of 140 mm (see Figure 7)

** Refer to Figure 20 for dC/da values used in the computation of G_c.

on $[(0_2/\pm45)_s]_s$ specimens. Tables 8 and 9 present corresponding data on $[0_2/\pm45_2/0_2]_s$ specimens, with and without flexure constraints, respectively.

The critical total strain energy release rates (G_c) in the mixed-mode CLS specimens were obtained using:

$$G_c = P_{cr}^2 \; (dC/da)/(2w) \tag{18}$$

where w = 2.54 cm (1 in.) for the specimens. Computed G_c values are also listed in Tables 7 to 9.

3.4 STRENGTH OF MATERIALS ANALYSIS OF CLS SPECIMENS

The following strength of materials analysis was carried out to approximately compute C, dC/da and G_c for the CLS test specimens (see Reference 18). The CLS specimen was modeled as shown in Figure 23, and bending effects due to load eccentricity in the 16-ply specimens were ignored. Let segments 1 and 2 have L_1 and L_2 as their lengths, A_1 and A_2 as their cross-sectional areas, and E_1 and E_2 as their longitudinal moduli. Both segments are subjected to the applied tensile load P_T. If u_1 and u_2 are the axial elongations of sections 1 and 2, the overall compliance (C) of the CLS specimen is given by:

$$C = (u_1 + u_2)/P_T = L_1/A_1E_1 + L_2/A_2E_2 \tag{19}$$

When the delamination propagates over a differential distance of "da", dL_1 = da and dL_2 = -da. Using this in equation (19), the following relationship may be obtained:

$$dC/da = (A_2E_2 - A_1E_1)/A_1A_2E_1E_2 \tag{20}$$

For the CLS specimens tested in this program $A_2=2A_1$ and $E_1=E_2$. Substituting these into equations (19) and (20), and noting that $L = L_1 + L_2$ (Figure 23),

$$C = (2L_1 + L_2)/(2A_1E_1) = (L + L_1)/A_2E_2 \tag{21}$$

$$dC/da = (2A_1E_1)^{-1} = (A_2E_2)^{-1} \tag{22}$$

Substituting the dC/da expression in equation (22) into equation (18), the critical total strain energy release rate (G_C) is expressed as:

$$G_C = P_{cr}^2/(4WA_1E_1) = P_{cr}^2/(2WA_2E_2) \tag{23}$$

TABLE 8. STATIC TENSION TEST DATA ON $[0_2/\pm45_2/0_2]_s$ CLS SPECIMENS WITH LATERAL (FLEXURE) CONSTRAINTS

a (mm)	P_{cr} (N)	u_{cr} (mm)	C (μ mm/N)	G_c^* (J/m^2)
		Specimen F-17		
50.8	8096	0.6604	81.60	433.4
82.6	7651	0.6858	89.65	387.2
95.3	7437	0.7061	94.96	365.8
101.6	7473	0.7341	98.21	369.3
114.3	7651	0.7874	102.90	387.2
		Specimen F-8		
50.8	8896	0.7239	81.37	546.6
101.6	7775	0.7569	97.36	417.5
125.7	7775	0.8407	108.15	417.5
		Specimen F-11		
99.1	7259	0.7442	102.50	453.6
114.3	7669	0.8458	110.32	506.1
133.4	8274	0.9728	117.57	589.1
		Specimen F-26		
114.3	7962	0.8255	103.70	521.9
127.0	8274	0.9017	109.01	563.4
139.7	9074	1.0465	114.32	677.7

* Refer to Figure 21 for dC/da values used in the computation of G_c.

TABLE 9. STATIC TENSION TEST DATA FROM UNCONSTRAINED $[0_2/\pm 45_2/0_2]_s$ CLS SPECIMENS

a (mm)	P_{cr} (N)	u_{cr} (mm)	C (μ mm/N)	G_c^* (J/m^2)
		Specimen F-10		
40.6	7329	0.5588	71.38	400.5
53.3	7740	0.5791	74.63	391.6
66.0	7651	0.6071	79.26	382.7
76.2	7740	0.6350	82.05	391.6
95.3	7740	0.6858	88.62	391.6
104.1	7953	0.7366	92.62	413.5
114.3	8007	0.7620	95.19	419.1
		Specimen F-6		
38.1	8274	0.6655	80.46	391.8
50.8	8274	0.6858	82.91	391.8
66.0	7989	0.6985	87.42	365.3
76.2	8007	0.7239	90.39	366.9
89.2	7918	0.7366	93.02	358.8
101.6	7829	0.7874	100.56	350.8
119.4	7793	0.8001	102.67	347.6
		Specimen F-16		
38.1	8398	0.6045	72.00	436.6
55.9	8398	0.6299	75.03	436.6
63.5	8274	0.6401	77.37	423.8
76.2	8345	0.6934	83.08	431.2
91.4	8185	0.7137	87.19	414.7
104.1	8007	0.7366	91.99	396.8
		Specimen F-1		
38.1	9074	0.6985	76.97	407.7
55.9	9039	0.7239	80.11	404.5
68.6	8985	0.7620	84.80	399.8

* Refer to Figure 22 for dC/da values used in the computation of G_c.

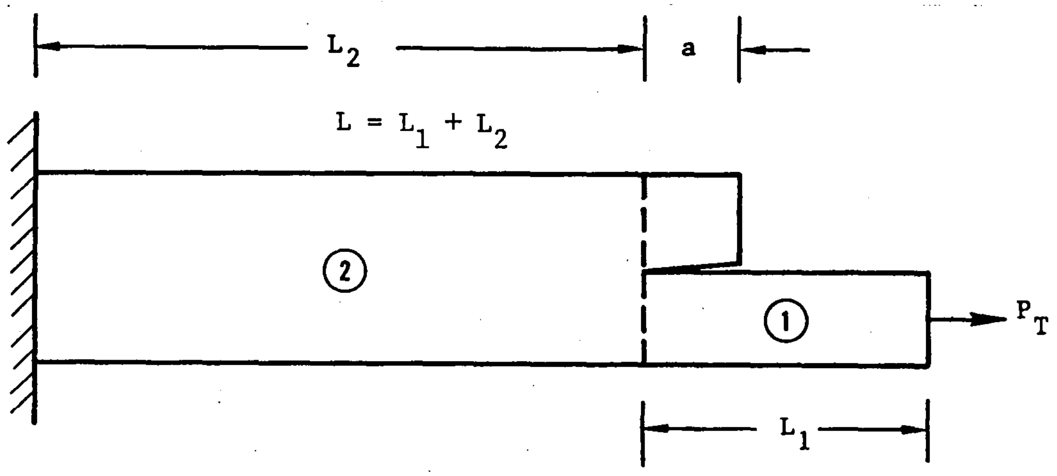

Figure 23. A Strength of Materials Model of the CLS Specimen

TABLE 10. AVERAGE STATIC TENSION TEST DATA ON $[(0_2/\pm45)_s]_s$ CLS SPECIMENS

Delamination Length, a (mm)	Average P_{cr} (N)	Average u_{cr} (mm)	Average C (μmm/N)	Average G_c* (J/m^2)
50.8	7962	0.4115	51.56	457.3
63.5	7918	0.4369	55.05	452.2
76.2	8007	0.4826	60.07	462.2
88.9	8047	0.5156	64.07	467.1
101.6	8025	0.5486	68.35	464.5
114.3	7949	0.5867	73.83	455.8
127.0	7989	0.6350	79.71	460.4

*This is computed using $dC/da = 0.3664 \mu N^{-1}$, based on a least squares linear fit through the average compliance data listed above.

The average A_2 value for the fabricated CLS specimens was measured to be 57.03 mm^2, yielding a ply thickness of 0.14 mm (0.0055 in) in the cured laminate. Back-to-back axial strain gages bonded to a $[(0_2/\pm 45)_s]_s$ test specimen (H-3) measured a Young's modulus of E_1=E_2 = 74.05 GPa. Likewise, back-to-back axial gages on a $[0_2/\pm 45_2/0_2]_s$ specimen (F-28) measured an E value of 70.05 GPa.

The average static test data on $[(0_2/\pm 45)_s]_s$ specimens are presented in Table 10. These were obtained from the data listed in Table 7. For the $[(0_2/\pm 45)_s]_s$ specimens, the variation in P_{cr} (and hence in G_c) with delamination size (a) is negligible--within 1% from the average value (see Table 10). Therefore P_{cr} and G_c may be assumed to be independent of a.

Substituting the measured areas, Young's modulus and P_{cr} into equations (21), (22) and (23), a strength of materials estimate for C, dC/da and G_c may be obtained. A comparison between experimental measurements and strength of materials estimates is presented in Table 11. It is seen that the measured compliances are 10 to 20% larger than the strength of materials prediction. dC/da and G_c values based on experimental data are approximately 35% higher than the strength of materials predictions.

Tests on $[0_2/\pm 45_2/0_2]_s$ CLS specimens were not conducted with extensometers. The gage length for these specimens corresponded to the distance between the centers of the two holes (see Figure 2). This was established by comparing the midplane strain based on this gage length with the direct strain gage measurement on specimen F-28. Table 12 presents a comparison between measurements and strength of materials estimates for laterally unconstrained $[0_2/\pm 45/0_2]_s$ specimens. The average measurements in Table 12 were obtained using the data presented in Table 9. Though P_{cr} (and G_c) differed by approximately 10% from the average value corresponding to the various delamination sizes in Table 9, they were again assumed to be independent of a. Measured average compliances, dC/da based on average C values, and G_c are approximately 6%, 20% and 17% larger than predictions, respectively.

TABLE 11. COMPARISON BETWEEN STRENGTH OF MATERIALS ESTIMATES AND ACTUAL MEASUREMENTS ON $[(0_2/\pm 45)_s]_s$ CLS SPECIMENS+

a (mm)	L_1 (mm)	C (μmm/N)		dC/da (μN^{-1})		G_c (J/m^2)	
		S.O.M.*	Measurement **	S.O.M.	Measurement	S.O.M.	Measurement
50.8	53.34	45.73	51.56	0.2360	0.3664	297.2	460.0
63.5	66.04	48.71	55.05	0.2360	0.3664	297.2	460.0
76.2	78.74	51.73	60.07	0.2360	0.3664	297.2	460.0
88.9	91.44	54.70	64.07	0.2360	0.3664	297.2	460.0
101.6	104.14	57.73	68.35	0.2360	0.3664	297.2	460.0
114.3	116.84	60.76	73.83	0.2360	0.3664	297.2	460.0
127.0	129.54	63.73	79.71	0.2360	0.3664	297.2	460.0

+ L is the extensometer gage length

$L = 139.7$ mm (see Figure 7)

$A_2 = 57.03\ mm^2$

$E_2 = E_1 = 74.05$ GPa

$L_1 = (a + 2.54)$ mm (See Figures 7 and 23)

* S.O.M. = strength of materials (equations 21, 22 and 23)

** Average Values from Table 10.

Average $P_{cr} = 7985$ N and average $G_c = 460.0\ J/m^2$ from Table 10

TABLE 12. COMPARISON BETWEEN STRENGTH OF MATERIALS ESTIMATES AND ACTUAL MEASUREMENTS ON LATERALLY UNCONSTRAINED $[0_2/\pm 45_2/0_2]_s$ CLS SPECIMENS+

a (mm)	L_1 (mm)	C (μmm/N)		dC/da (μN^{-1})		G_c (J/m^2)	
		S.O.M.*	Measure- ment**	S.O.M.	Measure- ment	S.O.M.	Measure- ment
38.1	76.2	73.09	75.03	0.2495	0.3147	327.2	396.3
50.8	88.9	76.29	77.54	0.2495	0.3147	327.2	396.3
63.5	101.6	79.49	81.31	0.2495	0.3147	327.2	396.3
76.2	114.3	82.63	85.20	0.2495	0.3147	327.2	396.3
88.9	127.0	85.82	88.68	0.2495	0.3147	327.2	396.3
101.6	139.7	89.02	94.33	0.2495	0.3147	327.2	396.3
114.3	152.4	92.16	98.61	0.2495	0.3147	327.2	396.3

\+ L is the distance between the centers of the holes in the CLS specimens, and is assumed to be the distance over which the recorded displacement occurred.

$L = 215.9$ mm (see Figure 2)

$A_2 = 57.03\ mm^2$

$E_2 = E_1 = 70.05$ GPa

$L_1 = (38.1 + a)$ mm (see Figures 2 and 23).

* S.O.M. = strength of materials (equations 21, 22 and 23)

** Average Values Obtained from Data in Table 9.

Average $P_{cr} = 8149$ N and average $G_c = 396.3\ J/m^2$ from Table 9

3.5 NONLINEAR FINITE ELEMENT ANALYSIS (NFEA) OF CLS SPECIMENS -- G_I, G_{II} and G_C COMPUTATIONS

Delamination growth in mixed mode CLS specimens is in general induced by an interaction among modes I, II and III. For the CLS specimens tested in this program, mode III effects were assumed to be negligible -- an assumption that has to be verified through a three-dimensional numerical analysis that was beyond the scope of the reported program. Therefore, the measured G_c values were assumed to have only G_I and G_{II} components which were computed as explained below.

Laterally unconstrained $[(0_2/\pm45)_s]_s$ CLS test specimens were analyzed using an appropriate finite element model. Finite element analysis was performed by the program project engineer at NASA, Langley Research Center. The geometry of the specimen was taken from Figure 2. Assuming the x and y coordinates to be along the loading and thickness directions, respectively, the 0° plies were assumed to have the following properties: E_x = 137.9 GPa, E_y = 14.5 GPa, ν_{yx} = 0.022, and G_{xy} = 5.86 GPa. The $\pm45°$ plies were assumed to have the following properties: E_x = 20.4 GPa, E_y = 15.0 GPa, ν_{yx} = 0.044, and G_{xy} = 5.86 GPa. The performed finite element analysis accounted for geometric nonlinearity, and a reduced integration scheme was employed. G_I and G_{II} were computed at the delamination boundary using a virtual crack closure technique (References 9 and 10). For each of three initial crack lengths (a = 51, 76 and 102 mm), G_I and G_{II} were computed for a range of loads that extended from below to above the measured P_{cr} values (see Table 13).

NFEA results in Table 13 indicate that G_I and G_{II} are practically unaffected by the delamination size (a) in the laterally unconstrained $[(0_2/\pm45)_s]_s$ CLS specimens. A least squares curve fit analysis of the average NFEA G_I and G_{II} values (corresponding to a=51, 76 and 102mm) provided the following expressions:

$$G_I = 0.72\ P^{2.15}\ \mathrm{J/m^2} \tag{24}$$

$$G_{II} = 3.77\ P^{1.95}\ \mathrm{J/m^2} \tag{25}$$

TABLE 13. G_I, G_{II} COMPUTATIONS BASED ON NFEA OF LATERALLY UNCONSTRAINED $[(0_2/\pm45)_s]_s$ CLS SPECIMENS

Load, P (kN)	Delamination Length(a) (mm)	G_I^* (J/m^2)	G_{II}^* (J/m^2)	G_I/G_{II}
4.448	50.8	17.69	68.82	.257
	76.2	17.86	69.00	.259
	101.6	18.04	69.18	.261
6.672	50.8	42.03	152.36	.276
	76.2	42.03	152.54	.276
	101.6	42.38	152.89	.277
8.896	50.8	78.28	266.19	.294
	76.2	78.28	266.19	.294
	101.6	78.81	267.94	.294
11.121	50.8	127.84	411.55	.311
	76.2	128.02	411.55	.311
	101.6	128.54	411.55	.312

* G_I, G_{II} were computed at the delamination boundary.

$$G_I/G_{II} = 0.19\ P^{0.20} \tag{26}$$

In the above equations, P is expressed in kN, and G_I and G_{II} are independent of a.

Referring to Table 10, it is seen that the critical loads corresponding to a=51, 76 and 102 mm are relatively unaltered. Incorporating the average critical load value (7.985 kN) from Table 11 into equations (24) to (26), one obtains:

$$G_I = 62.69\ J/m^2,\ G_{II} = 216.66\ J/m^2,\ G_I/G_{II} = 0.289 \tag{27}$$

corresponding to delamination growth in $[(0_2/\pm45)_s]_s$ CLS specimens, for any delamination size (a). The sum of G_I and G_{II} yields the total strain energy release rate at any load level. Therefore, the critical total strain energy release rate (G_c) for the $[(0_2/\pm45)_s]_s$ CLS specimen, based on NFEA results, is (see equation 27):

$$G_c = 62.69 + 216.66 = 279.35\ J/m^2 \tag{28}$$

Referring to Table 11, it is seen that G_c based on NFEA results agrees well with the strength of materials prediction, but is 39% lower than the measured value.

3.6 ANALYTICAL PREDICTION OF G_{IIC}

Static DCB tests measured G_{IC} for T300/5208 to be 102.6 J/m^2. Finite element analysis of the $[(0_2/\pm45)_s]_s$ CLS specimens estimated G_I and G_{II} corresponding to static delamination growth to be 62.7 and 216.7 J/m^2, respectively. An estimation of G_{IIC} may be obtained by incorporating the mentioned G_{IC}, G_I and G_{II} values into a failure criterion. Since none has yet been established to be valid, the following three failure criteria were selected:

$$G_I/G_{IC} + G_{II}/G_{IIC} = 1 \tag{29}$$

$$(G_I/G_{IC})^2 + (G_{II}/G_{IIC})^2 = 1 \tag{30}$$

$$(G_I/G_{IC})^2 + (G_{IIC}/G_{IIC})^2 + (G_I/G_{IC})(G_{II}/G_{IIC}) = 1 \tag{31}$$

Substituting G_{IC} = 102.6 J/m^2, G_I = 62.7 J/m^2 and G_{II} = 216.7 J/m^2 into equations (29), (30) and (31), G_{IIC} values of 587.0, 279.0 and 414.9

J/m^2, respectively, were obtained. Only a pure shear test and the concomitant G_{IIC} measurement will establish the best choice among equations (29), (30) and (31).

In section 3.5, G_c based on NFEA was shown to be 39% lower than the G_c based on test results. If the NFEA estimations of G_I and G_{II}, used in G_{IIC} computation above, are scaled up (by a factor of 1.64) to estimate G_I and G_{II} corresponding to test results, G_I is seen to be equal to G_{IC} (103 J/m^2). This indicates that static delamination growth in the $[(0_2/\pm45)_s]_s$ CLS specimens is influenced largely by the opening mode (mode I). Also, G_{IIC} will be computed to be larger than the reported values if the scaled-up G_I and G_{II} are substituted into the selected failure criteria ($G_{II}/G_{IIC} \rightarrow 0$ as $G_I/G_{IC} \rightarrow 1$).

3.7 CLS FATIGUE TEST RESULTS

Constant amplitude tension fatigue tests on CLS specimens were conducted at $R = 0.05$ and $\omega = 10$ Hertz. The tests were displacement-controlled and the maximum cyclic displacements (u_{max}) were selected, based on static test data, to yield initial delamination growth rates (da/dN) in the neighborhood of 2.54 mm (0.1 in.) per 200 cycles. These maximum cyclic displacement values were reset in most cases to a higher value after a 12.7 mm (0.5 in.) growth in the delamination (see Section 2.6). Compliance measurements and cycle counts were recorded at Δa intervals of 2.54 mm (0.1 in.). Figure 24 shows a typical static compliance variation with delamination growth. Recorded data also yielded da/dN values for various a, u_{max} values (see Tables 14 to 16).

The maximum cyclic value of the total strain energy release rate (G_{max}) in CLS specimens can be expressed in a form similar to equation (11):

$$G_{max} = u_{max}^2 \, (dC/da)/(2wC^2) \qquad (32)$$

where w = 25.4 mm (1 in) for the tested CLS specimens. Recalling that compliance is a linear function of the delamination length (see Figures 20 to 22), it is seen that G_{max} is proportional to a^{-2} in CLS specimens:

$$G_{max} \;\alpha\; a^{-2} \qquad (33)$$

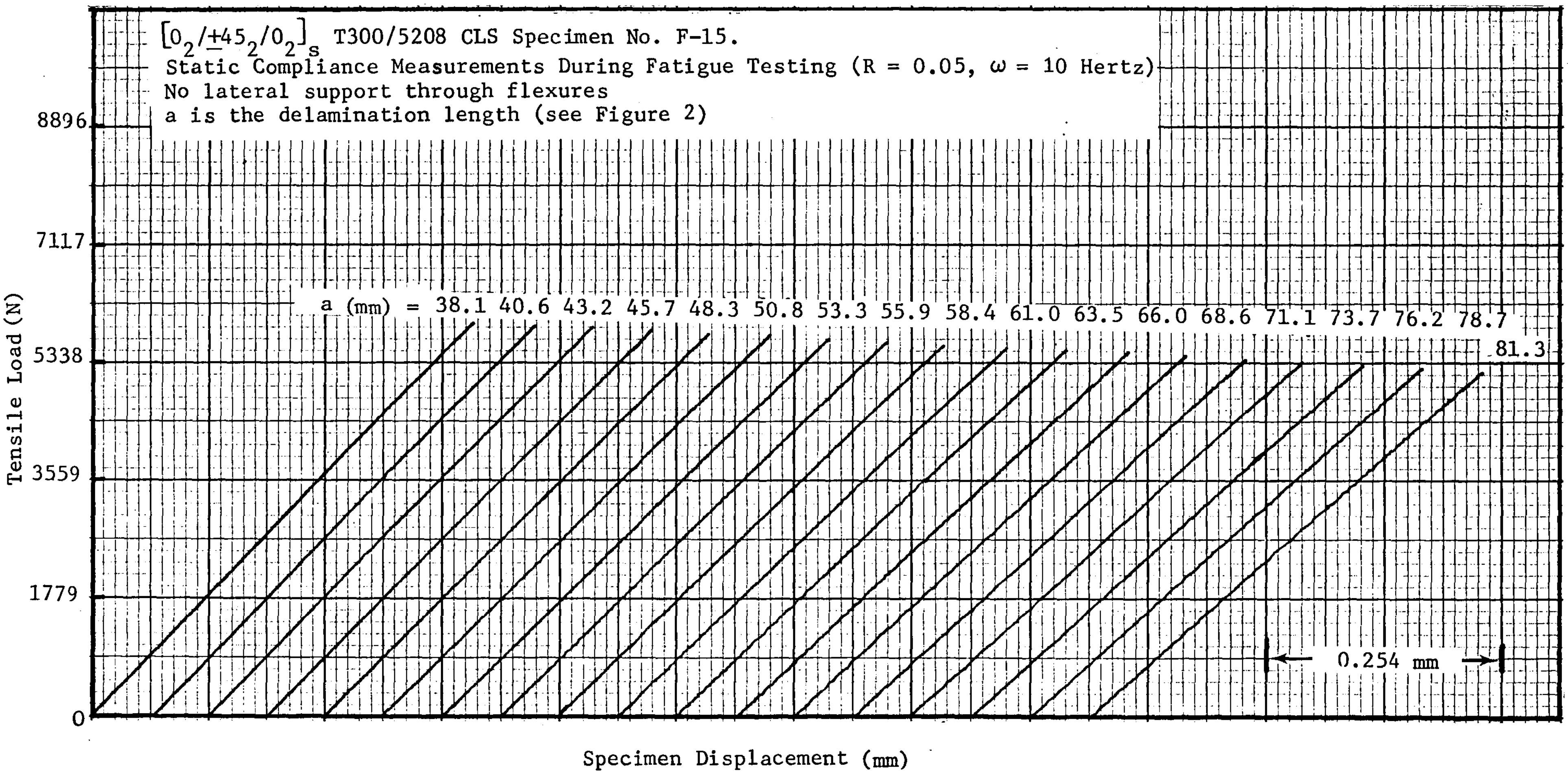

Figure 24. Typical Static Compliance Measurements During Fatigue Testing of CLS Specimens.

TABLE 14. TENSION FATIGUE TEST DATA ON $[(0_2/\pm45)_s]_s$ T300/5208 CLS SPECIMENS AT R=0.05 AND ω=10 HERTZ

Specimen H-17			Specimen H-12			Specimen H-11		
a (mm)	da/dN (μmm/cycle)	G_{max} (J/m^2)	a*	da/dN*	G^*_{max}	a*	da/dN*	G^*_{max}
28.4	7493	353	30.5	60477	484	50.8	9548	310
38.1	3505	304	38.1	39065	425	63.5	5570	263
50.8	2718	253	50.8	27305	348	76.2	1857	226
63.5	879	215	63.5	14122	291	88.9	737	197
76.2	869	184	76.2	3454	246	101.6	368	173
88.9	177	160	88.9	1026	211	114.3	155	153
101.6	85	140	101.6	518	183	124.5	56	139
114.3	17	123	114.3	84	160			
119.4	12	118	124.5	57	145			

A least squares curve-fit analysis of the presented data yielded the following equation:

$$da/dN = 7.7279 \times 10^{-12} \, G_{max}^{6.0660} \quad \mu mm/cycle \text{ where } G_{max} \text{ is expressed in } J/m^2$$

* Same units as shown for specimen H-17.

TABLE 15. TENSION FATIGUE TEST DATA ON $[0_2/\pm45_2/0_2]_s$ T300/5208 CLS SPECIMENS WITH LATERAL FLEXURE CONSTRAINTS (R=0.05, ω=10 HZ)

Specimen F-29			Specimen F-31			Specimen F-35			Specimen F-23		
a (mm)	da/dN (μmm/cycle)	G_{max} (J/m^2)	a*	da/dN*	G^*_{max}	a*	da/dN*	G^*_{max}	a*	da/dN*	G^*_{max}
50.8	1681	262	38.1	21166	397	38.9	916	207	38.9	361	226
63.5	1090	237	43.2	10584	382	40.6	609	204	50.8	216	211
76.2	1450	220	48.3	9769	371	43.2	179	202	63.5	254	187
88.9	752	205	63.5	8758	364	48.3	168	188	76.2	163	180
101.6	330	209	78.7	640	209	55.9	72	185	88.9	140	169
114.3	249	193	86.4	259	199	63.5	171	174	101.6	150	153
121.9	183	187	91.4	836	223	68.6	135	169	111.8	33	143
			101.6	485	205						

A least squares curve-fit analysis of the presented data yielded the following equation:

$$da/dN = 2.7536 \times 10^{-11} G_{max}^{5.6873} \quad \mu mm/cycle \text{ where } G_{max} \text{ is expressed in } J/m^2$$

* Same units as shown for specimen F-29.

TABLE 16. TENSION FATIGUE TEST DATA ON LATERALLY UNCONSTRAINED $[0_2/\pm 45_2/0_2]_s$ T300/5208 CLS SPECIMENS (R=0.05, ω=10 HZ)

Specimen F-33			Specimen F-15			Specimen F-25			Specimen F-37		
a (mm)	da/dN (μ mm/cycle)	G_{max} (in-lb/in^2)	a*	da/dN*	G^*_{max}	a*	da/dN*	G^*_{max}	a*	da/dN*	G^*_{max}
66.0	8458	353	38.1	3785	335	38.1	22479	362	61.5	227	149
71.1	6045	337	40.6	2896	327	40.6	14427	359	63.5	171	146
76.2	5080	316	43.2	2540	323	43.2	16383	350	66.0	147	144
78.7	12700	358	45.7	2289	317	58.4	5410	356	68.6	131	141
81.3	9398	365	53.3	12090	338	61.0	4801	344	76.2	55	136
86.4	7468	344	58.4	8458	326	63.5	4089	341	83.8	66	131
104.1	25400	376	63.5	7950	312	66.0	5766	342	91.4	69	126
106.7	15875	374	68.6	6350	313	73.7	4039	315	94.0	48	124
109.2	9779	371	71.1	4699	305				97.0	40	124
			73.7	3962	296						

A least squares curve-fit analysis of the presented data yielded the following equation:

$$da/dN = 4.3942 \times 10^{-9} \; G_{max}^{4.8273} \quad \mu mm/cycle \text{ where } G_{max} \text{ is expressed in } J/m^2$$

* Same units as shown for specimen F-33.

The average dC/da value was taken from Figures 20 to 22, and C was computed from records similar to Figure 24. G_{max} was computed by substituting C, dC/da and the imposed u_{max} values into equation (32). Subsequently, plots of da/dN versus G_{max} were generated for the $(0_2/\pm 45)_{s\ s}$ and $0_2/\pm 45_2/0_{2\ s}$ CLS specimens (see Figures 25 to 27).

A least squares curve-fit analysis of the delamination growth data presented in Tables 14 to 16 (Figures 25 to 27) yielded the following expressions:

For the $[(0_2/\pm 45)_s]_s$ CLS specimens,

$$da/dN = 7.73 \times 10^{-12}\ G_{max}^{6.07} \quad \mu mm/cycle \tag{34}$$

For the $[0_2/\pm 45_2/0_2]_s$ CLS specimens with lateral (flexure) constraints,

$$da/dN = 2.75 \times 10^{-11}\ G_{max}^{5.69} \quad \mu mm/cycle \tag{35}$$

For the laterally unconstrained $[0_2/\pm 45_2/0_2]_s$ CLS specimens,

$$da/dN = 4.39 \times 10^{-9}\ G_{max}^{4.83} \quad \mu mm/cycle \tag{36}$$

In the above equations, G_{max} is expressed in J/m^2. It is also noted that these delamination growth relationships were obtained from constant amplitude fatigue tests run at a frequency of 10 Hertz with the minimum cyclic total strain energy release rate (G_{min}) maintained to be equal to 0.0025 G_{max}. Equations (34) to (36) are therefore valid only for ω = 10 Hz and R = 0.05. The differences in the coefficient and exponent values in the three equations is due to different G_I/G_{II} ratios in the corresponding test cases. G_I/G_{II} will vary with the laminate layup, and for the same layup, will vary with the specimen support conditions (lateral constraints).

3.8 G_I, G_{II} CONTRIBUTIONS TO DELAMINATION GROWTH RATE IN CLS SPECIMENS

CLS specimens are mixed mode specimens in which delamination growth is potentially influenced by all the strain energy release rate components (G_I, G_{II} and G_{III}). In the preceding section, a least squares curve fit analysis of the experimental data on $[(0_2/\pm 45)_s]_s$ CLS specimens was per-

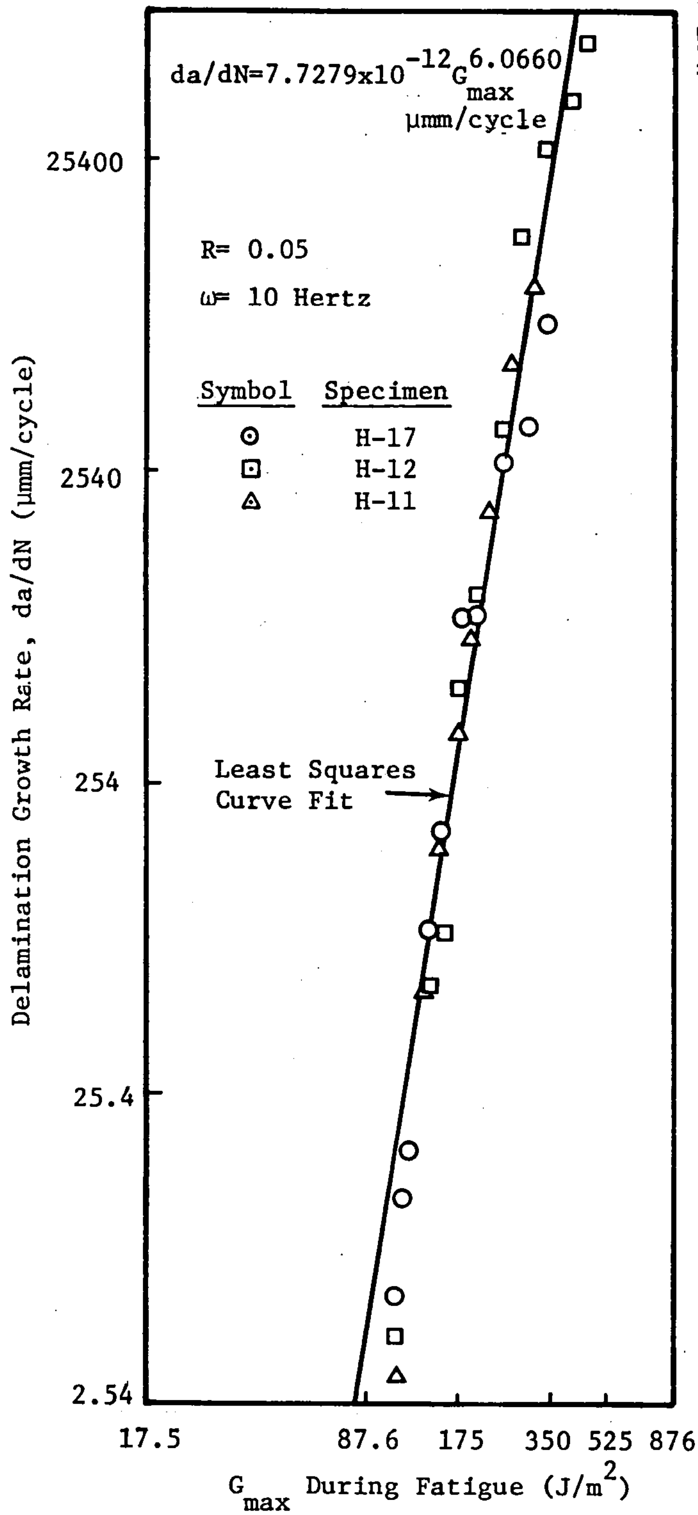

Figure 25. Variation of Delamination Growth Rate With Maximum Cyclic Strain Energy Release Rate in $[(0_2/\pm45)_s]_s$ T300/5208 CLS Specimens.

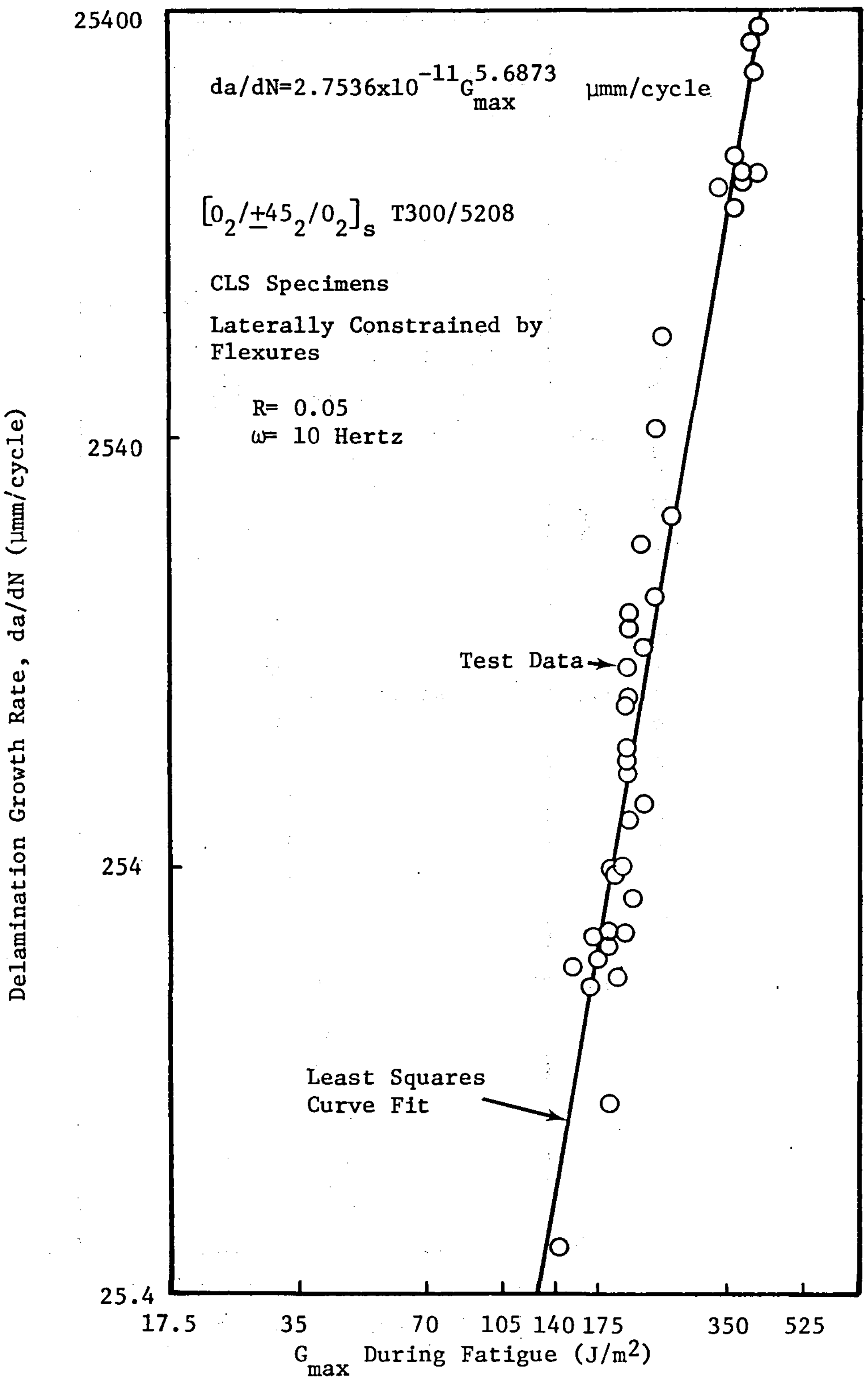

Figure 26. Variation of Delamination Growth Rate with Strain Energy Release Rate in $[0_2/\pm45_2/0_2]_s$ CLS Specimens with Lateral Constraints.

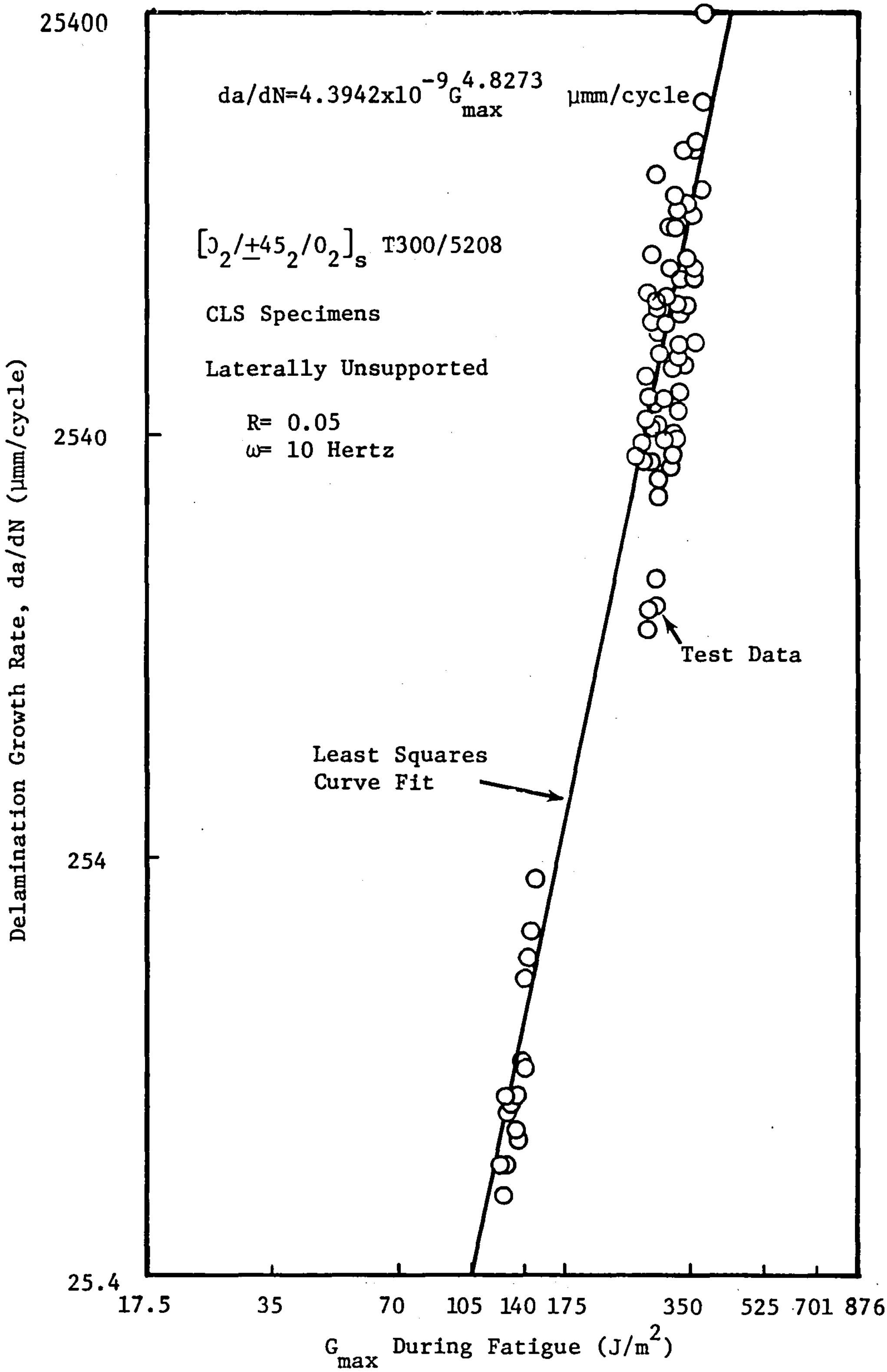

Figure 27. Variation of Delamination Growth Rate with Strain Energy Release Rate in $[0_2/\pm45_2/0_2]_s$ CLS Specimens Without Lateral Constraints.

formed to obtain a power law approximation (equation 34) relating delamination growth rate (da/dN) to the maximum cyclic total strain energy release rate (G_{max}). Individual mode contributions to da/dN are implicitly included in this relationship, and useful information regarding the CLS specimen behavior can be obtained by separating these values. Assuming that G_{III} effects are negligible in the $[(0_2/\pm45)_s]_s$ CLS specimens, modes I and II were assumed to contribute to delamination growth rate according to the following equation:

$$da/dN = C_1(G_{I_{max}}/G_{IC})^{n_1} + C_2(G_{II_{max}}/G_{IIC})^{n_2} \tag{37}$$

$$\text{where } G_{I_{max}} + G_{II_{max}} = G_{max} \tag{38}$$

In section 3.2, it was shown that the mode I contribution to delamination growth was adequately represented by C_1 = 0.0283 mm/cycle and n_1 = 8, when da/dN is expressed in mm/cycle (see equation 16). This was based on fatigue test data on DCB specimens in which G_{II} (and G_{III}) effects were absent. Also, static tests on DCB specimens yielded a G_{IC} value of 102.6 J/m^2. Substituting these values into equation (37) yields:

$$da/dN = 0.0283\ (G_{I_{max}}/103)^8 + C_2\ (G_{II_{max}}/G_{IIC})^{n_2} \tag{39}$$

In the above equation, da/dN and C_2 are expressed in mm/cycle, and $G_{I_{max}}$, $G_{II_{max}}$ and G_{IIC} are expressed in J/m^2. In section 3.6, G_{IIC} was computed to be 587, 279, and 415 J/m^2, assuming the failure criteria in equations (29), (30) and (31), respectively. The choice of G_{IIC} will only affect C_2 in equation (39), and not n_2. The values of C_2 and n_2 are computed below using finite element results and tension fatigue test data on the $[(0_2/\pm45)_s]_s$ CLS specimen.

NFEA of the $[(0_2/\pm45)_s]_s$ CLS specimen provided the expressions in equations (24) to (26) for G_I, G_{II} and G_I/G_{II} as a function of the applied load, P. These expressions are independent of the delamination size (a). During fatigue, u_{max} was set to be a specified value. The compliance variation with a and the delamination growth rate (da/dN) were measured. The maximum cyclic load (P_{max}) corresponding to any delamination size (a) was computed using the C versus a records and the imposed u_{max} value. Substituting P_{max} into equation (26), $G_{I_{max}}/G_{II_{max}}$ was computed. The average dC/da from Figure 20 and the computed P_{max} yielded G_{max} expressed as P^2_{max} (dC/da)/(2w). G_{max} was subsequently divided into $G_{I_{max}}$ and $G_{II_{max}}$ components using the calculated $G_{I_{max}}/G_{II_{max}}$ ratios and equation (38).

In equation (39), the mode I contribution to da/dN was assumed to be $0.0283\ (G_{I_{max}}/103)^8$ mm/cycle, when $G_{I_{max}}$ is expressed in J/m^2. Computed $G_{I_{max}}$ values were substituted into this expression, and the results were subtracted from the measured da/dN values to obtain the mode II contribution to da/dN, expressed as $C_2\ (G_{II_{max}}/G_{IIC})^{n_2}$ in equation (39). Table 17 presents the relevant delamination growth data for $[(0_2/\pm45)_s]_s$ CLS specimens. A least squares analysis of the computed mode II contributions to da/dN yielded the following results:

$$n_2 = 5.7865 \tag{40}$$

C_2 = 1.1237, 0.0152 or 0.1511 mm/cycle if G_{IIC} = 587, 279 or 415 J/m^2, respectively. (41)

It is interesting to note that n_2 in equation (40) is approximately equal to the exponent in equation (34). Also, Table 17 reveals that the mode I contribution to da/dN is very small in comparison to the mode II contribution to da/dN, especially for low G_{max} values. Delamination growth in the $[(0_2/\pm45)_s]_s$ CLS specimens is, therefore, predominantly influenced by mode II.

In summary, delamination growth rate in T300/5208 laminates may be quantified by:

$$da/dN = 0.0283\ (G_{I_{max}}/103)^8 + C_2\ (G_{II_{max}}/G_{IIC})^6 \tag{42}$$

where C_2 for three G_{IIC} values are given by equation (41). The expression in equation (42) assumes negligible G_{III} effects, and is restricted to constant amplitude fatigue loading at R=0.05 and ω = 10 Hertz.

TABLE 17. MODE II CONTRIBUTION TO DELAMINATION GROWTH IN $[(0_2/\pm45)_s]_s$ CLS SPECIMENS

Specimen	a (mm)	u_{max} (mm)	C (μmm/N)	P_{max} (kN)	G_{max} (J/m^2)	da/dN (μmm/cycle)	$G_{I_{max}}$ (J/m^2)	$G_{II_{max}}$ (J/m^2)	$C_2\left(\frac{G_{II_{max}}}{G_{IIC}}\right)^{n_2}$ + (μmm/cycle)
H-12	30.5	0.3226	38.69	8.340	484	60477	109	375	32177
H-12	38.1	0.3226	41.28	7.816	425	39065	95	330	24244
H-12	50.8	0.3226	45.60	7.073	348	27305	76	272	24818
H-12	63.5	0.3226	49.92	6.463	291	14122	63	228	13568
H-12	76.2	0.3226	54.25	5.947	246	3454	53	193	3315
H-12	88.9	0.3226	58.57	5.507	211	1026	44	167	995
H-12	101.6	0.3226	62.89	5.129	183	518	38	145	508
H-12	114.3	0.3226	67.21	4.800	160	84	33	127	81
H-12	124.5	0.3226	70.67	4.564	145	57	30	115	56
H-11	50.8	0.3531	52.93	6.672	310	9548	67	243	8641
H-11	63.5	0.3531	57.42	6.147	263	5570	56	207	5354
H-11	76.2	0.3531	61.90	5.703	226	1857	48	178	1794
H-11	88.9	0.3531	66.39	5.316	197	737	41	156	719
H-11	101.6	0.3531	70.88	4.982	173	368	36	137	362
H-11	114.3	0.3531	75.37	4.684	153	155	31	122	153
H-11	124.5	0.3531	78.96	4.471	139	56	28	111	55

+ Refer to equation (39).

(Continued)

TABLE 17. MODE II CONTRIBUTION TO DELAMINATION GROWTH in $[(0_2/\underline{+}45)_s]_s$ CLS SPECIMENS (CONCLUDED)

Specimen	a (mm)	u_{max} (mm)	C (μ mm/N)	P_{max} (kN)	G_{max} (J/m^2)	da/dN (μ mm/cycle)	$G_{I_{max}}$ (J/m^2)	$G_{II_{max}}$ (J/m^2)	$C_2\left(\frac{G_{II_{max}}}{G_{IIC}}\right)^{n_2}$ (μmm/cycle)$^+$
H-17	28.4	0.3048	42.80	7.122	353	7493	78	275	4432
H-17	38.1	0.3048	46.13	6.610	304	3505	66	238	2701
H-17	50.8	0.3048	50.49	6.036	253	2718	54	199	2556
H-17	63.5	0.3048	54.86	5.556	215	879	45	170	841
H-17	76.2	0.3048	59.22	5.147	184	869	38	146	859
H-17	88.9	0.3048	63.59	4.795	160	177	33	127	174
H-17	101.6	0.3048	67.95	4.484	140	85	29	111	84
H-17	114.3	0.3048	72.32	4.212	123	17	25	98	17
H-17	119.4	0.3048	74.06	4.115	118	12	24	94	12

+ Refer to equation (39).

3.9 STATIC COMPRESSION TEST RESULTS ON SPECIMENS WITH ITTW DELAMINATIONS

Specimens with imbedded through-the-width (ITTW) delaminations had the geometry shown in Figure 3, and were tested under static compression as shown in Figure 9. Specimens with three laminate configurations were tested. Laminate A had a $[0_4/(0/45/90/-45)_7]_s$ layup with a 19 mm (0.75 in.) long initial delamination between plies 3 and 4. Laminate B had a $[0/45_2/0/(0/45/90/-45)_7]_s$ layup with a 25 mm (1 in.) long initial delamination between plies 4 and 5. Laminate C had a $[0/45/90_2/45/0_3/(0/45/90/-45)_6]_s$ layup with a 32 mm (1.25 in.) long initial delamination between plies 6 and 7. In every case, the delamination was imbedded at a 0/0 interface.

Static compression loads were introduced at a slow rate, and the transverse deflection of the delaminated set of plies at midlength was monitored. The far-field axial strain and the strain in the delaminated region at midlength were measured in selected specimens. If the ITTW delamination propagated over only a short distance, the new length and the corresponding location of the maximum transverse deflection were recorded as shown in Figure 11.

Static compression test results on laminate A specimens are presented in Tables 18 to 21. With the exception of one specimen (A-4), the ITTW delamination propagated in an unstable manner, initially to one tab edge, and subsequently to the other. In specimen A-4, a stable delamination growth was observed initially prior to its abrupt propagation to the tab region. In one specimen (A-3), the 25.4 mm (1 in.) wide delaminated $[0]_{3T}$ plies split between fibers, 19.1 mm (0.75 in.) from one edge. The 19.1 mm (0.75 in.) wide delamination propagated to the tab region first, and the 6.4 mm (0.25 in.) wide delamination followed it at a higher load level.

Static compression test results on laminates B and C with ITTW delaminations are presented in Table 22. Delamination failure -- propagation of the ITTW delamination to the tab region -- was abrupt (without any stable growth) during these load-controlled tests. In laminate B, the delaminated $[0/45]_s$ segment exhibited fiber failures and splitting

TABLE 18. STATIC COMPRESSION TEST RESULTS ON SPECIMEN A-1+

Applied Stress ksi (MPa)	Event	2a * in (mm)	Measured Strain far-field μmm/mm	ε_L * μmm/mm	δ_L * in (mm)	X_{max} * in (mm)
-26.26 (-181.1)	Kapton Separation	0.75 (19.1)	-3330	-2796	0.125 (3.18)	2.25 (57.15)
-29.18 (-201.2)	--	0.75 (19.1)	-3700	-2695	0.130 (3.30)	2.25 (57.15)
-35.02 (-241.4)	--	0.75 (19.1)	-4405	-2617	0.135 (3.43)	2.25 (57.15)
-39.39 (-271.6)	Propagation of delamination to one tab edge	2.63 (66.8)	-4995	364	0.239 (6.07)	1.32 (33.4)
-44.35 (-305.8)	Propagation of delamination to the other tab edge (Delam. Failure)	4.50 (114.3)	-5624	1001	--	2.25 (57.15)
-621.5 (-428.5)	Total Failure	---	-7781			

+ $[0_4/(0/45/90/-45)_7]_s$ T300/5208 laminate. The top $[0_3]$ layers were initially delaminated over 19.1 mm (0.75 in.) through the entire width (25.4 mm).
E = 54.38 GPa (7.89 Msi); Cross-sectional area = 221.1 mm^2 (0.3427 in^2)

* See Figure 11

TABLE 19. STATIC COMPRESSION TEST RESULTS ON SPECIMEN A-2+

Applied Stress ksi (MPa)	Event	$2a^*$ in (mm)	δ_L^* in (mm)	X_{max}^* in (mm)
-13.99 (- 96.5)	Kapton Separation	0.88 (22.2)	0.007 (0.18)	2.13 (53.98)
-22.38 (-154.3)	--	0.88 (22.2)	0.014 (0.36)	2.13 (53.98)
-29.3 (-202.6)	Propagation of delamination to one tab edge	2.63 (66.7)	0.049 (1.24)	1.31 (33.34)
-33.58 (-231.5)	--	2.63 (66.7)	0.051 (1.30)	1.31 (33.34)
-39.17 (-270.1)	--	2.63 (66.7)	0.100 (.254)	1.31 (33.34)
-44.49 (-306.7)	Propagation of delamination to the other tab edge	4.5 (114.3)	0.245 (6.22)	2.25 (57.15)
-62.95 (-434.1)	Total Failure	--	--	--

+ $[0_4/(0/45/90/-45)_7]_s$ T300/5208 laminate. The top $[0_3]$ layers were initially delaminated over 9.53 mm (0.75 in.) through the entire width (25.4 mm)
Cross-sectional area = 230.6 mm^2 (0.3574 in^2)

* See Figure 11

TABLE 20. STATIC COMPRESSION TEST RESULTS ON SPECIMEN A-3$^+$

Applied Stress ksi (MPa)	Event	2a * in (mm)	δ_L * in (mm)	X_{max} * in (mm)
-21.93 (-151.2)	Kapton Separation	0.75 (19.1)	0.010 (0.25)	2.25 (57.15)
-27.41 (-189.0)	--	0.75 (19.1)	0.014 (0.36)	2.25 (57.15)
-31.25 (-215.5)	Delamination propagated on one side	1.75 (44.5)	0.015 (0.37)	2.13 (53.98)
-32.89 (-226.8)	--	1.75 (44.5)	0.015 (0.38)	2.13 (53.98)
-39.47 (-272.2)	Delamination propagated to tab edge on either side over a 3/4" width	4.5 (114.3)	0.175 (4.45)	2.25 (57.15)
-46.60 (-321.3)	Delamination propagated to tab edge on either side over a 1/4" width	4.5 (114.3)	---	2.25 (57.15)
-74.00 (-510.3)	Total Failure	---	---	---

+ $[0_4/(0/45/90/-45)_7]_s$ T300/5208. The top $[0_3]$ layers were initially delaminated over 19.1 mm (0.75 in.) through the entire width (25.4 mm)

Cross-sectional area = 235.3 mm^2 (0.3648 in^2)

* See Figure 11.

TABLE 21. STATIC COMPRESSION TEST RESULTS ON SPECIMEN A-4+

Applied Stress ksi (MPa)	Event	$2a^*$ in (mm)	$\delta_L{}^*$ in (mm)	$X_{max}{}^*$ in (mm)
-163.39 (-113.0)	Kapton Separation	0.75 (19.1)	0.005 (0.13)	2.25 (57.15)
- 21.86 (-150.7)	--	0.75 (19.1)	0.013 (0.33)	2.25 (57.15)
- 27.32 (-188.4)	--	0.75 (19.1)	0.020 (.051)	2.25 (57.15)
- 30.60 (-211.0)	Delamination propagated 25.4 mm upward	1.75 (44.5)	0.023 (0.58)	2.13 (53.98)
- 32.79 (-226.1)	--	1.75 (44.5)	0.024 (0.61)	2.13 (53.98)
- 39.21 (-270.3)	Delamination propagated to the upper tab	2.63 (66.8)	0.020 (0.51)	1.32 (33.4)
- 47.81 (-329.7)	Delamination propagated to the lower tab	4.50 (114.3)	0.210 (5.33)	2.25 (57.15)
- 73.50 (-506.7)	Total Failure	--	--	--

+ $[0_4/(0/45/90/-45)_7]_s$ T300/5208. The top $[0_3]$ layers were initially delaminated over 19.1 cm (0.75 in.) through the entire width (25.4 mm)
Cross-sectional area = 230.6 mm^2 (0.3574 in^2)

* See Figure 11.

TABLE 22. STATIC COMPRESSION TEST RESULTS ON LAMINATES B AND C*

Specimen	Cross-Sectional Area cm^2 (in^2)	Applied Stress in MPa (ksi) Corresponding to		Modulus GPa (Msi)
		Delamination Failure	Total Failure	
B-2	2.257 (0.3499)	321.2 (46.585)	419.7 (60.875)	---
B-3	2.309 (0.3579)	321.7 (46.661)	454.6 (65.940)	---
B-4	2.337 (0.3623)	348.3 (50.511)	443.4 (64.311)	43.50 (6.31)+
B-5	2.345 (0.3635)	322.5 (46.768)	383.1 (55.571)	---
Average →	---	328.4 (47.631)	425.2 (61.674)	---
C-1	2.108 (0.3268)	379.8 (55.080)	451.5 (65.483)	49.64 (7.20)
C-2	2.245 (0.3480)	299.2 (43.391)	400.2 (58.046)	---
C-3	2.315 (0.3589)	337.5 (48.947)	418.8 (60.741)	---
C-4	2.348 (0.3640)	284.1 (41.209)	394.0 (57.143)	---
Average		325.1 (47.157)	416.1 (60.353)	---

* Laminate B has a $[0/45_2/0/(0/45/90/-45)_7]_s$ layup, with a 25.4 mm long Kapton inclusion between plies 4 and 5, across the 25.4 mm width. Laminate C has a $[0/45/90_2/45/0_3/(0/45/90/-45)_6]_s$ layup with a 31.8 mm long Kapton inclusion between plies 6 and 7, across the 25.4 mm width.

\+ This modulus is lower than the expected value (49.6 MPa<E<54.4 MPa) between fibers in the 0° and 45° plies at delamination failure. Laminate C exhibited similar local failures in the delaminated $[0/45/90]_s$ portion. All the laminates were loaded beyond delamination failure to measure strengths corresponding to total failure.

The static compression test results presented above can, and should, be used to identify the appropriate delamination failure criterion among equations (29), (30) and (31). This would require the computation of G_I and G_{II} values for the test laminates for various delaminations sizes (a) and load levels. A rigorous analysis or a numerical approximation of the analysis (Reference 5) may be employed for this purpose. Computed G_I and G_{II} values corresponding to delamination failure loads should then be incorporated into equations (29), (30), and (31) to identify a suitable delamination failure criterion.

3.10 COMPRESSION FATIGUE TEST RESULTS ON SPECIMENS WITH ITTW DELAMINATIONS

Constant amplitude compression fatigue tests were conducted at R = 10 and ω = 10 Hertz (see Figure 10). The Kapton inclusions (ITTW delaminations) were initially "released" by cycling the specimens at a compressive stress amplitude below the static delamination failure value. Fatigue tests were restarted after this to record the presented data. Cyclic delamination growth was monitored by constantly observing the marked free edges under a microscope. Table 23 presents the delamination growth rate data for laminate A specimens. Presented results are averages of data from three tests, at each σ_{min} value, on specimens that exhibited "clean" delamination growth. In a few specimens, the delaminated $[0]_{3T}$ plies exhibited splitting between fibers, and the split regions propagated to the tab region at different rates. Results from these tests are not included in Table 23. It is evident from the presented results that a higher absolute cyclic stress amplitude induces faster delamination growth. Also, the delamination growth rate reduces sharply as the delamination size (2a) increases.

Delamination growth rate results for laminate A (Table 23) were subsequently analyzed, using a least squares curve fit algorithm, to yield the following results:

TABLE 23. SUMMARY OF DELAMINATION GROWTH RATES AT TWO STRESS AMPLITUDES IN LAMINATE A SPECIMENS*

a (mm)	Average da/dN (μmm/cycle) **	
	σ_{min} = - 144.2 MPa+	σ_{min} = -129.8 MPa+
9.525	14631	8675
15.875	4428	2472
22.225	1123	661
28.575	377	202
34.925	187	92
41.275	110	51
47.625	79	36
53.975	18	13

* $[0_4/(0/45/90/-45)_7]_s$ T300/5208 Laminate.

The top three 0° plies were initially delaminated over a 19.1 mm (0.75 in.) length, through the 25.4 mm (1 in.) width.
2a is the total delamination length.

** Presented results are averages of data from three tests, at each σ_{min} value, on specimens that exhibited "clean" delamination growth.

\+ Average applied stress at which the imbedded delamination propagated to the tab edges during the static tests = -315.9 MPa. The listed stress amplitudes therefore correspond to stress ratios of 0.46 and 0.41, respectively, with respect to the applied static stress value at delamination failure.

$$da/dN = 88.24\ a^{-3.69}\ \text{mm/cycle for}\ \sigma_{min} = -144\ \text{MPa} \qquad (43)$$

$$da/dN = 56.50\ a^{-3.74}\ \text{mm/cycle for}\ \sigma_{min} = -130\ \text{MPa} \qquad (44)$$

In the above equations, a is expressed in mm.

Fatigue tests on laminates B and C posed a special problem (see Section 2.7). These specimens suffered delamination failures when they were cycled to "release" the imbedded Kapton film, prior to initiating fatigue tests. Subsequent specimens were tightly clamped over 37.1 from either tab edge (see Figure 11) to preclude delamination failures when Kapton inclusions were "released". While this procedure did not succeed in every case, it contained the imbedded delamination over at least 37.1 mm in most of the specimens. After the Kapton inclusion was "released", fatigue loading at R = 10 and ω = 10 Hertz was introduced to record delamination growth rate data. Tables 24 and 25 present da/dN data for laminates B and C. Again, a higher absolute cyclic stress amplitude induces faster delamination growth, and the growth rate reduces substantially as the delamination size (2a) increases.

Using a least squares curve fit algorithm, the results in Tables 24 and 25 were analyzed to yield delamination growth rate equations. For laminate B,

$$da/dN = 23.27\ a^{-2.81}\ \text{mm/cycle for}\ \sigma_{min} = -138\text{MPa} \qquad (45)$$

Only the above relationship is presented because insufficient results were obtained for the other σ_{min} cases. Laminate C results were also too limited in number, and the range of a values, to yield reliable delamination growth rate expressions.

The results presented in equations (43), (44) and (45) for laminates with ITTW delaminations can, and should, be analyzed further to verify the delamination growth rate expression in equation (42). The G_I, G_{II} values for these laminates, for various delamination lengths and load levels, should be determined using a rigorous analysis or a numerical approximation of the analysis (Reference 5). Computed G_I and G_{II} values should then be incorporated into equation (42) to obtain da/dN values. The expres-

TABLE 24. SUMMARY OF DELAMINATION GROWTH RATES IN LAMINATE B SPECIMENS*

a (mm)	da/dN (μmm/cycle) at σ_{min}=-197 MPa	a (mm)	da/dN (μmm/cycle) at σ_{min}=-138 MPa	a (mm)	da/dN (μmm/cycle) at σ_{min}=-99 MPa
41.3	12700	15.2	6960	26.4	762
44.5	5080	25.0	4641	27.1	381
47.6	2311	30.2	2159	28.8	216
50.8	584	32.0	1506	29.9	152
		42.0	931	31.4	48
		48.8	203	32.4	38
				33.7	13

* Laminate B has a $[0/45_2/0/(0/45/90/-45)_7]_s$ layup and a 25.4 mm long Kapton inclusion between plies 4 and 5, across the entire (25.4 mm) width.

Average applied stress corresponding to delamination failure in laminate B = -328.4 MPa

R = 20, ω = 10 Hertz.

2a is the total delamination length.

TABLE 25. SUMMARY OF DELAMINATION GROWTH RATES IN LAMINATE C SPECIMENS*

a (mm)	da/dN (μmm/cycle) at σ_{min} =-179 MPa	a (mm)	da/dN (μmm/cycle) at σ_{min} =-130 MPa	a (mm)	da/dN (μmm/cycle) at σ_{min} =-98 MPa
42.9	8026	46.4	1270	42.7	4877
46.0	3886	47.6	846	46.0	218
49.2	2362	48.9	254	49.2	79
52.4	838	49.5	32	52.4	48
		50.2	25		

* Laminate C has a $[0/45/90_2/45/0_3/(0/45/90/-45)_6]_s$ layup and a 31.8 mm long Kapton inclusion between plies 6 and 7, across the entire (25.4 mm) width.

Average applied stress corresponding to delamination failure in laminate C = -325.1 MPa.

R = 20, ω = 10 Hertz.

2a is the total delamination length.

sion in equation (42) is based on test results obtained at $R = 0.05$ and $\omega = 10$ Hertz. If the predictions based on equation (42) agree well with the results expressed by equations (43) to (45), the difference in the R values can be established to have a minimal effect on delamination growth rate. Also, equation (42) can be established to be a reliable delamination growth rate equation for $\omega = 10$ Hertz, when G_{III} effects are negligible.

3.11 SUMMARY OF RESULTS

The results discussed in the preceding sections are summarized below:

(1) $G_{IC} = 103\ J/m^2$ for the T300/5208 graphite/epoxy material system. G_{IC} was computed using static DCB test data and compares well with the result in Reference 14 (see Table 26). G_{IC} computations based on width-tapered DCB test results (Reference 3) yielded a G_{IC} value ($205\ J/m^2$) that is twice the value obtained in this program and in Reference 14. A comparison of G_{IC} for T300/5208 with G_{IC} for other material systems is presented in Table 26.

(2) The contribution of mode I alone to delamination growth rate in T300/5208 laminates may be expressed by equation (16):
$da/dN = C_1(G_{I_{max}}/G_{IC})^8$ for $R = 0.05$, $\omega = 10$ Hertz.
where $C_1 = 0.0283$ mm/cycle, $G_{IC} = 103\ J/m^2$, and da/dN is expressed in mm/cycle:

(3) In displacement-controlled, constant amplitude fatigue tests on DCB specimens (see equations 12 and 16):

$G_{I_{max}} \ \alpha \ a^{-4}$, and

$da/dN \ \alpha (G_{I_{max}}/G_{IC})^8$

Therefore, $da/dN \ \alpha \ a^{-32}$

Hence the drastic reduction in the delamination growth rate with an increase in a, in displacement-controlled fatigue tests on DCB specimens.

TABLE 26. COMPARISON OF AVAILABLE G_{IC}, G_{IIC} DATA WITH GENERATED RESULTS

Material	G_{IC} J/m^2	G_{IIC} J/m^2	Reference, Comments
T300/5208 (Narmco)	103	279-587	This report
T300/5208 (Narmco)	88	154	Ref. 14
T300/934 (Fiberite) and T300/5208 (Narmco)	205	--	Ref. 3--Width-tapered DCB tests
T300/P1700 (U.S. Polymeric)	380	--	Ref. 3--Width-tapered DCB tests
T300/BP907 (American Cyanamid)	306^{+}; 937^{++}	--	+ based on crack initiation load (Ref. 3) ++ based on maximum load (Ref. 3)
AS/3501-6 (Hercules)	131	322	Ref. 17
AS/3501 (Hercules)	--	825	Ref. 8--Delamination at the midplane of a beam under 3-point bending
AS4/2220-3 (Hercules)	245	--	Ongoing Northrop IRAD Project.
AS/3502 (Hercules)	133	--	Ref. 16
T300/V378-A (U.S. Polymeric)	79^{+}; 149^{*}	193^{*}	+Ref. 16; *Ref. 17
AS1/Polysulfone	655	--	Ref. 16

(4) Results from displacement-controlled, constant amplitude fatigue tests on DCB specimens indicate that, if $G_{I_{max}}/G_{IC}$ is less than 0.5, da/dN is reduced to below 0.25 μmm/cycle, approaching a "no growth" state. A $G_{I_{max}}$ value of 0.5 G_{IC} may therefore be referred to as the "threshold" $G_{I_{max}}$ value below which no significant mode I delamination growth will be observed.

(5) A reliable static failure criterion, accounting for the presence of G_I and G_{II}, does not exist. Therefore, static CLS test data were analyzed by incorporating G_{IC} and nonlinear finite element results into three assumed failure criteria (equations 29 to 31). G_{IIC} for the T300/5208 material system was computed to be between 279 and 587 J/m^2, based on the assumed failure criteria. A validated failure criterion is mandatory for the computation of a reliable G_{IIC}, using the generated static CLS test results. Only pure shear tests (like a torsion tube test) will provide reliable G_{IIC} values. A comparison of G_{IIC} for T300/5208 with G_{IIC} for other material systems is presented in Table 26.

(6) The contribution of mode II alone to delamination growth rate in T300/5208 laminates may be expressed by (see equation 42):

$$da/dN = C_2(G_{II_{max}}/G_{IIC})^6 \text{ for } R = 0.05,\ \omega = 10 \text{ Hertz}$$

where C_2 = 0.1511 mm/cycle if G_{IIC} = 415 J/m^2, and da/dN is expressed in mm/cycle.

(7) In displacement-controlled, constant amplitude fatigue tests on CLS specimens (see equations 33 and 42),

G_{max} ($\approx G_{II_{max}}$) α a^{-2} , and

$da/dN \;\alpha\; (G_{II_{max}}/G_{IIC})^6$

Therefore, $da/dN \;\alpha\; a^{-12}$

Hence the drastic reduction in the delamination growth rate, with an increase in a, in displacement-controlled fatigue tests on CLS specimens. A comparison with the expression in item (3) indicates that the delamination growth rate reduces faster in displacement-controlled DCB specimens.

(8) Results from displacement-controlled, constant amplitude fatigue tests on $[(0_2/\pm 45)_s]_s$ specimens indicate that a "no growth" situation (growth rates below 0.25 μmm/cycle) will be realized only when G_{max}/G_C is below 0.2. Since delamination growth in these specimens is predominantly under mode II, the "threshold $G_{II_{max}}$" value is approximately 0.2 G_{IIC}.

(9) Delamination growth rate in T300/5208 laminates with negligible G_{III} effects, subjected to constant amplitude fatigue loading at R = 0.05 and ω = 10 Hertz, may be quantified by (equation 42):

$$da/dN = C_1(G_{I_{max}}/G_{IC})^8 + C_2(G_{II_{max}}/G_{IIC})^6$$

where C_1, C_2, G_{IC} and G_{IIC} are defined in items (2) and (6). da/dN, C_1 and C_2 possess the same units.

(10) Specimens with ITTW delaminations generated static and fatigue test data that can be used to arrive at a reliable static delamination failure criterion, and to validate the delamination growth rate equation in item (9). This requires the development of a reliable analysis to predict G_I and G_{II} as a function of delamination size and load levels in these specimens.

(11) Assuming that mode III effects are similar to mode II effects, the delamination growth rate expression in equation (42) may be extended as follows for a general situation:

$$da/dN = C_1(G_{I_{max}}/G_{IC})^8 + C_2(G_{II_{max}}/G_{IIC})^6 + C_3(G_{III_{max}}/G_{IIIC})^6 \qquad (46)$$

This expression must be verified through tests (at $R = 0.05$ and $\omega = 10$ Hertz) on, and analysis of, specimens with imbedded delaminations that grow in a two-dimensional manner along the imbedded interface.

(12) Quantification of the effect of a realistic delamination on the strength and lifetime of a laminate subjected to constant amplitude fatigue loading requires: (a) measurement of G_{IC}, G_{IIC} and G_{IIIC} for the material; (b) establishment of a valid static delamination failure criterion; (c) measurement of "threshold" values for $G_{I_{max}}$, etc; (d) establishment of a valid delamination growth rate equation; and (e) analytical (approximate) expressions for G_I, etc. as function of delamination size, delamination location and applied loads. If $G_{I_{max}}$, $G_{II_{max}}$, etc. corresponding to the absolute maximum cyclic load satisfy the static failure criterion, an abrupt delamination failure (not necessarily total failure) will occur. If this is not the case, $G_{I_{max}}$, etc. must be compared with the corresponding "threshold" values to determine if there will be any significant (>0.25 μmm/cycle) delamination growth. If it is determined that there will be a stable cyclic growth of the imbedded delamination, the growth rate can be computed using the validated delamination growth rate equation. Over ΔN cycles at this growth

rate, the delamination size increases by Δa. $G_{I_{max}}$ and $G_{II_{max}}$ corresponding to the enlarged a value are incorporated into the static failure criterion to determine if the stable delamination growth is terminated by an abrupt delamination. This procedure is repeated for Δa increments until the maximum permissible delamination growth is realized, or until an abrupt delamination failure occurs. The residual strength and lifetime of a delaminated specimen may thus be computed.

SECTION 4

CONCLUSIONS AND RECOMMENDATIONS

4.1 CONCLUSIONS

An experimental program was conducted to investigate the roles played by G_I and G_{II} in inducing delamination growth under static and fatigue loading. Double cantilever beam (DCB) specimens were used for pure mode I tests, and cracked lap shear (CLS) specimens were used for mixed mode tests. In addition, static compression and constant amplitude compression fatigue tests were also conducted on specimens with imbedded through-the-width (ITTW) delaminations. All the specimens were fabricated using T300/5208 graphite/epoxy.

G_{IC} for T300/5208, computed using static DCB test results, agrees well with the value in Reference 14. The exponent in the da/dN versus $G_{I_{max}}$ relationship, obtained using a least squares curve fit analysis of the DCB fatigue test results, is different from the value reported in Reference 14.

The computation of G_{IIC} using static CLS test results requires a validated failure criterion that does not exist. Presented G_{IIC} values are based on failure criteria that were selected without validation. A better estimation of G_{IIC} can be made with the reported results if a validated failure criterion were to be available in the future. The G_{IIC} value in Reference 14 is lower than the values computed in this report. But, in Reference 14, a linear three-dimensional finite element analysis of the CLS specimen was performed, and G_{III} effects were accounted for in an invalidated failure criterion.

A least squares curve fit analysis of the CLS fatigue test data, using NFEA and DCB results, provided a delamination growth rate (da/dN) equation that accounts for the effects of G_I and G_{II} on da/dN. The growth rate equation is based on test results generated at R=0.05 and ω = 10 Hertz. This equation should be validated through additional tests on other mixed mode test specimens at R=0.05 and ω = 10 Hertz.

Static compression test results from specimens with ITTW delaminations should be analyzed to establish a valid static delamination failure criterion. This will require the development of a reliable analysis of the delaminated specimen to relate G_I and G_{II} to applied load levels, for various delamination sizes and locations. Constant amplitude compression fatigue test results from these specimens should also be analyzed in a similar manner to verify the applicability and adequacy of the delamination growth rate equation obtained using CLS test results.

4.2 RECOMMENDATIONS

(1) Measured compliances were larger (up to 20%) than analytical predictions, and dC/da and G_c computations based on test results were even larger (up to 39%) than the corresponding analytical predictions, in mixed mode CLS specimens. To investigate the causes for these differences, additional testing and analysis of CLS specimens are recommended.

(2) A valid delamination failure criterion must be established through additional tests on specimens with different G_I/G_{II} ratios. This will provide a means for reliable G_{IIC} computation. A pure shear situation is desirable, but is difficult to create in a test coupon.

(3) A reliable analysis of specimens with ITTW delaminations should be developed to relate G_I and G_{II} to applied load levels, for various delamination sizes and locations.

(4) The applicability of the developed delamination growth rate expression (equation 42) should be verified through additional tests at $R = 0.05$ and $\omega = 10$ Hertz, on specimens with ITTW delaminations (one-dimensional growth)

(5) The proposed extension of the delamination growth rate expression to include G_{III} effects (equation 46) should be verified through tests on, and analysis of, coupons and structural elements (like a stiffened panel) with imbedded delaminations. The coupons and elements should be subjected

to compressive loading at $R = 20$ and $\omega = 10$ Hertz to cause instability-induced delamination growth in a general (two-dimensional) manner along the imbeddment surface.

(6) In the presented delamination growth rate expressions, only the absolute maximum cyclic G_I and G_{II} values have been incorporated. The minimum-to-maximum cyclic load ratio (R) and frequency (ω) will likely influence delamination growth significantly. A systematic test program, addressing the effects of R and ω on imbedded delamination growth, is highly recommended.

SECTION 5

REFERENCES

1. Ramkumar, R.L., "Fatigue Degradation in Compressively Loaded Composite Laminates," NASA Contractor Report No. 165681, April 1981.

2. Ramkumar, R. L., "Environmental Effects on Composite Damage Criticality," Naval Air Development Center Report No. NADC-79067-60, January 1982.

3. Byers, B. A., "Behavior of Damaged Graphite-Epoxy Laminates Under Compression Loading," NASA Contractor Report 159293, August 1980.

4. Whitcomb, J. D., "Analysis of Instability-Related Delamination Growth," Proceedings of the Mechanics of Composites Review, Bergamo Center, Dayton, Ohio, October 1980.

5. Whitcomb, J. D., "Finite Element Analysis of Instability-Related Delamination Growth," NASA Technical Memorandum 81964, March 1981.

6. Whitcomb, J. D., "Delamination Growth in Compressively Loaded Laminates," Presented at the ASTM Symposium on Effects of Defects in Composite Materials, San Francisco, California, December 1982.

7. Ramkumar, R. L., Kulkarni, S. V. and Pipes, R. B., "Definition and Modeling of Critical Flaws in Graphite Fiber Reinforced Epoxy Resin Matrix Composite Materials," Naval Air Development Center Report No. NADC-76228-30, January 1978.

8. Chatterjee, S. N., Hashin, Z. and Pipes, R. B., "Definition and Modeling of Critical Flaws in Graphite Fiber Reinforced Resin Matrix Composite Materials," Naval Air Development Center Report No. NADC 77278-30, August 1979.

9. Rybicki, E. F., Schmueser, D. W. and Fox, J., "An Energy Release Rate Approach for Stable Crack Growth in the Free-Edge Delamination Problem," Journal of Composite Materials, Vol. 11, October 1977, pp. 479-487.

10. Rybicki, E. F. and Kanninen, M. F., "A Finite Element Calculation of Stress Intensity Factors by a Modified Crack Closure Integral," Engineering Fracture Mechanics, Vol. 9, 1977, pp. 931-938.

11. Wang, A. S. D. and Slomiana, M., "Fracture Mechanics of Delamination - Initiation and Growth," Naval Air Development Center Report No. NADC-79056-60, January 1982.

12. Chatterjee, S. N. and Pipes, R. B., "Composite Defect Significance," Proceedings of the Mechanics of Composites Review Meeting, Dayton, Ohio, October 1982.

13. "Standard Test Method for Peel Resistance of Adhesives (T-Peel Test)," ASTM Standard Number D1876-72.

14. Wilkins, D. J., Eisenmann, J. R., Camin, R. A., Margolis, W. S. , and Benson, R. A., "Characterizing Delamination Growth in Graphite-Epoxy," Damage in Composite Materials: Basic Mechanisms, Accumulation, Tolerance, and Characterization, ASTM STP XXX, American Society for Testing and Materials, 1981.

15. Devitt, D. F., Schapery, R. A. and Bradley, W. L., "A Method for Determining the Mode I Delamination Fracture Toughness of Elastic and Viscoelastic Composite Materials," Journal of Composite Materials, Vol. 14, October 1980, pp. 270-285.

16. Whitney, J. M., "Characterization of Interlaminar Fracture Toughness," Proceedings of the Mechanics of Composites Review Meeting, Dayton, Ohio, October 1982.

17. Wilkins, D. J., "A Comparison of the Delamination and Environmental Resistance of a Graphite-Epoxy and a Graphite-Bismaleimide," Naval Air Systems Command Report No. NAV-GD-0037, September 1981.

18. Roderick, G. L., Everett, R. A., Jr. and Crews, J. H., Jr., "Cyclic Debonding of Unidirectional Composite Bonded to Aluminum Sheet for Constant-Amplitude Loading," NASA TN D-8126, January 1976.

1. Report No.	2. Government Accession No.	3. Recipient's Catalog No.
NASA CR-166046		

4. Title and Subtitle	5. Report Date
Performance of a Quantitative Study of Instability-Related Delamination Growth	March 1983
	6. Performing Organization Code
7. Author(s)	8. Performing Organization Report No.
R. L. Ramkumar	NOR 83-70
9. Performing Organization Name and Address	10. Work Unit No.
Northrop Corporation Aircraft Division One Northrop Avenue Hawthorne, CA 90250	11. Contract or Grant No. NAS1-16727
12. Sponsoring Agency Name and Address	13. Type of Report and Period Covered Contractor Report
National Aeronautics and Space Administration Washington, D.C. 20546	14. Sponsoring Agency Code

15. Supplementary Notes

Langley Technical Monitor: John D. Whitcomb
Final Report

16. Abstract

An experimental program was conducted to quantify instability-induced imbedded delamination growth. Static tests on double cantilever beam (DCB) specimens yielded the critical mode I strain energy release rate (G_{IC}) for T300/5208 graphite/epoxy. Static tests on mixed mode cracked lap shear (CLS) specimens, and a nonlinear finite element analysis (NFEA) of the CLS specimen to separate mode I and mode II effects, yielded the critical mode II strain energy release rate (G_{IIC}) for T300/5208. Constant amplitude fatigue tests on DCB and CLS specimens, along with the NFEA results on CLS specimens, quantified mode I and mode II contributions to delamination growth rate. Fatigue tests were conducted at a frequency (ω) of 10 Hertz, maintaining the minimum to maximum cyclic load ratio (R) at 0.05.

Static compression and constant amplitude compression fatigue tests were also conducted on specimens with imbedded through-the-width (ITTW) delaminations. Kapton imbeddments were located below 3, 4 or 6 plies in a 64-ply laminate, during layup, to simulate ITTW delaminations. The onset of instability (local buckling), the transverse displacement of the delaminated region, and the load level corresponding to the propagation of the ITTW delamination to the tab boundary (delamination failure) were monitored during the static tests. Under cyclic compressive loading ($R=10$, $\omega = 10Hz$), delamination growth rates were measured at various maximum cyclic compressive load values.

17. Key Words (Suggested by Author(s))	18. Distribution Statement
Graphite/Epoxy, Delamination, Instability-induced growth, Compression Loading, Critical Strain Energy Release Rates, Delamination Growth Rate Equations	Unclassified-Unlimited

19. Security Classif. (of this report)	20. Security Classif. (of this page)	21. No. of Pages	22. Price
Unclassified	Unclassified		

 For sale by the National Technical Information Service, Springfield, Virginia 22161

End of Document